Few- and many-body physics of Rydberg polaritons

Dissertation

Matthias Moos

Vom Fachbereich Physik der Technischen Universität Kaiserslautern zur Verleihung des akademischen Grades „Doktor der Naturwissenschaften“ genehmigte Dissertation

Betreuer: Prof. Dr. Michael Fleischhauer

Zweitgutachter: Prof. James Anglin, Ph.D.

Datum der wissenschaftlichen Aussprache: 15. Dezember 2017

D 386

Contents

Abstract

Quantum computers and quantum simulators are two exciting fields harnessing the extraordinary properties of quantum-mechanical systems to solve problems which can practically not be computed on classical computers and to understand fundamental physical models, respectively. Many different ideas exist for building quantum computers and simulators. One promising recent approach is Rydberg quantum optics, a field combining the extraordinary control of light-matter coupling established in quantum optics with the strong nonlinearities between highly excited Rydberg atoms. The fundamental quasi-particles in this field, *Rydberg polaritons*, are suited for many applications in quantum information science, for instance optical transistors or phase gates, that ultimately may pave the way for all-optical quantum computation. Moreover, beyond these quantum information applications Rydberg polaritons provide a promising platform for creating many-body states of photons that may allow to investigate open problems of condensed-matter physics. Furthermore they will allow to address entirely new questions beyond the standard realm of solid-state physics such as the competition between interactions and single-particle dynamics with couplings to tailored reservoirs.

In the present thesis I study few- and many-body physics of one-dimensional Rydberg polaritons. I contribute to the understanding of the properties of interacting Rydberg polaritons and derive an effective many-body theory of these. I propose and analyze a scheme to reach a regime of strongly repulsive polaritons enabling the creation of correlated many-body states by a dynamical protocol. Moreover, I investigate the regime of weak attractive interactions, where photonic molecules can be observed.

The coherent control of light-matter interactions by electromagnetically induced transparency (EIT) leads to the formation of slowly propagating quasi-particles, termed dark-state polaritons. Using Rydberg states in this setup mediates strong interactions between individual photons, or interacting *Rydberg polaritons*. In general, interacting Rydberg polaritons have to be described as open systems, as the atomic interaction induces a coupling of dark states to a reservoir of bright states which are subject to decay. In Chapter 2 I derive an effective master equation of Rydberg polaritons and analyze conditions when the system can be described by a one-dimensional model. In an off-resonant driving scheme the open system can approximately be described by a unitary system, yielding many-body theory of Rydberg polaritons. To verify this model I employ numerical wave-function simulations of

two excitations and compare them with exact diagonalization for two excitations.

In one spatial dimension the low-energy physics of a many-body Rydberg polariton system is described by a moving-frame Luttinger liquid with strong repulsive interactions suggesting the possibility of Wigner crystallization. I argue that this regime of strongly interacting polaritons cannot be accessed in a typical continuous wave EIT setup. In Chapter 3 I show that a solution to this limitation consists in using a time-dependent protocol, i.e., dynamically storing the Rydberg polaritons in the medium. I employ numerical simulations to show that storage of Rydberg polaritons is possible – despite the strong interactions. A time-dependent Luttinger liquid theory shows that a dynamical protocol allows to generate a many-body state with quasi-long range correlations, i.e., a crystalline order over a finite length.

Finally, I consider the limit of weakly interacting Rydberg polaritons. Recent experiments have shown the existence of bunching in this regime, indicating the existence of bound pairs of Rydberg polaritons. Chapter 4 of the thesis contributes to the understanding of these experiments and investigates the properties and time evolution of Rydberg polariton pair states by employing a Green's function approach and numerical wave-function simulations. The bunching can be explained by a superposition of bound and scattering states. I investigate the interplay of these two contributions giving rise to the possibility of filtering bound and continuum states enabling the creation and observation of photonic molecules.

Kurzfassung

Quantencomputer und Quantensimulatoren sind zwei spannende Felder der Physik, die die außergewöhnlichen Eigenschaften quantenmechanischer Systeme nutzbar machen, um Probleme zu lösen, die praktisch nicht auf klassischen Computern berechnet werden können, bzw. um fundamentale physikalische Modelle zu verstehen. Es existieren viele unterschiedliche Ideen, um Quantencomputer und Quantensimulatoren zu bauen. Ein vielversprechender Ansatz ist die Rydberg-Quantenoptik, ein Forschungsfeld, das die bemerkenswerte Kontrolle von Licht-Materie-Wechselwirkungen, die in der Quantenoptik etabliert ist, mit starken Wechselwirkungen hochangeregter Rydberg-Atome kombiniert. Die fundamentalen Quasiteilchen dieses Feldes, *Rydberg-Polaritonen*, eignen sich für viele Anwendungen in der Quanteninformationstechnologie, z.B. optische Transistoren oder Phasengatter, die letztendlich den Weg für rein-optische Quantencomputer bahnen könnten. Über Anwendungen in der Quanteninformationstechnologie hinaus sind Rydberg-Polaritonen eine vielversprechende Plattform, um Vielteilchenzustände von Photonen zu erzeugen, die es möglich machen, offene Probleme der Physik der kondensierten Materie zu untersuchen. Weiterhin werden sie erlauben, völlig neue Fragestellungen über den Bereich der Festkörperphysik hinaus zu untersuchen, wie z.B. die Konkurrenz von Wechselwirkungen und Einteilchen-Dynamik mit Kopplungen zu zugeschnittenen Reservoirs.

In der vorliegenden Arbeit untersuche ich Systeme weniger Teilchen und Vielteilchensysteme von Rydberg-Polaritonen. Ich trage zum Verständnis von Eigenschaften wechselwirkender Rydberg-Polaritonen bei und leite eine effektive Vielteilchentheorie von Rydberg-Polaritonen her. Ich schlage ein Schema vor, um ein Regime stark wechselwirkender Photonen zu erreichen, was es möglich macht, mit einem dynamischen Protokoll korrelierte Vielteilchenzustände zu erzeugen. Weiterhin untersuche ich das Regime schwacher attraktiver Wechselwirkungen, wo photonische Molekülzustände beobachtet werden können.

Die kohärente Kontrolle von Licht-Materie-Wechselwirkungen durch elektromagnetisch induzierte Transparenz (EIT) führt zur Bildung langsam propagierender Quasiteilchen, genannt Dunkelzustandspolaritonen. Das Nutzen von Rydbergzuständen in diesem Setup vermittelt eine starke Wechselwirkung zwischen einzelnen Photonen, oder wechselwirkende Rydberg-Polaritonen. Im Allgemeinen müssen wechselwirkende Rydberg-Polaritonen als offene Systeme beschrieben werden, da die atomaren Wechselwirkungen eine Kopplung von Dunkelzuständen mit einem Reservoir von Hellzuständen

erzeugt, welche zerfallen. In Kapitel 2 leite ich eine effektive Mastergleichung für Rydberg-Polaritonen her und untersuche Bedingungen, wenn das System durch ein eindimensionales Modell beschrieben werden kann. Unter nicht-resonantem Treiben kann das offene System näherungsweise durch ein unitäres System beschrieben werden, was zu einer Vielteilchentheorie von Rydberg-Polaritonen führt. Um das Modell zu verifizieren, nutze ich numerische Wellenfunktions-Simulationen zweier Anregungen, die ich mit exakter Diagonalisierung zweier Anregungen vergleiche.

In einer räumlichen Dimension wird die Niedrigenergie-Physik von Vielteilchen-Rydberg-Polariton-Systemen durch eine Luttinger-Flüssigkeit mit starken repulsiven Wechselwirkungen beschrieben, die die Möglichkeit einer Wigner-Kristallisation andeuten. Ich argumentiere, dass dieses Regime stark wechselwirkender Polaritonen in einem typischen *continuous wave*-EIT-setup nicht erreicht werden kann. In Kapitel 3 zeige ich, dass durch Nutzen eines zeitabhängigen Protokolls, d.h., durch Speichern von Rydberg-Polaritonen im Medium, diese Limitierung überwunden werden kann. Ich nutze numerische Simulationen, um zu zeigen, dass ein Speichern von Polaritonen trotz starker Wechselwirkungen möglich ist. Eine zeitabhängige Luttinger-Theorie zeigt, dass ein dynamisches Protokoll erlaubt, Vielteilchenzustände mit quasi-langreichweitigen Korrelationen zu erzeugen, d.h., eine kristalline Ordnung über eine endliche Distanz.

Im letzen Teil betrachte ich den Grenzwert schwach wechselwirkender Rydberg-Polaritonen. Neuere Experimente zeigen, dass hier ein Bunching von Photonen existiert, was auf eine Existenz gebundener Zustände von Rydberg-Polaritonen hinweist. Kapitel 4 trägt zum Verständnis dieser Experimente bei und untersucht Eigenschaften und die Zeitentwicklung von Rydberg-Polariton-Paarzuständen durch Anwenden eines Greensfunktions-Ansatzes und numerischen Wellengleichung-Simulationen. Das Bunching kann durch eine Superposition von gebundenen und Kontinuumszuständen erklärt werden. Ich untersuche die Wechselwirkung dieser zwei Beiträge, was es ermöglicht, photonische Moleküle zu erzeugen und zu beobachten.

Chapter 1

General introduction

The main subject of this thesis are Rydberg polaritons, interacting quasi-particles of propagating light and stationary matter excitations. We investigate few- and many-body properties of Rydberg polaritons. In this section we want to introduce the fundamental physical and theoretical concepts underlying the results in the main text.

In Section 1.1 we will introduce the phenomenon of electromagnetically induced transparency (EIT) [1], describing the lossless propagation of photons in a system of three-level atoms. In the case of a (weak) quantized probe field, this can be explained in terms of dark-state polaritons [2, 3] as a superposition of light and atomic excitation. These are massive quasi-particles and allow for an explanation of slow light [4] and light storage [2]. In Section 1.2 we consider the interactions of Rydberg states of atoms [5, 6]. By combining electromagnetically induced transparency with Rydberg atoms, strong interactions between photons, respectively polaritons can be mediated [7]. These so-called Rydberg polaritons, which will be introduced in Chapter 2, are the fundamental concept of the present thesis giving rise to many interesting few-body effects, e.g. a strong suppression of the correlation function at short distances [8]. In Chapter 2 we will derive a many-body theory of Rydberg polaritons by a perturbative approach in tracing out the remaining degrees of freedom. This will be done by following a standard approach of quantum optics to describe open systems [9]. In Section 1.3 we will introduce this approach and derive a master equation in Lindblad form by employing Born and Markov approximations. Finally, Section 1.4 introduces the concept of bosonization [10], an effective description of gap-less one-dimensional many-body systems, in particular photons propagating in one dimension. This method will be employed in Chapter 3 to analyze the many-body dynamics in Rydberg-polariton setups.

Remark. Throughout the thesis we set $\hbar = 1$ unless otherwise noted.

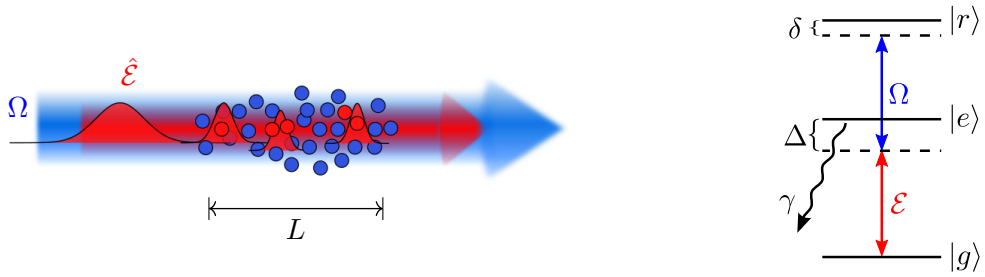

(a) Setup (b) Level scheme

Figure 1.1: (a) Schematic setup of an EIT experiment with a cloud of atoms of length L a control field Ω and a probe field $\hat{\mathcal{E}}$. (b) Effective atomic level scheme for EIT with Rydberg atoms in a ladder configuration. The probe field $\hat{\mathcal{E}}$ is off-resonantly coupled to the atomic transition $|\mathrm{g}\rangle \leftrightarrow |\mathrm{e}\rangle$ with a single-photon detuning Δ and the (strong) control field Ω is driving the transition $|\mathrm{e}\rangle \leftrightarrow |\mathrm{r}\rangle$ with a resulting two-photon detuning δ.

1.1 Electromagnetically induced transparency and dark polaritons

The research field of quantum optics investigates the interaction of light fields and atomic matter from the quantum-mechanical single-particle level up to semi-classical descriptions. An important concept of quantum optics is the effect of electromagnetically induced transparency (EIT) [1] describing the lossless propagation of a light field in a medium of three-level atoms under the influence of an additional control light field, rendering an otherwise opaque medium transparent.

In this section we first introduce the fundamental Hamiltonian governing the propagation of light in a gas of three-level atoms dressed by a control field and derive equations of motion for electric field and atomic operators. We will discuss the phenomenon of EIT and slow light for classical light fields in terms of the linear-response susceptibility and furthermore introduce the concept of dark- and bright-state polaritons. These are light-matter quasi-particles that allow us to explain the effect of light storage and, moreover, lead to an interacting many-body theory of photons by using Rydberg interactions as will be subject of Section 2.2.

A more detailed derivation of the light-matter coupling will be given in appendix A.

1.1.1 Light-matter coupling and wave equation

In this section we want to derive the fundamental Hamiltonian describing the coupling of two light fields to three-level atoms as sketched in Figure 1.1. Specifically, we consider the propagation of a probe field $\hat{\mathbf{E}}_\mathrm{p}$ in an ensemble of three-level atoms in ladder configuration consisting of a ground state $|\mathrm{g}\rangle$, a (meta-) stable (Rydberg) state $|\mathrm{r}\rangle$ and an excited state $|\mathrm{e}\rangle$ that is subject to spontaneous decay with rate γ. The probe field is a weak quantized field $\hat{\mathbf{E}}_\mathrm{p}(\mathbf{r},t) = \sqrt{\frac{\omega_\mathrm{p}}{2\epsilon_0}}\boldsymbol{\epsilon}_\mathrm{p}\hat{\mathcal{E}}(\mathbf{r},t)e^{\mathrm{i}(k_\mathrm{p}z-\omega_\mathrm{p}t)} + \mathrm{H.a.}$ with carrier frequency ω_p and wave number k_p. This field couples the atomic transition $|\mathrm{g}\rangle \leftrightarrow |\mathrm{e}\rangle$

resonantly or off-resonantly with a single-photon detuning $\Delta = \omega_{\mathrm{eg}} - \omega_{\mathrm{p}}$. Here $\omega_{\mu\nu} = (E_\mu - E_\nu)/\hbar$ denotes the transition frequency between atomic states $|\mu\rangle$ and $|\nu\rangle$. The control field is assumed to be a classical coherent field $\mathbf{E}_{\mathrm{c}}$ with carrier frequency ω_{c} that is driving the transition $|\mathrm{e}\rangle \leftrightarrow |\mathrm{r}\rangle$ with a single photon detuning $\Delta_{\mathrm{c}} = \omega_{\mathrm{re}} - \omega_{\mathrm{c}}$. We denote the resulting two-photon detuning by $\delta = \Delta + \Delta_{\mathrm{c}}$. The operators $\hat{\mathcal{E}}^\dagger, \hat{\mathcal{E}}$ are normalized creation and annihilation operators of the probe field and, in particular, we assume that they are slowly varying in time and space and obey bosonic commutation relations, i.e.,

$$[\hat{\mathcal{E}}(\mathbf{r}, t), \hat{\mathcal{E}}^\dagger(\mathbf{r}', t)] = \delta(\mathbf{r} - \mathbf{r}'), \tag{1.1}$$

cf. Eq. (A.4) in the appendix. The polarization and spin coherence are microscopically defined by spin flip operators $\hat{\sigma}_{\mu\nu} = |\mu\rangle\langle\nu|$. We assume that there are many atoms on length scales where the light field varies. Consequently, we can introduce coarse-grained continuous atomic operators $\hat{\sigma}_{\mu\nu}(\mathbf{r})$ by averaging over a small volume centered at position $\mathbf{r}$. These obey the commutation relations

$$[\hat{\sigma}_{\alpha\beta}(\mathbf{r}), \hat{\sigma}_{\mu\nu}(\mathbf{r}')] = \frac{\delta(\mathbf{r} - \mathbf{r}')}{n(\mathbf{r})}[\delta_{\beta,\mu}\hat{\sigma}_{\alpha\nu}(\mathbf{r}) - \delta_{\nu,\alpha}\hat{\sigma}_{\mu\beta}(\mathbf{r})], \tag{1.2}$$

where $n(\mathbf{r})$ denotes the continuous atomic density. See appendix A for details.

The interaction of an atom with a quantized or classical light field can in general be described in dipole approximation by the Hamiltonian $\hat{\mathcal{H}}_{\mathrm{dipole}} = -\hat{\mathbf{d}} \cdot \hat{\mathbf{E}}$, [11], where the dipole operator of an atom is defined by $\hat{\mathbf{d}} = \sum_{\mu,\nu} \wp_{\mu\nu}\hat{\sigma}_{\mu\nu} + \mathrm{H.a.}$, with $\wp_{\mu\nu}$ being the dipole matrix element of the transition $|\mu\rangle \leftrightarrow |\nu\rangle$. Extending this interaction Hamiltonian to an ensemble of many three-level atoms interacting with two fields, a probe field and a classical control field and performing the continuum limit and the rotating wave approximation [12] we arrive at the Hamiltonian

$$\hat{\mathcal{H}} = \int \mathrm{d}^3\mathbf{r}\, n(\mathbf{r}) \left\{ \Delta\hat{\sigma}_{\mathrm{ee}}(\mathbf{r}) + \delta\hat{\sigma}_{\mathrm{rr}}(\mathbf{r}) - \left[g\hat{\mathcal{E}}^\dagger(\mathbf{r})\hat{\sigma}_{\mathrm{ge}}(\mathbf{r})e^{-\mathrm{i}k_{\mathrm{p}}z} + \Omega^*\hat{\sigma}_{\mathrm{re}}(\mathbf{r})e^{-\mathrm{i}k_{\mathrm{c}}z} + \mathrm{H.a.} \right] \right\}. \tag{1.3}$$

Here we introduced the probe field coupling strength $g = \sqrt{\frac{\omega_{\mathrm{p}}}{2\epsilon_0}}\wp_{\mathrm{ge}} \cdot \boldsymbol{\epsilon}_{\mathrm{p}}$ and the control field Rabi frequency $\Omega = \wp_{\mathrm{er}} \cdot \mathbf{E}_{\mathrm{c}}$. A more detailed derivation of (1.3) will be given in Appendix A. We remark that the Hamiltonian (1.3) is a well established model of light-matter interactions in quantum optics [11] and will together with the paraxial wave equation be the fundamental model for Chapters 2–4 of the present thesis. The time evolution of the (quantized) probe light field is governed by Maxwell's wave equation,

$$\left[\frac{\partial^2}{\partial t^2} - c^2\nabla^2\right]\hat{E}_{\mathrm{p}}(\mathbf{r}, t) = -\frac{1}{\epsilon_0}\frac{\partial^2}{\partial t^2}\hat{P}(\mathbf{r}, t), \tag{1.4}$$

where $\hat{P}(\mathbf{r}) = n(\mathbf{r})\wp_{\mathrm{ge}}\hat{\sigma}_{\mathrm{ge}}(\mathbf{r})$ denotes the polarization of the medium in the continuum limit, where we dropped the vectorial character of the fields and considered only the polarization corresponding to the $|g\rangle \leftrightarrow |e\rangle$-transition, as can be justified by a proper choice of probe and control field polarization,

see appendix A for details. Making use of the fact that the probe field is almost monochromatic and defining a slowly varying polarization $\hat{P} = \hat{\mathcal{P}} \exp[\mathrm{i}(k_\mathrm{p} z - \omega_\mathrm{p} t)] + \text{H.a.}$ leads to the truncated paraxial wave equation

$$\left[\frac{\partial}{\partial t} + c\frac{\partial}{\partial z} - \mathrm{i}\frac{c}{2k_\mathrm{p}}\nabla_\perp^2\right]\hat{\mathcal{E}}(\mathbf{r},t) = \mathrm{i}\sqrt{\frac{\omega_\mathrm{p}}{2\epsilon_0}}\hat{\mathcal{P}}(\mathbf{r},t) = \mathrm{i}gn(\mathbf{r})\hat{\sigma}_\mathrm{ge}(\mathbf{r},t). \tag{1.5}$$

Here we used the dispersion relation of the free probe field $\omega_\mathrm{p} = ck_\mathrm{p}$ and neglected the first and second time derivatives of the slowly varying polarization $\hat{\mathcal{P}}$. Furthermore, we absorbed a spatial oscillation of $\hat{\sigma}_\mathrm{ge}$ with wave vector k_p into the operator according to (A.32).

1.1.2 Heisenberg-Langevin equations

Let us now derive equations of motion for the atomic operators, where we want to include the spontaneous decay of the excited atomic states. The state $|\mathrm{r}\rangle$ is assumed to be a highly excited Rydberg state throughout the remainder of the thesis, which typically is a metastable state. Thus the decay of this state plays only a small role on typical experimental time scales and for simplicity we neglect its decay in the following, unless otherwise mentioned. The probe field is a weak quantized field, therefore we treat the equations of motion in linear response with respect to $g\hat{\mathcal{E}}$. To regard the spontaneous decay of the excited state $|\mathrm{e}\rangle$ we derive Heisenberg-Langevin equations of motion. After a transformation of the operators $\hat{\sigma}_\mathrm{ge}$ and $\hat{\sigma}_\mathrm{gr}$ according to (A.32) to absorb a factor $1/\sqrt{n(\mathbf{r})}$ and spatial oscillations with wave vector k_p and $k_\mathrm{p} - k_\mathrm{c}$, respectively, we obtain finally

$$\begin{aligned}
\frac{\partial}{\partial t}\hat{\sigma}_\mathrm{ge}(\mathbf{r},t) &= -\Gamma\hat{\sigma}_\mathrm{ge}(\mathbf{r},t) + \mathrm{i}g\sqrt{n(\mathbf{r})}\hat{\mathcal{E}}(\mathbf{r},t) + \mathrm{i}\Omega\hat{\sigma}_\mathrm{gr}(\mathbf{r},t) + \hat{F}_\mathrm{ge}(\mathbf{r},t),\\
\frac{\partial}{\partial t}\hat{\sigma}_\mathrm{gr}(\mathbf{r},t) &= -\mathrm{i}\delta\hat{\sigma}_\mathrm{gr}(\mathbf{r},t) + \mathrm{i}\Omega\hat{\sigma}_\mathrm{ge}(\mathbf{r},t),
\end{aligned} \tag{1.6}$$

where $\Gamma = \gamma + i\Delta$ combines spontaneous decay rate and probe field detuning into an effective complex detuning. $\hat{F}_\mathrm{ge}$ denotes a Langevin noise operator [13], which has to be added to preserve the commutation relations of the decaying operators. This noise operator is δ-correlated in space and time with zero expectation value,

$$\begin{aligned}
\langle\hat{F}_\mathrm{ge}(\mathbf{r},t)\rangle &= 0,\\
\langle\hat{F}_\mathrm{ge}^\dagger(\mathbf{r},t)\hat{F}_\mathrm{ge}(\mathbf{r}',t')\rangle &= D_\mathrm{ge}\delta^3(\mathbf{r}-\mathbf{r}')\delta(t-t'),
\end{aligned} \tag{1.7}$$

where D_ge is called diffusion coefficient and can be determined using the dissipation-fluctuation theorem [13]. Typically, the decay of the excited state $|\mathrm{e}\rangle$ can be described by coupling to a thermal (or vacuum) reservoir. In this case $D_\mathrm{ge} \propto \gamma$. Since the noise results from excitation of the state $|\mathrm{e}\rangle$, which we have set $\langle\hat{\sigma}_\mathrm{ee}\rangle = 0$ in linear response, the Langevin noise operator can safely be neglected.

We note that in the derivation of equations (1.6) further approximations have been made that will not be covered in detail here but will be presented appendix A.

1.1.3 Electromagnetically induced transparency

Electromagnetically induced transparency is a coherence effect that does not require quantum properties of the light field but can be explained with classical fields. This makes it possible to understand the effect in terms of the response of the medium, i.e. the susceptibility χ, that is defined by the relation $P = \epsilon_0 \chi E$. We get the equations of motion for the classical fields readily from the Heisenberg-Langevin equations of motion (1.6) by replacing the quantized probe field by a classical field $E = \mathcal{E} e^{-\mathrm{i}\omega_\mathrm{p} t}$ and the atomic spin-flip operators by density-matrix coherences, i.e., $\hat{\sigma}_{\mu\nu} \to \rho_{\nu\mu} = \langle \nu | \hat{\rho} | \mu \rangle$, for which we get the following equations of motion in linear response

$$\begin{aligned} \partial_t \rho_\mathrm{eg} &= -\Gamma \rho_\mathrm{eg} + \mathrm{i} d_\mathrm{ge} \mathcal{E} e^{-\mathrm{i}\omega_\mathrm{p} t} + \mathrm{i}\Omega \rho_\mathrm{rg}, \\ \partial_t \rho_\mathrm{rg} &= -\mathrm{i}\delta \rho_\mathrm{rg} + \mathrm{i}\Omega \rho_\mathrm{eg}. \end{aligned} \tag{1.8}$$

Solving these equations for the steady state and using the definition of the Polarization $P = n d_\mathrm{ge} \rho_\mathrm{eg}$ yields the susceptibility

$$\chi(\omega_\mathrm{p}) = -\frac{n |d_\mathrm{ge}|^2}{\epsilon_0} \frac{\delta}{\Omega^2 + \mathrm{i}(\gamma + \mathrm{i}\Delta)\delta}, \tag{1.9}$$

as a function of the probe field frequency ω_p, since both, the single photon detuning Δ and the two-photon detuning δ are dependent on ω_p. In Figure 1.2 we display real and imaginary part of the susceptibility as function of the probe field frequency in the case of zero and non-zero control field detuning. In both cases the absorption vanishes for $\Delta = -\Delta_\mathrm{c}$, i.e. for $\delta = 0$, indicating that the medium becomes transparent.

Using the susceptibility (1.9) we can calculate the transmission coefficient for the transmission of probe light through a medium of length L under EIT conditions. According to Beer's absorption law the transmission coefficient, defined as the ratio of input and output intensity, $|E(0)|^2$ and $|E(L)|^2$, respectively,

$$T = \frac{|E(L)|^2}{|E(0)|^2} = e^{-2\Im[\chi] k L} \approx 1 - 2kL \frac{n d_\mathrm{ge}^2}{\epsilon_0} \frac{\gamma \delta^2}{(\Omega^2 - \gamma\Delta)^2 + \gamma^2 \delta^2}, \tag{1.10}$$

where in the last step we approximated the exponential function for small arguments, i.e. for small $\Im[\chi]$. Here we can directly read off that the transmission coefficient becomes unity, if the two-photon detuning δ goes to zero and hence the absorption of the probe field vanishes. This phenomenon is called electromagnetically induced transparency (EIT) and can be explained by an interference effect of different excitation paths. Note that this is a purely classical effect [14]. It has first been observed by [15].

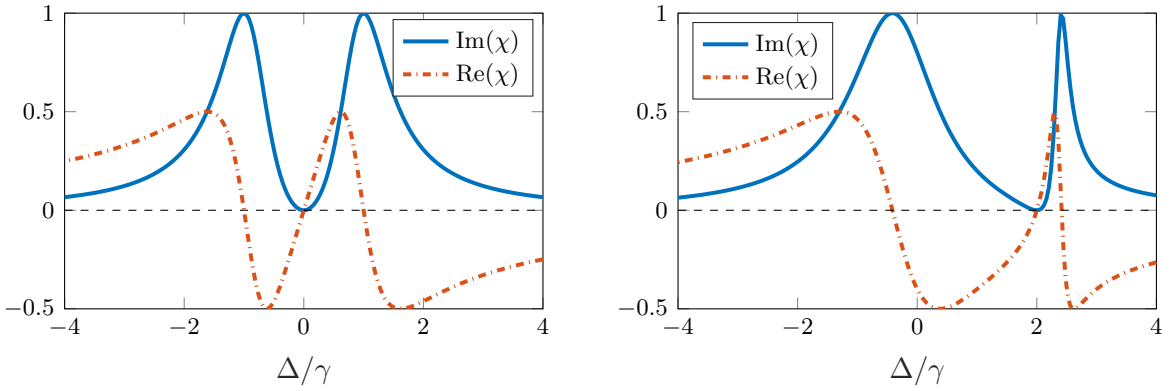

(a) $\Delta_c = 0$ (b) $\Delta_c = 2\gamma$

Figure 1.2: Imaginary (solid blue lines) and real part (dash-dotted red lines) of the EIT susceptibility χ as function of single-photon detuning Δ/γ. (a) Resonant driving, no control field detuning. (b) Control field detuning $\Delta_c = 2\gamma$, the two-photon resonance is shifted to $\Delta = 2\gamma$. In both cases the imaginary part vanishes on two-photon resonance, i.e. the medium becomes transparent.

For zero control field detuning, we can rewrite Eq. (1.10) in the form

$$T(\Delta \approx 0) \approx 1 - \frac{\Delta^2}{\Delta\omega_{\mathrm{tr}}^2}, \tag{1.11}$$

where $\Delta\omega_{\mathrm{tr}}$ denotes the spectral width of the EIT transparency feature, the so-called EIT transparency window,

$$\Delta\omega_{\mathrm{tr}} = \frac{1}{\sqrt{d}}\frac{\Omega^2}{\gamma} \tag{1.12}$$

with $d = \frac{3}{8\pi} n\lambda^3 kL$ being the resonant optical depth in absence of EIT.

Not only the imaginary part of the susceptibility becomes strongly modified by the control field but also the real part of the susceptibility, which is connected to the imaginary part by the Kramers-Kronig relations [16]. As can be seen in Figure 1.2 the real parts of the susceptibility become very steep and show for the resonant case a linear dispersion. Since the group velocity of the probe field is defined by $v_g = c/(1 + \frac{\omega}{2}\frac{\partial \Re\chi}{\partial\omega})$ the real part of the susceptibility becomes very steep corresponding to a strong reduction of the group velocity of the probe field, i.e. $v_g \ll c$. This phenomenon is called slow light, pointed out in [4] and observed in [17, 18] and led to the observation of a light speed reduction of $17\,\mathrm{m\,s^{-1}}$ [19].

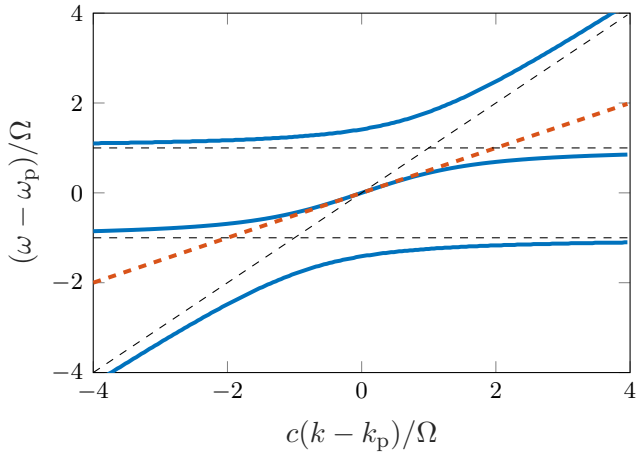

Figure 1.3: Dispersion relation of electromagnetically induced transparency obtained by diagonalizing the matrix in Eq. (1.13) for $g\sqrt{n} = \Omega$, $\gamma = \Delta = \delta = 0$. The branch corresponding to the dark-state polariton is given by the blue solid curve in the middle, which is exhibits a slow, linear dispersion in the vicinity of $k = k_\mathrm{p}$, as indicated by the dashed red line.

1.1.4 Dark-state polaritons

As we have seen in the previous section, the dressing of an ensemble of three-level atoms with a control field results in a strongly modified optical response for a probe field. In particular, the group velocity of light propagating in such a medium can become very small compared to the vacuum speed of light, giving rise to slow light and even allowing for the storage of light pulses, which will be introduced in the next section. These effects can be understood by introducing quasi-particles consisting of light and matter excitation, the so-called dark-state polaritons. The strong coherent admixture of massive and stationary atomic excitation to the propagating light field then leads to a strong reduction of the group velocity. In the following we want to introduce these quasi-particles. See appendix A for details.

For simplicity we will assume a perfectly one-dimensional setup of light-fields propagating through a cloud of atoms as sketched in Figure 1.1(a). Then the truncated paraxial wave equation (1.8) and the Heisenberg-Langevin equations (1.6) reduce to one spatial dimension and the transversal mass term in the wave equation vanishes. Together these equations form a closed set of equations for the electromagnetic and atomic field operators, the so-called Maxwell-Bloch equations (see also Eq. (A.33) in Appendix A), that can be written in the form of a Schrödinger equation with a non-Hermitian Hamiltonian,

$$\mathrm{i}\frac{d}{dt}\begin{pmatrix}\hat{\mathcal{E}}\\ \hat{\sigma}_\mathrm{gr}\\ \hat{\sigma}_\mathrm{ge}\end{pmatrix} = \begin{pmatrix}-ck & 0 & -g\sqrt{n}\\ 0 & \delta & -\Omega\\ -g\sqrt{n} & -\Omega & -\mathrm{i}\Gamma\end{pmatrix}\begin{pmatrix}\hat{\mathcal{E}}\\ \hat{\sigma}_\mathrm{gr}\\ \hat{\sigma}_\mathrm{ge}\end{pmatrix}, \tag{1.13}$$

where we applied a Fourier transform of the space coordinate z according to $f(z) = \int \mathrm{d}k\, e^{-\mathrm{i}kz} f(k)$. Next, we make a canonical transformation, rotating $\hat{\Psi} = \cos\theta\hat{\mathcal{E}} - \sin\theta\hat{\sigma}_{\mathrm{gr}}$ and $\hat{\Phi} = \sin\theta\hat{\mathcal{E}} + \cos\theta\hat{\sigma}_{\mathrm{gr}}$, [2]. As can easily be calculated, $\hat{\Psi}$ is a zero energy eigenstate of the matrix in Eq. (1.13) in the case $ck = \delta = 0$, i.e., defines a dark-state polariton of the system. $\hat{\Phi}$ on the other hand denotes a bright state polariton. The mixing angle $\theta = \mathrm{atan}(g\sqrt{n}/\Omega)$ characterizes the mixture of $\hat{\mathcal{E}}$ and $\hat{\sigma}_{\mathrm{gr}}$ in the polaritons. We now want to analyze the effect of k and δ on the dynamics of the dark-state polariton and treat them as a perturbation. Furthermore, we want to allow for a time-dependence of the mixing angle, which introduces a coupling between $\hat{\Psi}$ and $\hat{\Phi}$, when transforming the equation of motion Eq. (1.13) and can also treated as perturbation. In second order perturbation theory we get the result

$$\begin{aligned}\mathrm{i}\frac{d}{dt}\hat{\Psi} = &\left(-v_{\mathrm{g}}k + \delta\sin^2\theta\right)\hat{\Psi} \\ &- \mathrm{i}[\partial_t\theta + \sin\theta\cos\theta(ck+\delta)]^2\left[\frac{\Gamma}{\Omega_{\mathrm{eff}}^2} - \frac{4\gamma}{|\Gamma|^2 + 4\Omega_{\mathrm{eff}}^2 + |\Gamma^2 - 4\Omega_{\mathrm{eff}}^2|}\right]\hat{\Psi},\end{aligned} \tag{1.14}$$

see Appendix A for details. $v_{\mathrm{g}} = c\cos^2\theta$ denotes the group velocity of the dark state polariton. As in k-space this is only an ordinary differential equation, it can easily be solved by integrating the time variable. Considering the case, where $\theta(t) = \text{const.}$ and $\delta = 0$, the first order perturbation yields the result $\hat{\Psi}(k,t) = \hat{\Psi}(k,0)\exp\{\mathrm{i}v_{\mathrm{g}}kt\}$, which transforms to the equation

$$\hat{\Psi}(z,t) = \hat{\Psi}(z - v_{\mathrm{g}}\tau, t-\tau), \tag{1.15}$$

in real space, i.e., that the dark-state polaritons propagate form-stable with the group velocity v_{g}. A finite two-photon detuning leads to further corrections that we consider in greater detail in the appendix or can be found in the literature, see e.g. [20, 21]. In the case $\Delta \gg \gamma$ we can simplify Eq. (1.14) to the form

$$\mathrm{i}\frac{d}{dt}\hat{\Psi} = \left[\delta\sin^2\theta\left(1 + \frac{\delta\Delta\cos^2\theta}{\Omega_{\mathrm{eff}}^2}\right) - kv_{\mathrm{g}}\left(1 - 2\sin^2\theta\frac{\delta\Delta}{\Omega_{\mathrm{eff}}^2}\right) + \frac{v_{\mathrm{g}}c\Delta\sin^2\theta}{\Omega_{\mathrm{eff}}^2}k^2\right]\hat{\Psi}, \tag{1.16}$$

i.e., a Schrödinger equation with unitary time-evolution. Here the first term is a constant energy offset, the second term a drift term with a modified group velocity and the last term describes a kinetic energy with an effective mass

$$m_{\parallel}{}^{-1} = 2c^2\frac{\sin^2\theta\cos^2\theta\Delta}{\Omega_{\mathrm{eff}}^2} \approx 2v_{\mathrm{g}}L_{\mathrm{abs}}\frac{\Delta}{\gamma}, \tag{1.17}$$

where $L_{\mathrm{abs}} = c\gamma/g^2n$ denotes the resonant absorption length of the medium in absence of electro-

magnetically induced transparency.

Length scale.
In deriving the result (1.16) using perturbation theory we assumed that

$$c|k| \ll \frac{\Omega_{\text{eff}}^2}{|\Gamma|} \tag{1.18}$$

has to be fulfilled for all relevant k modes of the polariton field $\hat{\Psi}$. We note that this condition sets a lower limit for the characteristic length scale of the dark-state polaritons

$$l_{\text{dsp}} \gg c\frac{|\Gamma|}{\Omega_{\text{eff}}^2} \approx \frac{|\Delta|}{\gamma} L_{\text{abs}}, \tag{1.19}$$

where in the second step we assumed $|\Delta| \gg \gamma$ and L_{abs} denotes the resonant absorption length of the medium in absence of EIT.

1.1.5 Light storage

In the previous chapter we have derived an effective Schrödinger equation for the time evolution of dark-state polaritons under constant EIT driving conditions. However, Eq. (1.14), describes also time-dependent driving and explains dynamics of EIT light storage [3]. Recalling the definition of the dark-state polariton, namely $\hat{\Psi} = \cos\theta\hat{\mathcal{E}} - \sin\theta\hat{\sigma}_{\text{gr}}$, we see that changing the mixing angle $\theta(t)$ dynamically, allows to turn an initial light pulse continuously into a stationary spin wave. Doing this adiabatically, the pulse is at all times described by the ground-state of the model, i.e., the dark-state polariton. To illustrate this, we show a numerical solution of Eq. (1.13) for a single excitation wave function in Fig. 1.4. As can be observed, an initial polariton consisting mostly of photonic excitation that propagates with the velocity v_{g}, gets turned into a stationary spin excitation and then back to photonic excitation. The rightmost picture clearly shows that the dynamics is at all times well described by a dark-state polariton wave function.

In a storage protocol, the corrections arising due to $\partial_t\theta$ become relevant. Considering the simple case $\delta = \Delta = 0$, i.e., single- and two-photon resonance, Eq. (1.14) becomes

$$\frac{\partial}{\partial t}\hat{\Psi} = \mathrm{i}v_{\text{g}}k\hat{\Psi} - \frac{\gamma}{2g^2n}\sin^2\theta[(\partial_t\theta)^2 + \sin\theta\cos\theta ck\partial_t\theta + \sin^2\theta\cos^2\theta c^2k^2]\hat{\Psi}. \tag{1.20}$$

This equation describes the time evolution of the dark polaritons with losses induced by non-adiabatic storage. Introducing a characteristic time T_{stor} for the storage process, setting a bound for the relative change of the mixing angle, $T_{\text{stor}} \leq \theta/\partial_t\theta$ allows to determine an adiabaticity condition from Eq. (1.20).

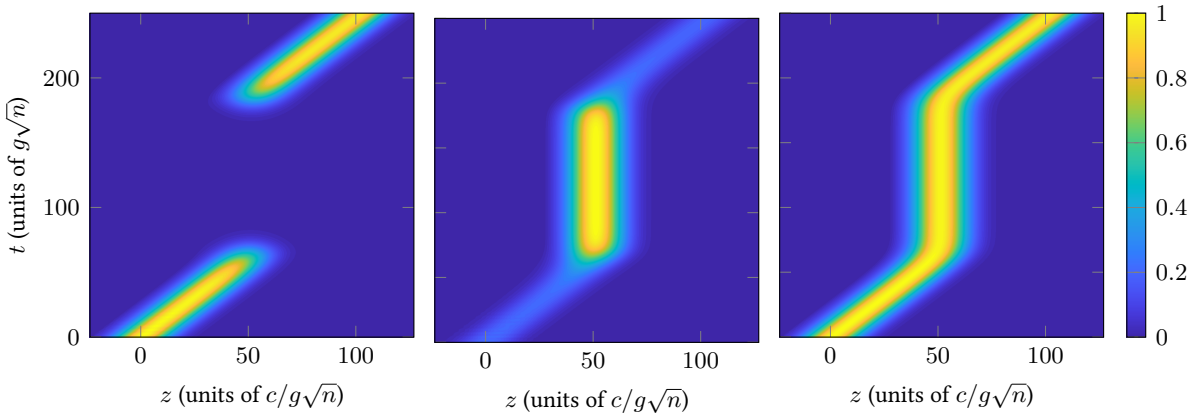

(a) $|\langle\hat{\mathcal{E}}(z,t)\rangle|^2$ (b) $|\langle\hat{\sigma}_{\mathrm{gr}}(z,t)\rangle|^2$ (c) $|\langle\hat{\Psi}(z,t)\rangle|^2$

Figure 1.4: Numerical simulation of storage of a dark-state polariton pulse. Intensity of (a) electric field $\hat{\mathcal{E}}$, (b) atomic coherence $\hat{\sigma}_{\mathrm{gr}}$ and (c) dark-state polariton $\hat{\Psi} = \cos\theta\hat{\mathcal{E}} - \sin\theta\hat{\sigma}_{\mathrm{gr}}$ components in arbitrary units. The initial group velocity is $v_{\mathrm{g}}(0) = 0.8\,c$.

If we assume slow light, i.e., $\theta \approx \cos\theta$, $\sin\theta \approx 1$ and set $\partial_t\theta = \theta/T_{\mathrm{stor}}$, adiabaticity requires

$$T_{\mathrm{stor}} \gg \left\{\frac{L_{\mathrm{abs}}}{c}, \frac{v_{\mathrm{g}}}{c}\right\}, \tag{1.21}$$

where L_{abs} denotes the resonant absorption length in absence of EIT. In the case of a setup with a finite single-photon detuning $|\Delta| \gg \gamma$, this condition has to be multiplied by $|\Delta|/\gamma$, see also the condition (1.19).

1.2 Rydberg atoms

In this section we want to give a brief introduction into Rydberg states of atoms, in particular their extraordinary properties and strong interactions compared to low-lying states of atoms. Detailed reviews about Rydberg atoms and their application in physics can be found in [5, 6]. We focus on alkali atoms like Rb and Cs as they possess only single valence electrons and are widely used in the relevant experiments. The term *Rydberg atom* denotes atoms with a highly excited valence electron which approximately behave like hydrogen atoms, i.e., their energies for a state with principal and angular quantum numbers n and l, respectively, are given by the Rydberg formula for the hydrogen atoms

$$E_{n,l} = -\frac{\mathrm{R}_\infty}{(n-\delta_l(n))^2}. \tag{1.22}$$

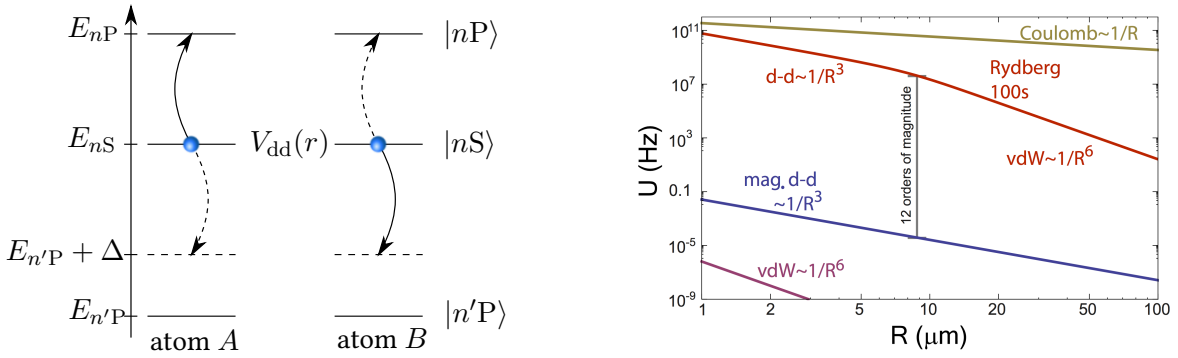

(a) Sketch of dipole-dipole interaction.

(b) Two-body interaction strengths.

Figure 1.5: (a) Sketch of dipole-dipole interaction between two Rydberg atoms A and B with single interaction channel. (b) Two-body interaction strengths for ion, ground state atom, $100s$ Rb atom. Taken from [6].

Here R_∞ denotes the Rydberg constant [1] and $\delta_l(n)$ the quantum defect that is a slowly varying function of the principal quantum number n [6]. The dipole moments of Rydberg atoms scale as $\sim n^2$ and the lifetime as $\sim n^3$, resulting in long-lived states suitable for applications in quantum information, slow light and light storage, as will be considered in this thesis. Moreover, as they are highly excited states one would need UV light to directly excite Rydberg levels from the ground state. For EIT setups we are interested in two-photon excitation schemes that are typically in the visible light range [23]. The dipole matrix elements for transitions between the ground state $|\phi_0\rangle$ and a Rydberg state $|\phi_\mathrm{r}\rangle$,

$$\langle\phi_0|e\mathbf{r}_i|\phi_\mathrm{r}\rangle = \langle n_0, l_0, j_0, m_0|e\mathbf{r}|n, l, j, m\rangle \tag{1.23}$$

become smaller with increasing n, as the overlap between the ground state and the spatially extended Rydberg state becomes smaller. As can be seen from Fermi's golden rule this results in an increasing radiative lifetime of the Rydberg state, scaling as $\tau \sim n^3$. Hence, the Rydberg states are very long-lived metastable states and we assume them to be stable on the time scales considered throughout the present thesis.

The dipole matrix element between neighboring Rydberg states, i.e., states of the same principle quantum number n, scales as

$$\langle n\mathrm{P}|e\mathbf{r}|n\mathrm{S}\rangle \propto n^2 \tag{1.24}$$

leading to very large polarizabilities scaling as $\alpha \sim n^7$. The large polarizabilities of Rydberg atoms make them strongly susceptible to electrical fields and leads to strong mutual interactions between Rydberg states in the absence of external fields. At large inter-atomic distances, $|\mathbf{r}| \gg n^2 a_0$, of two

[1] $\mathrm{R}_\infty = 10\,973\,731.568\,508(65)\,\mathrm{m}^{-1}$, [22]

Rydberg atoms A and B, the dipole-dipole interaction is given by

$$\hat{V}_{\mathrm{dd}}(\mathbf{r}) = \frac{e^2}{4\pi\epsilon_0}\frac{1}{|\mathbf{r}|^3}\left[\mathbf{r}_a\cdot\mathbf{r}_b - 3(\mathbf{r}_a\cdot\hat{\mathbf{r}})(\hat{\mathbf{r}}\cdot\mathbf{r}_b)\right], \tag{1.25}$$

where $\hat{\mathbf{r}} = \mathbf{r}/|\mathbf{r}|$ and $\mathbf{r}_a$ and $\mathbf{r}_b$ denote the distances of the respective electrons from the atomic cores. We are interested in the coupling of a Rydberg pair state $|\phi\rangle = |nlj, nlj\rangle$ to other pair states $|\psi\rangle = |n_a, l_a, j_a, n_b, l_b, j_b\rangle$ with the coupling energy $\langle\psi|\,\hat{V}_{\mathrm{dd}}\,|\phi\rangle$ as sketched in Figure 1.5(a). We do not want to consider state exchange processes between $|\phi\rangle$ and $|\psi\rangle$ but rather the energy shift acting on the pair state $|\phi\rangle$ in presence of neighboring states $|\psi\rangle$ due to dipole-dipole interaction. While in general a manifold of neighboring levels contributes to this level shift, it has been shown [24] that the shift is dominated by only two neighboring states, i.e., a single channel. To derive the interaction potential we choose a Rydberg state $|\phi\rangle = |n\mathrm{S}, n\mathrm{S}\rangle$ with the neighbors $n\mathrm{P}$ and $(n-1)\mathrm{P}$, such that we can write the pair state $|\psi\rangle = \frac{1}{\sqrt{2}}(|n\mathrm{P}, (n-1)\mathrm{P}\rangle + |(n-1)\mathrm{P}, n\mathrm{P}\rangle)$ as shown in Figure 1.5(a), when choosing $n' = n-1$. For simplicity we neglect the degeneracy of these states, a more rigorous derivation can be found in [6, 25]. We denote the energy mismatch of these states (for $r = \infty$) by $\Delta = E_{n_a,l_a} + E_{n_b,l_b} - 2E_{n,l}$. In this single-channel approximation the interaction Hamiltonian is given by the operator

$$\begin{pmatrix} \Delta & V_{\mathrm{dd}}(\mathbf{r}) \\ V_{\mathrm{dd}}^{\dagger}(\mathbf{r}) & 0 \end{pmatrix}, \tag{1.26}$$

acting on the vector of states $(|\phi\rangle, |\psi\rangle)^t$. Diagonalizing this operator leads to the eigenenergies

$$E_{\pm} = \frac{\Delta}{2} \pm \sqrt{\frac{\Delta^2}{4} + \hat{V}_{\mathrm{dd}}^{\dagger}(\mathbf{r})\hat{V}_{\mathrm{dd}}(\mathbf{r})} \tag{1.27}$$

Two regimes can be distinguished. If $\hat{V}_{\mathrm{dd}}(r) \gg \Delta$, i.e., for small distances (or the special case of vanishing Δ) the interaction energy is given by $\hat{V}_{\mathrm{dd}} \sim |\mathbf{r}|^{-3}$, which is the regime of the so-called Förster resonance. We are, however, interested in a second regime, where $\hat{V}(\mathbf{r}) \ll \Delta$, the so-called van der Waals regime. Here the relevant pair-state energy is approximately

$$E(r) = -\frac{V_{\mathrm{dd}}(\mathbf{r})^2}{\Delta} = -\frac{C_6}{r^6}, \tag{1.28}$$

scaling as $|\mathbf{r}|^{-6}$where C_6 denotes the van der Waals interaction strength. As $V_{\mathrm{dd}}(\mathbf{r}) \sim n^4$ and $\Delta \sim n^{-3}$ the interaction strength scales like n^{11}, i.e., becomes very strong for large n. This is shown in Figure 1.5(b). For our choice of states the interaction is isotropic, which is the relevant case for the present thesis, however, in general the interaction can be anisotropic as has been considered for binary interactions in [24].

Finally, when neglecting coupling between different Rydberg states, the interaction Hamiltonian of

two atoms at positions $\mathbf{r}_1$ and $\mathbf{r}_2$ can be written as

$$\hat{\mathcal{H}} = \hat{\sigma}_{\mathrm{rr}}^{(1)} V(\mathbf{r}_1 - \mathbf{r}_2) \hat{\sigma}_{\mathrm{rr}}^{(2)}, \tag{1.29}$$

where $\hat{\sigma}_{\mathrm{rr}}^{(j)} = |\mathrm{r}\rangle_j \langle \mathrm{r}|_j$ denotes the projector onto the Rydberg state of atom j.

1.3 Open systems

Time evolution of quantum mechanical systems, as described by the Schrödinger equation, are unitary processes and reversible in time [26]. However, real systems have vast numbers of degrees of freedom such that it is impossible to track all of them microscopically and irreversible processes can be observed in many experiments. For instance, spontaneous decay of an excited atom or absorption of a photon are of interest in quantum optics [11]. These and other irreversible processes can be described by introducing the concept of open systems [9], i.e., systems that are in contact with an environment or reservoir, that has a very large or even infinite number of degrees of freedom. Under certain assumptions these degrees of freedom can be traced out leading to an equation of motion describing the effective non-unitary time evolution of the system. This equation is called master equation [9].

1.3.1 System-plus-reservoir approach

The standard approach in quantum optics to describe an open system starts in splitting the full Hilbert space into a system, the degrees of freedom of interest, and a reservoir, containing all degrees of freedom of the environment. These environment degrees of freedom will subsequently be traced out, leading to an effective equation of motion for the system [9].

We start with the Hamiltonian in the Schrödinger picture, that has been split into a term containing the system degrees of freedom, a term containing the reservoir degrees of freedom and a term that contains the coupling of both,

$$\hat{\mathcal{H}} = \hat{\mathcal{H}}_{\mathrm{S}} + \hat{\mathcal{H}}_{\mathrm{R}} + \hat{\tilde{\mathcal{H}}}_{\mathrm{sr}} \tag{1.30}$$

The dynamics of the full system is governed by the von Neumann equation of the density operator $\tilde{\chi}$ of the full system. We transform to an interaction picture with respect to $\hat{\mathcal{H}}_{\mathrm{S}} + \hat{\mathcal{H}}_{\mathrm{R}}$, according to

$$\chi(t) = e^{\frac{\mathrm{i}}{\hbar}(\hat{\mathcal{H}}_{\mathrm{S}} + \hat{\mathcal{H}}_{\mathrm{R}})t} \tilde{\chi}(t) e^{-\frac{\mathrm{i}}{\hbar}(\hat{\mathcal{H}}_{\mathrm{S}} + \hat{\mathcal{H}}_{\mathrm{R}})t} \tag{1.31}$$

$$\hat{\mathcal{H}}_{\mathrm{sr}}(t) = e^{\frac{\mathrm{i}}{\hbar}(\hat{\mathcal{H}}_{\mathrm{S}} + \hat{\mathcal{H}}_{\mathrm{R}})t} \hat{\tilde{\mathcal{H}}}_{\mathrm{sr}} e^{-\frac{\mathrm{i}}{\hbar}(\hat{\mathcal{H}}_{\mathrm{S}} + \hat{\mathcal{H}}_{\mathrm{R}})t}, \tag{1.32}$$

leads to the von Neumann equation in the interaction picture

$$\frac{\partial}{\partial t}\chi(t) = -\frac{\mathrm{i}}{\hbar}\left[\hat{\mathcal{H}}_{\mathrm{sr}}(t), \chi(t)\right]. \tag{1.33}$$

Formally integrating this equation yields

$$\chi(t) = \chi(0) - \frac{\mathrm{i}}{\hbar}\int_0^t \mathrm{d}\tau\ \left[\hat{\mathcal{H}}_{\mathrm{sr}}(\tau), \chi(\tau)\right] \tag{1.34}$$

and reinserting this into Eq. (1.33) leads to

$$\frac{\partial}{\partial t}\chi(t) = -\frac{\mathrm{i}}{\hbar}\left[\hat{\mathcal{H}}_{\mathrm{sr}}(t), \chi(0)\right] - \frac{1}{\hbar^2}\int_0^t \mathrm{d}\tau\ \left[\hat{\mathcal{H}}_{\mathrm{sr}}(t), \left[\hat{\mathcal{H}}_{\mathrm{sr}}(\tau), \chi(\tau)\right]\right]. \tag{1.35}$$

This seems to be a more complex form of Eq. (1.33) but its form allows us to derive a simplified effective equation of motion for the system part of the density matrix only, when making certain assumptions.

First, we assume that initially for $t = 0$ system and reservoir are uncorrelated, i.e., $\chi(0) = \tilde{\chi}(0) = \rho(0) \otimes \rho_{\mathrm{R}}(0)$ and, moreover, that the expectation value of the coupling Hamiltonian with respect to the initial reservoir state vanishes at all times, i.e., $\mathrm{tr}_{\mathrm{R}}[\rho_{\mathrm{R}}\hat{\mathcal{H}}_{\mathrm{sr}}(t)] \equiv 0$. The latter assumption is not essential to the derivation but is usually fulfilled in typical systems and simplifies the further discussion.

Applying a partial trace over the reservoir degrees of freedom yields an equation of motion for the density matrix of the system operator, $\rho(t) = \mathrm{tr}_{\mathrm{R}}\,\chi(t)$,

$$\frac{\partial}{\partial t}\rho(t) = -\frac{1}{\hbar^2}\int_0^t \mathrm{d}\tau\ \mathrm{tr}_{\mathrm{R}}\left\{\left[\hat{\mathcal{H}}_{\mathrm{RS}}(t), \left[\hat{\mathcal{H}}_{\mathrm{RS}}(\tau), \chi(\tau)\right]\right]\right\}. \tag{1.36}$$

To simplify this equation we perform the Born approximation and Markov approximation. Typically the reservoir has a large (infinite) number of degrees of freedom such that the coupling of system and reservoir only affects system degrees of freedom. The reservoir degrees of freedom are thus stable and we can assume that the reservoir stays in its initial equilibrium-state $\rho_{\mathrm{R}}(t) \approx \rho_{\mathrm{R}}(0)$. Note that the free evolution of the reservoir has been transformed away by transforming to the interaction picture. This is called the Born approximation. If additionally the initial state has no system-reservoir correlations, as assumed above, the full state can be written as $\chi(t) = \rho(t) \otimes \rho_{\mathrm{R}}(0)$.

Equation (1.36) is still an integro-differential equation. A substantial simplification arises, if we assume that the reservoir coupling destroys the memory of the system. Then we can replace $\rho(\tau)$ by $\rho(t)$ in Eq. (1.36). This is called the Markov approximation and leads finally to the master equation in

Born-Markov approximation,

$$\frac{\partial}{\partial t}\rho(t) = \frac{1}{\hbar^2}\int_0^t \mathrm{d}\tau\ \mathrm{tr}_\mathrm{R}\left\{\left[\hat{\mathcal{H}}_\mathrm{RS}(t), \left[\hat{\mathcal{H}}_\mathrm{RS}(\tau), \rho(t)\otimes\rho_\mathrm{R}(0)\right]\right]\right\}. \tag{1.37}$$

As will be exemplified in the following, the Markov approximation is justified, if reservoir correlations decay on time scales that are much shorter than the characteristic time scale governing the time evolution of the system.

1.3.2 Master equation

We consider now a simple example of a system described by bosonic operators $\hat{a}_i$ coupled to a reservoir with operators $\hat{b}_j$ by a coupling Hamiltonian with the interaction picture representation

$$\hat{\mathcal{H}}_\mathrm{SR}(t) = \hbar\sum_j \hat{a}_j^\dagger\hat{b}_j + \mathrm{H.c.} \tag{1.38}$$

Inserting this into the master equation and using cyclic permutations in the trace yields

$$\begin{aligned}\frac{\partial}{\partial t}\rho(t) = \sum_{ij}\int_0^t \mathrm{d}\tau\ \Big[&\langle\hat{b}_i\hat{b}_j\rangle_\mathrm{R}\left(\hat{a}_j^\dagger\rho\hat{a}_i^\dagger - \hat{a}_i^\dagger\hat{a}_j^\dagger\rho\right) + \langle\hat{b}_i^\dagger\hat{b}_j^\dagger\rangle_\mathrm{R}\left(\hat{a}_j\rho\hat{a}_i - \hat{a}_i\hat{a}_j\rho\right)\\ &+\langle\hat{b}_i^\dagger\hat{b}_j\rangle_\mathrm{R}\left(\hat{a}_j^\dagger\rho\hat{a}_i - \hat{a}_i\hat{a}_j^\dagger\rho\right) + \langle\hat{b}_i\hat{b}_j^\dagger\rangle_\mathrm{R}\left(\hat{a}_j^\dagger\rho\hat{a}_i^\dagger - \hat{a}_i^\dagger\hat{a}_j\rho\right) + \mathrm{H.c.}\Big]\end{aligned} \tag{1.39}$$

where all operators with index i are to be evaluated at time t and operators with index j at time τ, respectively, and $\langle\cdot\rangle_\mathrm{R}$ denotes the expectation value with respect to the reservoir. In the following we assume for simplicity that the reservoir operators fulfill bosonic commutation relations, i.e., $[\hat{b}_i, \hat{b}_j^\dagger] = \delta_{ij}$, and, moreover, that all anomalous reservoir correlation functions vanish at all times, i.e., $\langle\hat{b}_i\hat{b}_j\rangle_\mathrm{R} = 0$. The Markov approximation is justified, if the reservoir operators are δ-correlated in time, i.e., if

$$\begin{aligned}\langle\hat{b}_i^\dagger(t)\hat{b}_j(\tau)\rangle_\mathrm{R} := \mathrm{tr}\left\{\rho_\mathrm{R}(0)\hat{b}_i^\dagger(t)\hat{b}_j(\tau)\right\} = \Gamma_{ij}\delta(t-\tau)\\ \langle\hat{b}_j^\dagger(\tau)\hat{b}_i(t)\rangle_\mathrm{R} = \Gamma_{ij}^*\delta(t-\tau).\end{aligned} \tag{1.40}$$

Then we can replace the upper limit of integration in Eq. (1.39) by ∞. Setting

$$\Gamma_{ij} = \gamma_{ij} + \mathrm{i}\Delta_{ij} = \gamma_{ji} + \mathrm{i}\Delta_{ji} \tag{1.41}$$

we get finally the equation of motion

$$\frac{\partial}{\partial t}\rho(t) = -\frac{\mathrm{i}}{2}\sum_{ij}\Delta_{ij}\left[\hat{a}_i^\dagger\hat{a}_j + \mathrm{H.c.}, \rho(t)\right] + \frac{1}{2}\sum_{ij}\gamma_{ij}\left[2\hat{a}_i\rho\hat{a}_j^\dagger - \hat{a}_j^\dagger\hat{a}_i\rho - \rho\hat{a}_j^\dagger\hat{a}_i\right]. \tag{1.42}$$

This is the Born-Markov master equation in Lindblad form. This form of the master equation is of special interest, as it has certain properties as follows. First, throughout a time evolution according to Eq. (1.42) the total probability is conserved, i.e., $\mathrm{tr}\,\rho(t) = 1$ at all times, which can be shown easily by using the invariance of the trace under cyclic permutations. Second, if $\gamma_{ij} \geq 0$, the positivity of the density operator is conserved at all times, i.e.,

$$\langle\psi|\rho(t)|\psi\rangle \geq 0 \tag{1.43}$$

for all times t and states $|\psi\rangle$. These properties ensure that the time evolution of a density operator always yields a density operator. Lastly, the Lindblad dynamics conserves the complete positivity of the density operator, i.e., not only $\rho(t)$, but in addition the extended density matrix upon an arbitrary completion with an ancillary system remains positive.

A master equation in Lindblad form can be derived for many well-known problems of quantum optics. Prime examples are the coupling of an harmonic oscillator to a reservoir representing the coupling of an optical cavity to external light fields or the coupling of a two-level atom to a harmonic oscillator. Generalizing Eq. (1.42) we write

$$\frac{d}{dt}\rho = -\mathrm{i}[\hat{\mathcal{H}}, \rho] - \frac{1}{2}\sum_{\mu}\left\{\hat{L}_{\mu}^{\dagger}\hat{L}_{\mu}\rho + \rho\hat{L}_{\mu}^{\dagger}\hat{L}_{\mu} - 2\hat{L}_{\mu}\rho\hat{L}_{\mu}^{\dagger}\right\}, \tag{1.44}$$

for $\hat{L}_{\mu}$ denotes an arbitrary system operator, called Lindblad operator. These are the generators of the dissipative dynamics.

1.3.3 Quantum trajectories

Instead of solving the Lindblad master equation (1.44) with the density matrix formalism, which is describing an ensemble average over many individual realizations of a quantum system, one can also calculate the time evolution of pure states such that it reproduces the master equation as a stochastic average. This is the principle of the quantum trajectory (or Monte-Carlo wave function) approach [27–29]. The time evolution is governed by the master equation (1.44), which can be written in the form

$$\frac{d}{dt}\rho = -\mathrm{i}\left(\hat{\mathcal{H}}_{\text{eff}}\rho - \rho\hat{\mathcal{H}}_{\text{eff}}^{\dagger}\right) + \sum_{\mu}\hat{L}_{\mu}\rho\hat{L}_{\mu}^{\dagger}, \tag{1.45}$$

with a non-Hermitian effective Hamiltonian

$$\hat{\mathcal{H}}_{\text{eff}} = \hat{\mathcal{H}} - \mathrm{i}\sum_{\mu}\hat{L}_{\mu}^{\dagger}\hat{L}_{\mu}. \tag{1.46}$$

Here the $\hat{L}_\mu$ are Lindblad operators, generating the dissipative dynamics. Evolving a pure state $|\psi\rangle$ under this non-Hermitian Hamiltonian for a time dt leads to a decay of the norm of the wave function, in first order in dt given by

$$\langle\psi(t+dt)|\psi(t+dt)\rangle \approx 1 - dp, \quad dp = dt \sum_\mu \langle\psi(t)|\hat{L}_\mu^\dagger \hat{L}_\mu|\psi(t)\rangle\,, \tag{1.47}$$

where dt is chosen, such that $dp \ll 1$. The probability $1 - dp$ gives the probability that the state remains in $|\psi(t+dt)\rangle$ evolved under the effective Hamiltonian. Then with a probability of dp the state does not remain but undergoes a projection,

$$|\psi\rangle = \frac{\hat{L}_\mu\,|\psi\rangle}{||\hat{L}_\mu\,|\psi\rangle\,||}, \tag{1.48}$$

i.e., a *quantum jump* [30]. Particularly, for multiple Lindblad operators $\hat{L}_\mu$, $dp = \sum_\mu dp_\mu$ is a probability distribution, summing up all probabilities of the different jumps. In the limit of $dt \to 0$ the time evolution appears as the continuous time evolution of the state ψ interrupted by jumps. Performing this time evolution many times while calculating the expectation values of observables throughout the time evolution and stochastically averaging these lead to the same result.

A direct numerical implementation of this algorithm by evolving with a fixed step size dt and evaluating the probabilities at every step is quite cumbersome. In typical implementations thus, the time at which a jump occurs is randomly selected [31] and well-established numerical methods can be used to calculate the time evolution under the effective Hamiltonian (1.46) between two jumps.

Note that using this method has the advantage that instead of the density matrix only the time evolution of wave functions has to be calculated. Thus a much larger system size can be calculated, when storage is the limiting factor in a numerical implementation. However, that comes at a cost of computational time, as the stochastic averaging requires many individual trajectories.

1.4 Bosonization

In this section we want to introduce the mathematical technique of *Bosonization*, a method that allows to solve any gapless interacting quantum system in (1+1) dimensions by mapping it to a system of massless, noninteracting bosons, called the Luttinger liquid. Extensive introductions can be found in the literature, for example in the book by Giamarchi [10] as well as [32–34] among many others. In this section we follow the notation of [10] building on the phenomenological derivation introduced in [35].

One-dimensional quantum many-body systems with a gapless spectrum can be described in terms of their low-energy excitations, by using the technique of bosonization. This method is an approach

describing the low-energy physics of a one-dimensional model by linearizing the spectrum around the Fermi energy and mapping the model to a quadratic bosonic model, called the Luttinger liquid model. This makes it possible to solve interacting problems nonperturbatively. The Luttinger liquid is fully characterized by two parameters, the speed of sound v_s, i.e., the characteristic velocity of the system and the dimensionless Luttinger parameter K, that depend on the microscopic model. The Luttinger liquid Hamiltonian is given by

$$\hat{\mathcal{H}}_\mathrm{LL} = \frac{1}{2\pi}\int \mathrm{d}x\, v_\mathrm{s} K \left[\nabla\hat{\theta}(x)\right]^2 + \frac{v_\mathrm{s}}{K}\left[\nabla\hat{\phi}(x)\right]^2. \tag{1.49}$$

Here the field $\hat{\Pi} = \frac{1}{\pi}\nabla\hat{\theta}$ is the canonically conjugate momentum to $\hat{\phi}$, i.e., they obey the commutation relation

$$\left[\hat{\phi}(x), \hat{\Pi}(y)\right] = \mathrm{i}\delta(x-y), \tag{1.50}$$

where, phenomenologically, $\nabla\hat{\phi}$ describes density fluctuations while $\hat{\Pi}$ describes phase fluctuations. Hamiltonian (1.49) is the most general Hamiltonian describing the low-energy properties of a massless one-dimensional system. The bosonization method maps a one-dimensional model to the Hamiltonian (1.49). The parameters v_s and K are dependent on the microscopic model. Introducing an interaction only leads to a renormalization of the parameters. A representation of the original physical fields in terms of the new bosonized fields can be given by

$$\hat{\Psi}^\dagger(x) = \sqrt{\hat{\rho}(x)}e^{-\mathrm{i}\hat{\theta}(x)}, \tag{1.51}$$

$$\hat{\rho}(x) = \left[\rho_0 - \frac{1}{\pi}\nabla\hat{\phi}(x)\right]\sum_p e^{\mathrm{i}2p(\pi\rho_0 x - \hat{\phi}(x))}, \tag{1.52}$$

where p is an integer.

The correlation functions of the Luttinger liquid are universally determined by the K parameter. For the ground state of a Luttinger liquid the first-order correlation function is given by

$$\langle\hat{\Psi}^\dagger(x)\hat{\Psi}(0)\rangle = \rho_0 A_1 \left(\frac{1}{x}\right)^{\frac{1}{2K}} \tag{1.53}$$

and the density-density correlation function is given by

$$\langle\hat{\rho}(x)\hat{\rho}(0)\rangle = \rho_0^2 - \frac{K}{2\pi^2}\frac{1}{x^2} + A_2\rho_0^2\cos(2\pi\rho_0 x)x^{-2K} + \rho_0^2 A_4\cos(4\pi\rho_0 x)x^{-8K} + \ldots \tag{1.54}$$

Comparing both correlation functions one finds that the asymptotic behavior of the Green's function is a power law with exponent $\frac{1}{2K}$ while the density-density correlation function is a power law with exponent $2K$. Thus, the point $K = 1/2$ marks a special point, indicating a cross-over from a regime

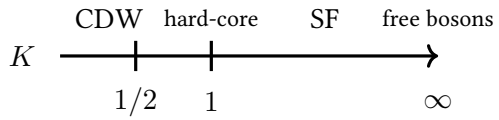

Figure 1.6: Sketch phase diagram for Luttinger liquid of bosons, cf. [10].

dominated by superfluid (SF) correlations for $K > 1/2$ to a charge-density wave (CDW) for $K < 1/2$. The limits of these regimes are the limit of free bosons for $K \to \infty$ and a Wigner crystal for $K \to 0$. The point $K = 1$ corresponds to the case of hard-core interacting bosons, the so-called Tonks gas, which is dual to free fermions. These observations can be put into a sketch phase-diagram, which we show in Figure 1.6. Note that these correlation functions get modified for non-zero temperature [34].

Chapter 2

Few-body quantum physics of Rydberg polaritons

Photons are well established as *qubits*, i.e. carriers of information in quantum science. Their noninteracting nature on the one hand makes them ideally suitable for quantum communication applications but on the other hand makes it hard to perform computational operations directly with photonic qubits. Instead one has to use different physical realizations, for instance superconducting qubits [36], for computation operations and convert them to photonic qubits for communication [37]. However, these conversion steps are difficult to be made efficient and lead to loss of fidelity.

From this perspective it seems desirable to take another path and engineer interactions between photons leading towards an *all-optical* realization. The high speed of an all-optical information processing is moreover of large importance, also in classical communication.

One possible approach to engineer interactions is used in Rydberg quantum optics [7], an emerging research field in physics that utilizes the theoretical knowledge and experimental expertise of quantum optics allowing for an extraordinary control of light-matter coupling and applies it to work with Rydberg states of atoms which give access to strong interaction potentials [5]. The long life-times and strong, non-local interactions make Rydberg states well suited for use in quantum information science [6]. Including these states in a setup of electromagnetically induced transparency [1] allows to mediate strong and long-range interactions between photons [38]. This so-called *Rydberg EIT* paves the way to address problems ranging from quantum communication to quantum computation and even beyond quantum information.

The first experiment to implement Rydberg EIT was done by Pritchard et al., [39] and was quickly understood theoretically [40] using Monte-Carlo sampling of atom dynamics and explained by introducing interacting superatoms [41].

While these first publications considered the attenuation of a classical probe field propagating through an atomic medium with Rydberg states, subsequent experiments extended the research to quantized light fields. On a quantum level, i.e., for a quantized probe field of few photons, the interactions lead to an extension of the fundamental model of dark-state polaritons [2, 3] to a theory

of interacting quasi-particles termed Rydberg polaritons. These have been shown to exhibit spatial correlations, a strongly avoided volume for short relative distances [8], as has been predicted by Gorshkov et al. using two-photon wave function simulations [42]. These first results showed that Rydberg polaritons are a promising setup for building optical quantum-computation devices and since then a single-photon switch [43] and all-optical transistors have been demonstrated by multiple groups [44, 45] and a CZ-gate [46] has been proposed leading to the possibility of all-optical quantum computation [47].

In this chapter we consider few-body quantum physics of Rydberg polaritons. We rigorously analyze the experimental setup of sending a quantized probe light field through a three-dimensional atomic Rydberg medium under conditions of EIT. We derive conditions, when the setup can be described by a one-dimensional model, which is the case when the size of the Rydberg blockade becomes larger than the transversal beam parameter. For this one-dimensional model we employ a perturbative system-plus-reservoir approach to trace out the bright state degrees of freedom to derive a theory that allows to describe the model in terms of a single quantum field, namely Rydberg polaritons. In doing so we arrive at a master equation governing the time evolution of Rydberg polaritons. We discuss the individual contributions to the dynamics described by the master equation and find conditions where the dissipative dynamics can be approximated by a unitary dynamics, i.e., by an effective Hamiltonian.

Finally, we use numerical simulations to compute the time evolution of few-body wave-functions under the full Heisenberg-Langevin equations to verify the effective polariton picture.

The results presented in this chapter are summarized in reference [Moos2015], which was a collaboration of Razmik Unanyan, Michael Fleischhauer and myself, with contributions from Michael Höning and numerical DMRG results provided by Dominik Muth. In particular all analytical calculations and the wave-function simulations were done by me.

2.1 Rydberg polaritons in one dimension

One-dimensional systems are of great interest, as the reduced dimensionality typically corresponds to an enhancement of quantum fluctuations due to correlations [10]. Typically, perturbative descriptions break down and non-classical states beyond mean-field description become relevant. Propagating photons can be created in single laser modes [48], and thus can be described by one-dimensional models. This holds true for polaritons due to their large transversal mass [49, 50]. This changes, however, when interactions have to be taken into account, which is the case for Rydberg polaritons [41]. Here, a coupling between different transversal modes is induced by photon-photon scattering. Although a restriction of transversal modes and a confinement to one dimension can be achieved by performing the experiment inside hollow core fibers [51–53], where excited transverse modes are energetically

separated, so far most Rydberg polariton experiments use three-dimensional atomic clouds [8, 39, 44, 45]. In the following we analyze the propagation of Rydberg polaritons in such three-dimensional setups and derive conditions where the descriptions by a one-dimensional model remains valid, even in the interacting case.

2.1.1 Paraxial light propagation

As introduced in Section 1.1, the propagation of a weak monochromatic quantized probe light field in an atomic medium under conditions of EIT is described by the truncated paraxial wave equation, Eq. (1.5),

$$\left(\frac{\partial}{\partial t} + c\frac{\partial}{\partial z} - \mathrm{i}\frac{c}{2k_\mathrm{p}}\nabla_\perp^2\right)\hat{\mathcal{E}}(\mathbf{r},t) = \mathrm{i}g\sqrt{n}\hat{\sigma}_\mathrm{ge}(\mathbf{r},t). \tag{2.1}$$

To derive a one-dimensional model we assume a cylindrical symmetry of the experimental setup. In a cylindrical setup the transverse mode functions of laser beams are the Laguerre-Gaussian modes, typically denoted $\mathrm{TEM}_{\mu\nu}$ modes [48, 54]. The width $w(z)$ of the Gaussian beam profile is given by [54]

$$w(z) = w_0\sqrt{\frac{R(z)}{z}}, \quad R(z) = z\left(1 + \frac{z^2}{z_\mathrm{R}^2}\right), \tag{2.2}$$

measured in distance z from the focus point of the laser, $R(z)$ gives the radius of curvature along z and $z_\mathrm{R} = \pi w_0^2/\lambda_\mathrm{p}$ denotes the Rayleigh length, indicating the distance from the focus point, where the beam width is a factor of $\sqrt{2}$ larger compared to the beam waist $w_0 = w(0)$.

We decompose the probe field into the transverse mode functions, denoted by $u_{pl}(r,\varphi,z)$, as

$$\hat{\mathcal{E}}(\mathbf{r},t) = \sum_{pl} u_{pl}(r,\varphi,z)\hat{\mathcal{E}}_{pl}(z,t). \tag{2.3}$$

The mode functions $u_{pl}(r,\varphi,z)$ are eigensolutions of the transverse Laplace's equation in two dimensions, $\nabla_\perp^2 u_{pl}(r,\varphi,z) = 0$, for fixed z given by [55]

$$u_{pl}(r,\varphi,z) = \frac{C_{pl}}{w(z)}\, s^{|l|}(r,z)e^{-r^2/w^2(z)+\mathrm{i}l\varphi}e^{-\mathrm{i}k_\mathrm{p}r^2/2R(z)}e^{\mathrm{i}(2p+|l|+1)\zeta(z)}L_p^{|l|}[s^2(r,z)], \tag{2.4}$$

where $s(r,z) \equiv \sqrt{2}r/w(z)$ and $\zeta(z) = \arctan(z/z_\mathrm{R})$ denotes the so called Gouy phase of the beam [48, 54]. The functions L_p^l are the associated Laguerre polynomials [56, 57], C_{pl} is a normalization constant and p and l denote the radial and azimuthal indexes of the mode functions, respectively. In Figure 2.1 we show a cross-section for $z = 0$ of some Laguerre-Gauss to illustrate the spatial structure of the modes. The associated Laguerre polynomials $L_p^l(x)$ form an orthogonal set over the interval

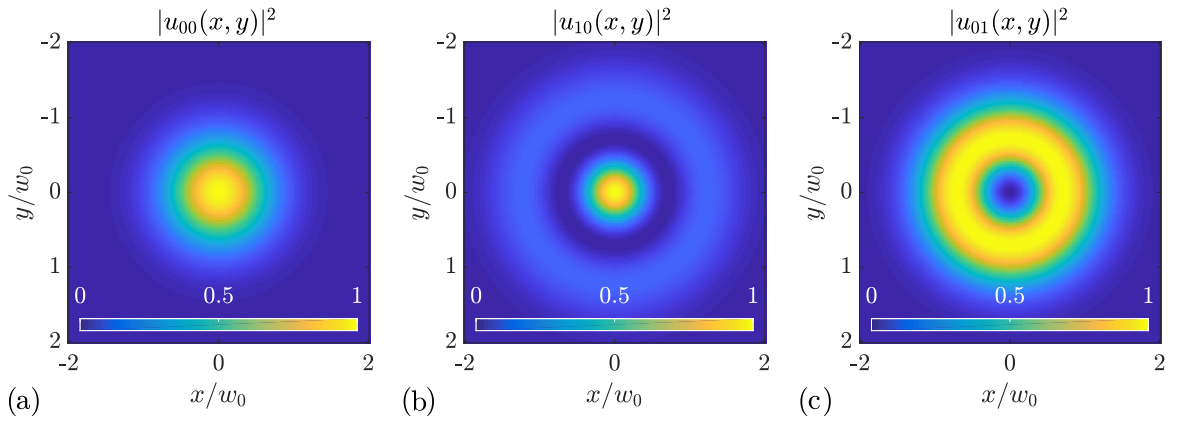

Figure 2.1: Examples of different Laguerre-Gauss modes. Plotted are normalized cross-sections $|u_{pl}(x,y)|^2$ in the plane $z = 0$ in arbitrary units.

$x \in [0, \infty)$ with respect to the weighting function $e^{-x}x^l$, i.e. it holds

$$\int_0^\infty \mathrm{d}x\, e^{-x} x^l L_p^l(x) L_q^l(x) = \frac{(p+l)!}{p!}\delta_{p,q}. \tag{2.5}$$

Moreover, the functions $\exp\{il\varphi\}$ form a complete orthogonal set on $\varphi \in [0, 2\pi)$ and therefore, when choosing the appropriate normalization constants given in Eq. (2.4), namely $C_{pl} = \frac{\pi}{2}\frac{(p+|l|)!}{p!}$ (see Appendix B for details), the mode functions u_{pl} form a complete orthonormal set in two dimensions (i.e., for fixed z), with the completeness relation

$$\int_0^\infty r\mathrm{d}r \int_0^{2\pi} \mathrm{d}\varphi\, u_{pl}(r,\varphi,z) u^*_{qm}(r,\varphi,z) = \delta_{pq}\delta_{lm}. \tag{2.6}$$

Thus we can conclude that the decomposition (2.3) is well-defined. Moreover, the orthogonality of the mode functions leads to the commutation relations of the normalized one-dimensional field operators,

$$[\hat{\mathcal{E}}_{pl}(z), \hat{\mathcal{E}}^\dagger_{qm}(z')] = \delta_{p,q}\delta_{l,m}\delta(z-z'). \tag{2.7}$$

We decompose the atomic field operators analogously,

$$\hat{\sigma}_{\mathrm{ge}}(\mathbf{r}) = \sum_{pl} u_{pl}(r,\varphi,z)\hat{\sigma}^{pl}_{\mathrm{ge}}(z), \quad \hat{\sigma}_{\mathrm{gr}}(\mathbf{r}) = \sum_{pl} u_{pl}(r,\varphi,z)\hat{\sigma}^{pl}_{\mathrm{gr}}(z), \tag{2.8}$$

into one-dimensional operators that fulfill similar commutation relations as (2.7).

Note that the original three-dimensional operators, $\hat{\sigma}_{\mathrm{ge}}(\mathbf{r})$ have a different physical dimension than the operators corresponding to single modes, $\hat{\sigma}^{\mu\nu}_{\mathrm{ge}}(z)$.

By using the decomposition of electromagnetic and atomic field operators and the completeness

relation of the mode functions we obtain from the paraxial wave equation (2.1)

$$\left(\frac{\partial}{\partial t}+c\frac{\partial}{\partial z}\right)\hat{\mathcal{E}}_{pl}(z,t)=\mathrm{i}g\sum_{\alpha,\beta}\left[\iint r\mathrm{d}r\,\mathrm{d}\varphi\,\sqrt{n(\mathbf{r})}u^{*}_{pl}(r,\varphi,z)u_{\alpha\beta}(r,\varphi,z)\right]\hat{\sigma}^{\alpha\beta}_{\mathrm{ge}}(z,t). \tag{2.9}$$

Thus, for a general atomic density distribution $n(\mathbf{r})$, the paraxial wave function couples all transversal modes. However, due to cylindrical symmetry, $n(\mathbf{r})$ becomes independent of the φ-coordinate. We may furthermore assume that $n(\mathbf{r})$ is only slowly varying in the radial coordinate, r, compared to the lower order mode functions $u_{pl}(r,\varphi)$, e.g. given by a Gaussian distribution that falls off much slower than the transverse mode functions. Then we can safely neglect the r-dependence of $n(\mathbf{r})$ in the integral in Eq. (2.9), i.e. replace it by $n=n(0)$ and the orthogonality of the modes yields a set of one-dimensional, decoupled paraxial wave equations for each of the transversal modes,

$$\left(\frac{\partial}{\partial t}+c\frac{\partial}{\partial z}\right)\hat{\mathcal{E}}_{pl}(z,t)=\mathrm{i}g\sqrt{n}\hat{\sigma}^{pl}_{\mathrm{ge}}(z,t). \tag{2.10}$$

The same arguments can be made for the Heisenberg-Langevin-equations (1.6), when assuming that the control field Rabi frequency Ω is independent of φ as well as slowly varying in r, leading also to a decomposition of the Heisenberg-Langevin equations for the different transversal modes,

$$\begin{aligned}\frac{\partial}{\partial t}\hat{\sigma}^{pl}_{\mathrm{gr}}(z,t)&=-\mathrm{i}\delta\hat{\sigma}^{pl}_{\mathrm{gr}}(z,t)+\mathrm{i}\Omega\hat{\sigma}^{pl}_{\mathrm{ge}}(z,t),\\ \frac{\partial}{\partial t}\hat{\sigma}^{pl}_{\mathrm{ge}}(z,t)&=-\Gamma\hat{\sigma}^{pl}_{\mathrm{ge}}(z,t)+\mathrm{i}g\sqrt{n}\hat{\mathcal{E}}_{pl}(z,t)+\mathrm{i}\Omega\hat{\sigma}^{pl}_{\mathrm{gr}}(z,t),\end{aligned} \tag{2.11}$$

with no coupling to other transversal modes.

In particular, this means that the propagation of the light field is reduced to a set of decoupled equations for each transversal mode that is described by one-dimensional equations of motion. We note, however, that this is only correct as long as the time evolution of the photons is described by the linear Maxwell-Bloch equations. Including nonlinearities, e.g. interactions between photons into the system changes the result in general. This will be subject of the next section.

2.1.2 Interactions

In a nonlinear medium, i.e., in the presence of interactions between polaritons, the result of the previous section holds no longer true. The interactions between Rydberg states of matter mediating interactions between photons lead in general to a scattering between different transverse Laguerre-Gaussian modes $u_{pl}(r,\varphi,z)$. Thus the propagation of dark-state polaritons in a Rydberg medium has in general to be considered as a three-dimensional problem. However, as can intuitively be guessed from the sketch in Figure 2.2, we expect the scattering between different transverse modes to be negligible, if the Rydberg blockade radius R_{B} is sufficiently large compared to the beam waist w_0 and

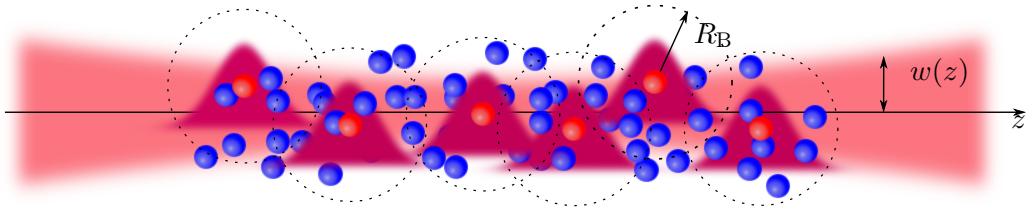

Figure 2.2: Sketch of a focused probe beam with beam waist $w(z)$ propagating through a medium of Rydberg atoms. Rydberg polariton excitations blockade further excitations in a radius of R_B. If the blockade radius is sufficiently large then only a single excitation is allowed for a certain z and the setup becomes effectively one-dimensional.

only single excitations are allowed to exist for a certain z-interval of the light beam because of the Rydberg blockade [58]. In the following we will derive conditions where this is fulfilled and also the propagation of polaritons in a Rydberg gas of atoms can be reduced to an effective one-dimensional description.

To begin with, we extend the interaction Hamiltonian (1.29) between two Rydberg atoms considered in Section 1.2 to an ensemble of many atoms, yielding the microscopic Hamiltonian

$$\hat{\mathcal{H}} = \frac{1}{2}\sum_{i,j\neq i} \hat{\sigma}^i_\mathrm{rr} V(\mathbf{r}_i - \mathbf{r}_j)\hat{\sigma}^j_\mathrm{rr}, \quad V(\mathbf{r}) = \frac{C_6}{|\mathbf{r}|^6}, \tag{2.12}$$

where the exact form of the potential V depends on the specific setup. We will assume a van der Waals potential $V(\mathbf{r}) = C_6/|\mathbf{r}|^6$ with an interaction strength C_6 in the following. $\hat{\sigma}^i_\mathrm{rr}$ denotes the projection operator onto the Rydberg state of an atom at position $\mathbf{r}_i$. If the density of Rydberg excitations is much smaller than the density of atoms, we can make the continuum limit as in Section A.1.2 and replace the sum over operators $\hat{\sigma}^i_\mathrm{rr}$ of individual atoms by an integral over coarse-grained operators $\hat{\sigma}_\mathrm{gr}(\mathbf{r})$. Furthermore, we make the assumption that $\hat{\sigma}_\mathrm{ee} \approx 0$ and apply a Holstein-Primakoff transformation [59], which allows us to replace the continuous operators $\hat{\sigma}_\mathrm{rr}(\mathbf{r}) \approx \hat{\sigma}_\mathrm{rg}(\mathbf{r})\hat{\sigma}_\mathrm{gr}(\mathbf{r})$. Finally, we transform the spin-flip operators to their slowly varying form $\hat{\sigma}_\mathrm{gr} \to n^{-1/2}\hat{\sigma}_\mathrm{gr}e^{\mathrm{i}(k_\mathrm{p}-k_\mathrm{c})z}$, see (A.32), leading to the continuous van der Waals interaction Hamiltonian,

$$\hat{\mathcal{H}}_\mathrm{int} = \frac{1}{2}\iint \mathrm{d}^3\mathbf{r}\,\mathrm{d}^3\mathbf{r}'\, V(\mathbf{r}-\mathbf{r}')\hat{\sigma}^\dagger_\mathrm{gr}(\mathbf{r})\hat{\sigma}^\dagger_\mathrm{gr}(\mathbf{r}')\hat{\sigma}_\mathrm{gr}(\mathbf{r}')\hat{\sigma}_\mathrm{gr}(\mathbf{r}). \tag{2.13}$$

Inserting the decomposition (2.8) of the operators into Laguerre-Gaussian modes into this interaction Hamiltonian, we can write the interaction as a sum over all kinds of effective interaction potentials between the different transversal modes,

$$\hat{\mathcal{H}}_\mathrm{int} = \frac{1}{2}\iint \mathrm{d}z\,\mathrm{d}z' \sum_{\mathbf{p},\mathbf{l}} \widetilde{V}_{\mathbf{pl}}(z,z')(\hat{\sigma}^{p_1 l_1}_\mathrm{gr}(z))^\dagger(\hat{\sigma}^{p_2 l_2}_\mathrm{gr}(z'))^\dagger\hat{\sigma}^{p_3 l_3}_\mathrm{gr}(z')\hat{\sigma}^{p_4 l_4}_\mathrm{gr}(z), \tag{2.14}$$

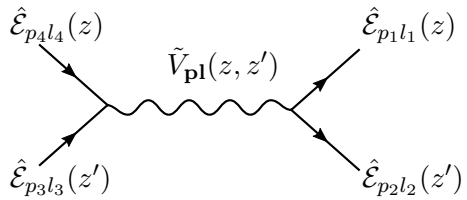

Figure 2.3: Diagrammatic representation of the scattering of two ingoing photons in modes (p_3, l_3) and (p_4, l_4) into two outgoing photons in modes (p_2, l_2) and (p_1, l_1).

where we defined the multi-indexes $\mathbf{p} = (p_1, p_2, p_3, p_4)$ and $\mathbf{l} = (l_1, l_2, l_3, l_4)$. $\widetilde{V}_{\mathbf{pl}}(z, z')$ denotes scattering matrix elements between different transversal modes as sketched in Figure 2.3, which are in general dependent on the positions z, z' of two interacting atoms. These can be obtained from the three-dimensional interaction potential by integrating over the transversal degrees of freedom, r, r' and φ, φ',

$$\widetilde{V}_{\mathbf{pl}}(z,z') := C_6 \iint_0^\infty r\mathrm{d}r\, r'\mathrm{d}r' \iint_0^{2\pi} \mathrm{d}\varphi\, \mathrm{d}\varphi' \frac{u^*_{p_1 l_1}(\mathbf{r}) u^*_{p_2 l_2}(\mathbf{r}') u_{p_3 l_3}(\mathbf{r}') u_{p_4 l_4}(\mathbf{r})}{[r^2 + r'^2 + 2rr'\cos(\varphi - \varphi') + (z - z')^2]^3}. \quad (2.15)$$

To get a reduction of the three-dimensional interacting Rydberg dark-state polariton model to one spatial dimension, the effective potentials $\widetilde{V}_{\mathbf{pl}}$ have to become diagonal. This is of course not possible to fulfill in general, but an approximate reduction of the model to one dimension is possible, as we show in the following. Let us first consider the integration over the angles φ, φ' in (2.15). Let us assume that the Rydberg blockade prevents photons to exist at zero mutual distance, i.e., $z = z'$ does not contribute to the interaction Hamiltonian. For $z \neq z'$ the integrand of Eq. (2.15) is non-vanishing. In this case the integration over φ, φ' can be performed analytically by means of residue integration, [60, 61], yielding

$$\begin{aligned} I^{\mathbf{l}}_{\varphi} :&= \iint_0^{2\pi} \mathrm{d}\varphi\, \mathrm{d}\varphi' \frac{e^{-\mathrm{i}(l_2 - l_3)\varphi'} e^{-\mathrm{i}(l_1 - l_4)\varphi}}{[r^2 + r'^2 + (z - z')^2 + 2rr'\cos(\varphi - \varphi')]^3} \\ &= 2\pi^2 \delta_{q,-q'} \left(\frac{\sqrt{\alpha^2 - \beta^2} - \alpha}{\beta} \right)^{|q|} \frac{(q^2 + 2)\alpha^2 - (q^2 - 1)\beta^2 + 3|q|\alpha\sqrt{\alpha^2 - \beta^2}}{(\alpha^2 - \beta^2)^{5/2}}, \end{aligned} \quad (2.16)$$

where we introduced $\alpha = r^2 + r'^2 + (z - z')^2$, $\beta = 2rr'$ and $q = l_1 - l_4, q' = l_2 - l_3$ denote the change of angular momentum in the scattering. A more detailed derivation of this is given in Appendix B. We observe that Eq. (2.16) is proportional to $\delta_{q,-q'} = \delta_{l_1 + l_2, l_3 + l_4}$, restricting the allowed processes to those conserving the sum of angular momentum. This conservation rule is expected, as we assumed a rotational symmetry of the model.

We are interested in the propagation of polaritons in the Gaussian, so-called TEM_{00} mode and the interaction between these as well the scattering from these modes into higher order modes. Thus

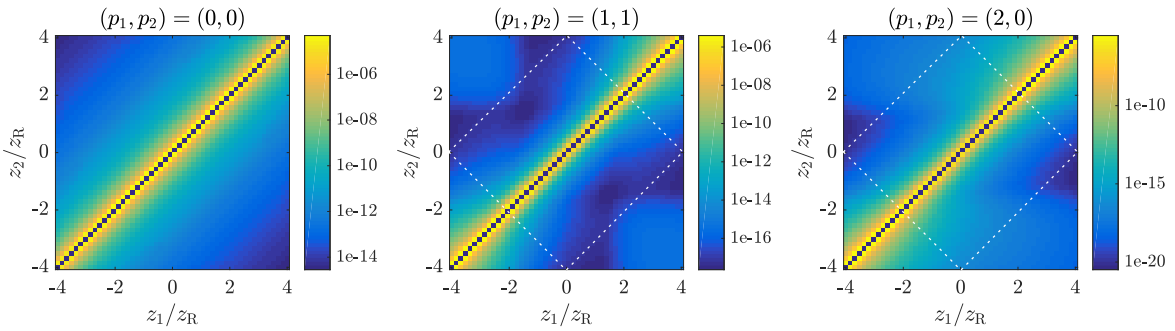

Figure 2.4: Two-dimensional plots of the absolute value of the effective potentials/scattering matrix elements $|\tilde{V}_{\mathbf{pl}}(z, z')|$ between photons initially in modes $p_3 = p_4 = 0$, $l_3 = l_4 = 0$ and final modes $l_1 = l_2 = 0$ and different angular mode numbers p_1, p_2. The dashed white rhombuses denote the region $(|z| + |z'|) \leq 2z_\mathrm{R}$, where the approximation $\tilde{V}_{\mathbf{pl}}(z, z') \approx \tilde{V}_{\mathbf{pl}}(|z - z'|)$ is justified.

we restrict ourselves to in-going modes of this type, i.e., we set $p_3 = p_4 = 0$ and $l_3 = l_4 = 0$ in the following. Further integration of (2.16) in the radial directions r_1, r_2 has to be done numerically. To this end we choose the ratio of the parameters z_R and w_0 as in typical experimental setups, see e.g. [62], namely $z_\mathrm{R} \approx 32 w_0$ and performed the numerical integration for different outgoing modes with radial and azimuthal indexes (p_1, p_2, l_1, l_4) in dependence of z and z'. The integration was done in MATLAB [63] using the CHEBFUN package [64]. In Figure 2.4 we show the resulting scattering potentials between initial Gaussian and different final modes. Before we analyze and compare these potentials in greater detail, we note that from these figures one recognizes that the assumption $|\tilde{V}_{\mathbf{pl}}(z, z')| \approx |\tilde{V}_{\mathbf{pl}}(|z - z'|)|$ is justified inside the region $(|z| + |z'|) \leq 2z_\mathrm{R}$, indicated by a dashed rhombus, although in general the scattering potentials depend on z, z'. Because of the Gouy phase of the Laguerre-Gaussian modes we can make this statement only for the absolute value of the scattering potentials. However, this is sufficient for comparison with the diagonal interaction elements, i.e. between identical ingoing and outgoing Laguerre-Gauss modes. For these, specifically, the relation $\tilde{V}_{\mathbf{pl}}(z, z') \approx \tilde{V}_{\mathbf{pl}}(|z - z'|)$ holds exactly, as can easily be observed from Eq. (2.15). In Figure 2.5 we show a log-log plot of different interaction and scattering potentials for ingoing Gaussian two-polariton modes as function of mutual distance. For different distances, three regimes are distinguishable. First, for small distances, $|z - z'| \leq w_0$, of the polaritons all potentials run in parallel, i.e., decay as a power law with a common exponent. At a distance w_0 there is a crossover to a regime where the potentials decay also as power laws, but with different exponents that depend on the azimuthal and radial mode numbers of the out-going modes. Finally, for distances $|z - z'| \gtrsim 2z_\mathrm{R}$ the potentials all behave differently, e.g. show zero crossings or approach again the diagonal interaction potential. In the regime of intermediate distances, where $z - z'$ is larger a few w_0 but smaller $2z_R$ we can derive an approximate solution, by making a series expansion of the full integral (2.16) for

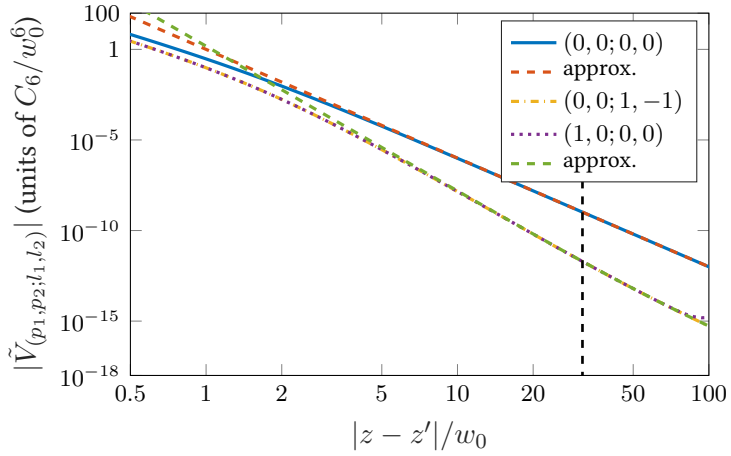

Figure 2.5: Interaction potentials $\tilde{V}_{p_1,p_2;l_1,l_2}$ for ingoing Gauss modes into different out-going Laguerre-Gauss modes. Shown is a log-log plot of the absolute values of the potentials for $z' = -z$ and $z_\mathrm{R} = 32w_0$, indicated by the vertical dashed black line. Plotted are numerically integrated exact potentials as well as approximate solutions according to Eq. (2.17). Note, that the approximate solution for the two higher order potentials is identical, as here $|z| = |z'|$.

$r, r' \ll |z - z'|$ yielding in leading order

$$\tilde{V}_{\mathbf{pl}}(z, z') \approx \delta_{l_1,-l_2}(-1)^l C_6 \frac{(l+p_1+p_2+2)!}{l!\,2^{l+p_1+p_2+1}} \sqrt{\frac{(l+p_1)!(l+p_2)!}{p_1!p_2!}} \frac{w(z)^{2p_1+l} w(z')^{2p_2+l}}{(z-z')^{6+2(l+p_1+p_2)}}, \tag{2.17}$$

where we defined $l = |l_1|$. In Figure 2.5 we have plotted these approximate potentials for the shown numerically integrated potentials, displaying a very good agreement for intermediate distances. Specifically, we can use Eq. (2.17) to read off the exponents of the power laws in the intermediate regime, which is given by $6 + 2(l + p_1 + p_2)$. That means, that higher order scattering potentials fall off much quicker than the interaction between Gaussian modes. In Figure 2.6 we show the ratio of higher order potentials $\tilde{V}_{p_1,p_2;l_1,l_2}$ compared to $\tilde{V}_{0,0;0,0}$. As can be seen, for inter-particle distances $|z - z'|$ larger $\approx 5w_0$ the potential $\tilde{V}_{1,0;0,0}$ is more than an order of magnitude smaller than $\tilde{V}_{0,0;0,0}$. All potentials describing scattering to higher order modes have an even smaller value, as can be seen from the inset in Figure 2.6, where the absolute value of different potentials is shown for fixed $z = w_0 = -z'$.

From these results we conclude that in the intermediate regime the dominant effective potential for in-going TEM_{00} modes is the interaction between the two modes, which allows to restrict the interaction Hamiltonian (2.14) to a single channel. Omitting the indexes p, l that are zero, we arrive at

$$\hat{\mathcal{H}}_\mathrm{int} = \frac{1}{2} \iint \mathrm{d}z\, \mathrm{d}z'\, V(z - z') \hat{\sigma}^\dagger_\mathrm{gr}(z) \hat{\sigma}^\dagger_\mathrm{gr}(z') \hat{\sigma}_\mathrm{gr}(z') \hat{\sigma}_\mathrm{gr}(z), \tag{2.18}$$

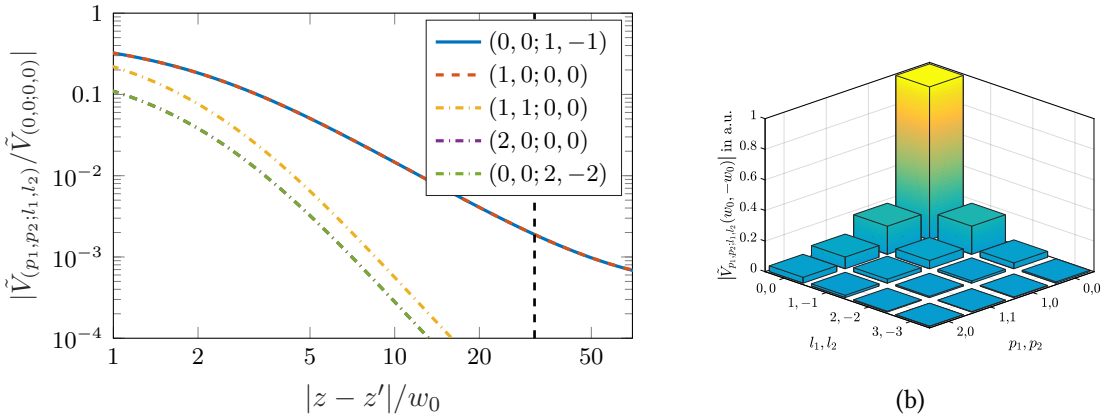

Figure 2.6: (a) Comparison of interaction potentials $\tilde{V}_{p_1,p_2;l_1,l_2}$ for in-going Gauss modes into different out-going Laguerre-Gauss modes and the repulsive interaction potential $\tilde{V}_{0,0;0,0}$. Shown is a log-log plot of the absolute values of the ratio of the potentials for $z_\mathrm{R} = 32w_0$, indicated by the dashed black line. (b) Comparison of interaction potentials $\tilde{V}_{p_1,p_2;l_1,l_2}$ for fixed $|z-z'| = 2w_0$ and different combinations $(p_1,p_2;l_1,l_2)$ of the out-going modes.

where $V(z-z') = C_6/(z-z')^6$ and $\hat{\sigma}_\mathrm{gr}(z) = \hat{\sigma}^{00}_\mathrm{gr}(z)$. Note, that these $1D$-operators have a different physical dimension as the original $3D$-operators $\hat{\sigma}_\mathrm{gr}(\mathbf{r})$. As a repulsive van der Waals interaction leads to an avoided volume, where only single excitations can exist, polaritons keep a minimal distance. Hence, if the interaction is sufficiently strong, the physics is restricted to the regime of intermediate distances, $|z-z'| \gg w_0$, where the coupling to higher Laguerre-Gauss modes is suppressed. Together with Eqs. (2.11) this yields an effective model in the sub-manifold of only TEM_{00}-mode, i.e., a one-dimensional model.

2.1.3 Rydberg polaritons

In Section 2.1.1 we showed that the propagation of photons through an EIT medium can, under certain conditions, be restricted to the physics of a single transversal mode with negligible coupling to other modes, i.e., by a one-dimensional model, governed by Eq. (2.9) and Eq. (2.11) in terms of fields $\hat{\mathcal{E}}, \hat{\sigma}_\mathrm{ge}, \hat{\sigma}_\mathrm{gr}$.

As derived in the introduction the fundamental quasi-particles of the non-interacting system are a superposition of light and matter excitation, the Rydberg polariton $\hat{\Psi}$ and the bright-state polariton $\hat{\Phi}$, defined by the rotation

$$\begin{pmatrix}\hat{\Psi}\\ \hat{\Phi}\end{pmatrix} = \begin{pmatrix}\cos\theta & -\sin\theta\\ \sin\theta & \cos\theta\end{pmatrix}\begin{pmatrix}\hat{\mathcal{E}}\\ \hat{\sigma}_\mathrm{gr}\end{pmatrix}. \tag{2.19}$$

The coherence $\hat{\sigma}_\mathrm{ge}$ can safely be eliminated under conditions of electromagnetically induced trans-

parency, see Section A.2.4 in the Appendix.

In the previous section we showed that additional interactions in general require a three-dimensional description, but for sufficiently small excitation densities and sufficiently strong repulsive interactions, the one-dimensional model is still a valid description. In that case, the interaction is governed by the Hamiltonian (2.18). This Hamiltonian changes the properties of the atomic medium in the polariton setup considered in the previous section. In particular, in a ladder-type EIT setup with the upper state $|\mathrm{r}\rangle$ being a Rydberg state the interactions between atoms mediate an interaction between photons, which is the basis for many interesting experiments and phenomena, e.g. the Rydberg blockade [8, 42] or bunching of photons [65, 66]. Consequently these Rydberg polaritons are promising candidates for applications in quantum information processing [6, 7, 44, 45] and beyond [67].

Let us now add these results up in a simple way. Elimination of the bright-state polariton from the paraxial Heisenberg Langevin equations (2.11) in one spatial dimension leads to the Schrödinger equation (1.16) describing the time-evolution of the Rydberg polariton. When assuming two-photon resonance, i.e., $\delta = 0$, it is straightforward to construct the Hamiltonian which is the generator of this equation in real space, see supplemental material to [Otterb2013] at [68]. Combining this Hamiltonian with (2.18) transformed to the polariton basis (2.19) we find in lowest non-vanishing order in $\cos\theta$

$$\hat{\mathcal{H}} = \int \mathrm{d}z\, \hat{\Psi}^\dagger(z) \left[\frac{\hat{p}_z^2}{2m} - v_\mathrm{g}\hat{p}_z\right] \hat{\Psi}(z) + \frac{C_6}{2} \iint \mathrm{d}z\, \mathrm{d}z'\, \frac{\hat{\Psi}^\dagger(z)\hat{\Psi}^\dagger(z')\hat{\Psi}^\dagger(z')\hat{\Psi}(z)}{|z-z'|^6}, \tag{2.20}$$

where we set $\sin\theta = 1$, $\hat{p}_z = -\mathrm{i}\partial_z$ and $m^{-1} = 2v_\mathrm{g}L_\mathrm{abs}\Delta/\gamma$. The interaction leads to an avoided volume, called the Rydberg blockade defined by the interaction strength being equal to the EIT linewidth, i.e., $V(R_\mathrm{B}) = C_6/|R_\mathrm{B}|^6 = \frac{\Omega^2}{|\Gamma|}$ [42, 58, 69], such that

$$R_\mathrm{B} = \left(\frac{|\Gamma|C_6}{\Omega^2}\right)^{1/6}. \tag{2.21}$$

The effective Hamiltonian (2.20) describes propagating massive Rydberg polaritons subject to van der Waals type interaction. In the following section we want to make a strict derivation of this model.

2.2 Master equation for Rydberg polaritons

In the previous section we considered the propagation of photons coherently coupled to an atomic three-level medium with Rydberg interactions and derived conditions for describing the system by a one-dimensional model. It is well known that the photon propagation under conditions of EIT can be described by a field theory of light-matter quasi-particles, dark-state polaritons [3]. Particularly, this holds true, even when incorporating interactions between three-level atoms as shown in the previous section.

In this section we attempt to derive a field theory for the Rydberg polaritons in one dimension by an elimination of the bright polaritons. To this end we identify multiple loss mechanisms for the bright polaritons depending on the detuning between electrical fields and atomic transitions. Treating the bright polaritons as a reservoir for the Rydberg polaritons in an open-system approach and performing perturbation theory in the coupling of the two fields, allows us to derive a Markovian master equation describing the time evolution of the Rydberg polaritons as an effective theory of a single-component field.

2.2.1 Maxwell-Bloch equations

The dynamics of photons propagating in a medium of Rydberg atoms is governed by a set of equations of motion, consisting of the Heisenberg-Langevin equations (2.11) for the atomic operators and the paraxial wave-equation (2.10) for the electric field operator. After adiabatic elimination of the coherence $\hat{\sigma}_{\mathrm{ge}}$ this set of equations is given in the polariton basis (2.19) by

$$\begin{aligned}\frac{d}{dt}\hat{\Psi} &= -c\cos^2\theta\frac{\partial}{\partial z}\hat{\Psi} - c\sin\theta\cos\theta\frac{\partial}{\partial z}\hat{\Phi}\\ \frac{d}{dt}\hat{\Phi} &= -\Gamma_{\mathrm{eff}}\hat{\Phi} - c\sin^2\theta\frac{\partial}{\partial z}\hat{\Phi} - c\sin\theta\cos\theta\frac{\partial}{\partial z}\hat{\Psi}\end{aligned} \tag{2.22}$$

where $\Gamma_{\mathrm{eff}} = \Omega_{\mathrm{eff}}^2/\Gamma = (\Omega^2 + g^2 n)/(\gamma + \mathrm{i}\Delta)$ and we assumed time-independent driving, i.e., $\partial_t\theta = 0$. We note that in the derivation of Eq. (2.11) and subsequently Eq. (2.22) we have dropped Langevin noise operators. See Appendix A.2.4, for details on the derivation. It is easy to construct an effective Hamiltonian $\hat{\mathcal{H}}_0$ which generates the equations of motion (2.22). Taking the interactions (2.18) into account the full interacting problem is described by

$$\hat{\mathcal{H}} = \hat{\mathcal{H}}_0 + \hat{\mathcal{H}}_{\mathrm{int}} = \hat{\mathcal{H}}_\Psi + \hat{\mathcal{H}}_\Phi + \hat{\mathcal{H}}_{\Psi\Phi}, \tag{2.23}$$

which consists of three parts describing the time evolution of the dark and bright polaritons, respectively, as well as the coupling between the two fields. The full coupling Hamiltonian between dark and bright state polaritons is given by

$$\begin{aligned}\hat{\mathcal{H}}_{\Psi\Phi} = &-\int \mathrm{d}z\,\left\{\mathrm{i}c\cos\theta\sin\theta\hat{\Psi}^\dagger(z)\partial_z\hat{\Phi}(z) + \mathrm{H.c.}\right\} - \sin\theta\cos\theta\\ &\times\iint \mathrm{d}z\,\mathrm{d}z'\,V(z-z')\hat{\Psi}^\dagger(z)\hat{\Phi}^\dagger(z')\left[\sin\theta\hat{\Psi}(z') - \cos\theta\hat{\Phi}(z')\right]\left[\sin\theta\hat{\Psi}(z) - \cos\theta\hat{\Phi}(z)\right] + \mathrm{H.c.},\end{aligned} \tag{2.24}$$

consisting of terms arising from the Maxwell-Bloch equations as well as from the interaction. Note that in the case of time-dependent driving fields an additional coupling arises $\propto \partial_t\theta(t)$.

Neglecting the coupling Hamiltonian and the interaction between Rydberg polaritons, the time evolution of the Rydberg polariton field $\hat{\Psi}$ is simply described by

$$\frac{d}{dt}\hat{\Psi}(z,t) = -c\cos^2\theta\partial_z\hat{\Psi}(z,t), \tag{2.25}$$

As already discussed in the introduction, see Eq. (1.15), this differential equation has the solution

$$\hat{\Psi}(z,t) = \hat{\Psi}(z - c\cos^2\theta\tau, t-\tau), \tag{2.26}$$

i.e., the free Rydberg polariton propagates lossless with a velocity $v_\mathrm{g} = c\cos^2\theta$ that is much smaller than the vacuum speed of light c, while keeping its spatial shape. Analogously, the free time evolution of bright-state polaritons $\hat{\Phi}$ is governed by

$$\frac{d}{dt}\hat{\Phi}(z,t) = -c\sin^2\theta\partial_z\hat{\Phi}(z,t) - \Gamma_\mathrm{eff}\hat{\Phi}(z,t) \tag{2.27}$$

$$\hat{\Phi}(z,t) = e^{-\Gamma_\mathrm{eff}\tau}\hat{\Phi}(z - c\sin^2\theta\tau, t-\tau). \tag{2.28}$$

Assuming slow light conditions, we observe that the bright polaritons propagate with the velocity $c\sin^2\theta$, which is much larger than v_g and are moreover subject to decay with the rate $\Re\{\Gamma_\mathrm{eff}\} = \gamma\Omega_\mathrm{eff}^2/|\Gamma|^2$, i.e., bright polariton excitations either decay or propagate out of the atomic medium, if we assume that the system has open boundaries. Hence, if there is no external driving of bright polariton excitations, their steady state is given by

$$\rho_\Phi = |\mathrm{vac}\rangle_\Phi\langle\mathrm{vac}|_\Phi\,, \tag{2.29}$$

i.e., the vacuum density matrix. Therefore, the coupling of Rydberg (dark) polaritons and bright polaritons via the Hamiltonian (2.24) constitutes an effective loss channel for the Rydberg polaritons. Making the assumption that $1/|\Gamma_\mathrm{eff}|$ defines the fastest time scale of the system, we can eliminate the bright polariton excitations from the dynamics, giving rise to a description of the Rydberg polariton $\hat{\Psi}$ as an effective field theory of an open system.

2.2.2 Master equation

Let us now consider the coupling (2.24) between bright- and dark-state polaritons and also take the interactions into account to derive an field theory for the Rydberg polariton $\hat{\Psi}$. Instead of calculating the corrections by performing perturbation theory in the momentum space, see Eq. (1.14), and adding the interaction term in lowest non-vanishing order $\cos\theta$, as lead to Eq. (2.20), we here use a systematic approach. Specifically, we employ the system-plus-reservoir approach, introduced in Section 1.3, to derive this field theory and the losses and corrections arising from the coupling to bright polaritons.

This approach is a standard procedure to describe open quantum systems, see e.g. [9, 11, 70–72]. We treat the bright polaritons $\hat{\Phi}$ as a reservoir for the dark polaritons, which will subsequently be traced out leading to a theory solely for $\hat{\Psi}$. We note that this approach allows us to treat both kinds of corrections to the free polariton evolution, arising from non-adiabatic as well as interaction-induced couplings between bright polaritons and Rydberg polaritons in an equal fashion.

We calculate the correlation functions of reservoir operators $\hat{\Phi}$ with respect to their steady state ρ_Φ from the solution (2.28). The correlation function of lowest non-vanishing order in bright polariton operators is the anti-normal ordered first-order correlation function, given by

$$\langle \hat{\Phi}(x,t)\hat{\Phi}^\dagger(y,t-\tau)\rangle \approx e^{-\Gamma_{\text{eff}}\tau}\delta(x-y), \qquad \tau>0, \tag{2.30}$$

where the expectation value $\langle\cdot\rangle = \mathrm{tr}\{\rho_\Phi\cdot\}_\Phi$ is defined as partial trace with respect to bright polariton degrees of freedom. The first-order correlation function (2.30) is δ-correlated in space and exponentially decaying in time. Apart from this correlation function, only the anti-normal ordered four-operator correlation function

$$\begin{aligned}
&\langle \hat{\Phi}(x,t)\hat{\Phi}(x',t)\hat{\Phi}^\dagger(y,t-\tau)\hat{\Phi}^\dagger(y',t-\tau)\rangle \\
&\quad\approx e^{-2\Gamma_{\text{eff}}\tau}\Big[\delta(x-y-c\sin^2\theta\tau)\delta(x'-y'-c\sin^2\theta\tau) \\
&\quad+\delta(x'-y-c\sin^2\theta\tau)\delta(x-y'-c\sin^2\theta\tau)\Big], \quad \tau>0
\end{aligned} \tag{2.31}$$

is non-vanishing while all other correlation functions of reservoir operators $\hat{\Phi}$ are zero for the vacuum steady state ρ_Φ.

As in Section 1.3 we can now derive an effective equation of motion for the Rydberg polaritons by tracing out the bright-state degrees of freedom. To this end, we start from the von Neumann equation of the full density matrix, $\partial_t\chi = -\mathrm{i}[\hat{\mathcal{H}},\chi]$ and transform to an interaction picture with respect to $\hat{\mathcal{H}}_\Psi + \hat{\mathcal{H}}_\Phi$. The Rydberg polariton degrees of freedom are described by a reduced density matrix that can be obtained from the full density matrix by tracing out the bright-state degrees of freedom, $\rho = \mathrm{tr}_\Phi(\chi)$. The effective equation of motion for this operator is in Born approximation given by the integro-differential equation

$$\frac{d}{dt}\rho(t) = -\int_0^\infty \mathrm{d}\tau\ \mathrm{tr}_\Phi\left\{[\hat{\mathcal{H}}_{\Psi\Phi}(t),[\hat{\mathcal{H}}_{\Psi\Phi}(\tau),\rho(\tau)\otimes\rho_\Phi]]\right\}. \tag{2.32}$$

Starting from this equation we use the correlation functions (2.30) and (2.31) of reservoir operators to derive an effective differential equation for the reduced system density matrix. This we will do in the following. In particular, since the reservoir correlation functions are exponentially fast decaying, the major contribution to the integrand comes from $t\approx 0$ and thus we can perform the Markov approximation and replace $\rho(\tau)\to\rho(t)$. For convenience let us introduce the nonlinear system

operator (i.e., Rydberg polariton operator)

$$\hat{L}(z) := -\sin^3\theta\cos\theta\left[\int \mathrm{d}s\, V(z-s)\hat{\Psi}^\dagger(s)\hat{\Psi}(s) + \mathrm{i}\frac{c\partial_z}{\sin^2\theta}\right]\hat{\Psi}(z), \tag{2.33}$$

which allows us to write the Hamiltonian $\hat{\mathcal{H}}_{\Psi\Phi}$ for the coupling between system and reservoir operators, i.e., between Rydberg and bright polaritons, in the interaction picture in the form

$$\begin{aligned}\hat{\mathcal{H}}_{\Psi\Phi}(t) = &\int \mathrm{d}z\left(\hat{\Phi}^\dagger(z)\hat{L}(z) + \hat{L}^\dagger(z)\hat{\Phi}(z)\right)\\ &+ \iint \mathrm{d}z\,\mathrm{d}z'\, V(z-z')\sin^2\theta\cos^2\theta\left(\hat{\Phi}^\dagger(z,t)\hat{\Phi}^\dagger(z',t)\hat{\Psi}(z',t)\hat{\Psi}(z,t) + \text{H.a.}\right) + \dots\end{aligned} \tag{2.34}$$

We omitted terms that are cubic in bright polaritons as they do not modify the effective dynamics of dark-state polaritons since the corresponding correlations functions are not of the form (2.30) or (2.31) and thus vanishing. By inserting this coupling Hamiltonian into the master equation, Eq. (2.32), performing the Markov approximation, i.e., replacing $\rho(\tau) \to \rho(t)$ and transforming back to a frame co-moving with the group velocity we finally arrive at the master equation in Lindblad form,

$$\begin{aligned}\frac{d}{dt}\rho = &\,\mathrm{i}\frac{\Delta}{\Omega_{\text{eff}}^2}\int \mathrm{d}z\,\left[\rho, \hat{L}^\dagger(z)\hat{L}(z)\right] + \mathrm{i}\frac{\sin^4\theta}{2}\iint \mathrm{d}z\,\mathrm{d}z'\, V(z-z')\left[\rho, \hat{\Psi}^\dagger(z)\hat{\Psi}^\dagger(z')\hat{\Psi}(z')\hat{\Psi}(z)\right]\\ &+ \mathrm{i}\frac{\Delta}{\Omega_{\text{eff}}^2}\sin^6\theta\cos^2\theta\iiint \mathrm{d}z\,\mathrm{d}s\,\mathrm{d}s'\, V(z-s')V(z-s)\left[\rho, \hat{\Psi}^\dagger(z)\hat{\Psi}^\dagger(s)\hat{\Psi}^\dagger(s)\hat{\Psi}(s')\hat{\Psi}(s')\hat{\Psi}(z)\right]\\ &+ \frac{\gamma}{\Omega_{\text{eff}}^2}\int \mathrm{d}z\,[2\hat{L}(z)\rho\hat{L}^\dagger(z) - \{\rho, \hat{L}^\dagger(z)\hat{L}(z)\}] + \frac{\gamma\sin^4\theta\cos^4\theta}{\Omega_{\text{eff}}^2}\\ &\times\iint \mathrm{d}z\,\mathrm{d}z'\, V^2(z-z')\left[2\hat{\Psi}(z')\hat{\Psi}(z)\rho\hat{\Psi}^\dagger(z)\hat{\Psi}^\dagger(z') - \{\rho, \hat{\Psi}^\dagger(z)\hat{\Psi}^\dagger(z')\hat{\Psi}(z')\hat{\Psi}(z)\}\right],\end{aligned} \tag{2.35}$$

where $\{\cdot,\cdot\}$ denotes the anti-commutator. The master equation (2.35) governs the effective time evolution of dark-state polaritons with non-adiabatic and interaction induced corrections arising from coupling to the bright-state polariton vacuum. It consists of unitary terms proportional to the single-photon detuning Δ, an interaction term, and dissipative terms proportional to the decay rate γ. In the following we will discuss the unitary and dissipative terms in detail to get some insight into the different processes contributing to the dynamics and analyze their interplay.

2.3 Discussion of the master equation

The master equation, Eq. (2.35) derived in the previous section denotes an effective field theory for the Rydberg polariton field $\hat{\Psi}$ taking into account interactions between Rydberg polaritons as well as corrections arising from coupling the Rydberg polaritons to a vacuum of bright polaritons. These

corrections can be divided into two types, unitary terms given by an effective Hamiltonian and dissipative terms given by a Lindbladian, which we want to analyze in the following. The terms in the master equation arising from coupling to bright polaritons are generated by the operator $\hat{L}$ we introduced in Eq. (2.33). To keep track of the individual contributions to the dynamics we split $\hat{L} = \hat{L}_1 + \hat{L}_2$ with

$$\begin{aligned} \hat{L}_1(z) &= -\sin^3\theta\cos\theta \int \mathrm{d}s\, V(z-s)\hat{\Psi}^\dagger(s)\hat{\Psi}(s)\hat{\Psi}(z), \\ \hat{L}_2(z) &= -\mathrm{i}\sin\theta\cos\theta c\frac{\partial}{\partial z}\hat{\Psi}(z). \end{aligned} \tag{2.36}$$

$\hat{L}_1$ corresponds to corrections to the time evolution due to a coupling of Rydberg and bright polaritons due to interaction, while $\hat{L}_2$ is due to non-adiabatic coupling.

Wave-function approach. The operator $\hat{L}_1(z)$ and thus the nonlinear terms in the master equation cannot be treated in mean-field approximation by replacing $\hat{\Psi}^\dagger(s)\hat{\Psi}(s)$ with its expectation value $\langle\hat{\Psi}^\dagger(s)\hat{\Psi}(s)\rangle$, since the integral over this single-particle density matrix multiplied with the potential diverges for $z = s$. To analyze the nonlinear terms and get insight into the few-body physics of Rydberg polaritons, we consider the time evolution of the simplest possible state showing nonlinear effects, a wave function consisting of two Rydberg polariton excitations. This two-excitation wave function is defined by

$$|\Psi_2(t)\rangle = \iint \mathrm{d}z\,\mathrm{d}z'\,\psi_2(z,z',t)\hat{\Psi}^\dagger(z)\hat{\Psi}^\dagger(z')\,|0\rangle\,, \tag{2.37}$$

with the normalized two-excitation amplitude $\psi_2(z,z',t) = \langle 0|\hat{\Psi}(z)\hat{\Psi}(z')|\Psi_2(t)\rangle$.

2.3.1 Unitary dynamics

The unitary dynamics of the master equation (2.35) is generated by an effective Hamiltonian

$$\hat{\mathcal{H}}_{\text{eff}} = \frac{\Delta}{\Omega_{\text{eff}}^2}\int \mathrm{d}z\,\hat{L}^\dagger(z)\hat{L}(z) + \frac{\sin^4\theta}{2}\iint \mathrm{d}z\,\mathrm{d}z'\,V(z-z')\hat{\Psi}^\dagger(z)\hat{\Psi}^\dagger(z')\hat{\Psi}(z')\hat{\Psi}(z) + \hat{\mathcal{H}}_{\text{3-body}}, \tag{2.38}$$

that consists of a term generated by $\hat{L}^\dagger(z)\hat{L}(z)$ and an interaction term, where $\hat{\mathcal{H}}_{\text{3-body}}$ denotes the three-body interaction. Expanding the product $\hat{L}^\dagger(z)\hat{L}(z)$ yields three different terms, namely a kinetic energy of the massive Rydberg polaritons, a drift term and corrections to the two-body interaction. In the following we will consider these terms separately and discuss them in greater detail.

Kinetic energy

The first term we consider is the kinetic energy contribution, given by the Hamiltonian

$$\hat{\mathcal{H}}_{\text{kin}} = \frac{\Delta}{\Omega_{\text{eff}}^2} c^2 \sin^2\theta \cos^2\theta \int \mathrm{d}z\, [\partial_z \hat{\Psi}^\dagger(z)][\partial_z \hat{\Psi}(z)]. \tag{2.39}$$

The existence of this term means that Rydberg polaritons are massive quasi-particles with an effective mass that can be read off as

$$m^{-1} = 2\frac{c^2 \Delta \sin^2\theta \cos^2\theta}{\Omega_{\text{eff}}^2} = 2 v_{\text{g}} L_{\text{abs}} \frac{\Delta}{\gamma} \sin^4\theta. \tag{2.40}$$

This mass is equal to the real part of the mass derived in [49]. This comes about, since the losses are treated separately in the master equation (2.35). In the limit of large single-photon detuning $|\Delta| \gg \gamma$ the expressions coincide. For a typical slow light setup the factor $\sin^4\theta \approx 1$ and we find that the polariton mass becomes comparable to the electron rest mass[1]. By adjusting the group velocity v_{g} or the ratio of detuning and decay rate, the magnitude of the mass can be tuned. Moreover, the sign of the effective mass can be changed by changing the sign of the single-photon detuning Δ and thus, depending on the sign of the interaction the Rydberg polaritons can be made attractively or repulsively interacting.

Drift term

The second contribution to the effective Hamiltonian is given by the product of $\hat{L}_1^\dagger$ and $\hat{L}_2$ and vice versa, i.e., by the terms linear in the interaction potential and in the derivative. This Hamiltonian is given by

$$\hat{\mathcal{H}}_{\text{drift}} = -\frac{v_{\text{g}}\Delta}{\Omega_{\text{eff}}^2} \sin^4\theta \iint \mathrm{d}z\, \mathrm{d}s\, V(z-s) \left\{ \hat{\Psi}^\dagger(z)\hat{\Psi}^\dagger(s)\hat{\Psi}(s)[\partial_z \hat{\Psi}(z)] - \text{H.c.} \right\}. \tag{2.41}$$

This Hamiltonian describes a drift term, i.e., the propagation of polaritons. As our frame of reference is co-moving with the particles with group velocity v_{g} this can be translated to a correction of the group velocity. This correction depends on the interaction, i.e., affects two polariton excitations depending on their relative distance r. For a two-excitation wave function ψ_2 this effect can be calculated leading to the equation of motion

$$\partial_t \psi_2(R, r, t) = \frac{2\Delta v_{\text{g}}}{\Omega_{\text{eff}}^2} \sin^4\theta\, V(r) \partial_R \psi_2(R, r, t), \tag{2.42}$$

[1] Using for instance realistic values of $\Delta/\gamma = 5$ and $v_{\text{g}} = 500\,\text{m/s}$ and reintroducing $\hbar$, we find a value of $m = 1 \times 10^4\,\text{s/m}^2 \times \hbar$, which is comparable to the electron rest mass [22].

where we introduced the coordinates $R = (x + y)/2$ and $r = x - y$ for center-of-mass and relative distance, respectively. Eq. (2.42) shows that for finite Δ, i.e., under off-resonant driving conditions the center-of-mass propagation velocity of two polaritons gets strongly modified at small distances in the presence of interactions. This can be understood by a simple argument as follows. The interaction shifts the energy of the upper level $|\mathrm{r}\rangle$ of the three-level atoms, i.e., induces a large two-photon detuning. If additionally a large single-photon detuning is present this leads to a complete decoupling of an incident probe field $\hat{\mathcal{E}}$ from the atoms, i.e., the medium becomes transparent and thus the probe field propagates with a large velocity up to the vacuum speed of light.

Interaction

The final contribution to the effective Hamiltonian is the interaction between Rydberg polaritons given by a combination of two- and three-body interaction,

$$\hat{\mathcal{H}}_{\text{int}} = \frac{1}{2} \iint \mathrm{d}z\, \mathrm{d}z'\, V_{\text{eff}}(z - z') \hat{\Psi}^\dagger(z) \hat{\Psi}^\dagger(z') \hat{\Psi}(z') \hat{\Psi}(z), \tag{2.43}$$

where the effective two-body interaction potential V_{eff} is given by the bare van der Waals interaction potential and corrections that are of second order in $\cos\theta$,

$$V_{\text{eff}}(r) \approx \sin^4\theta \left[V(r) + \frac{\Delta}{\Omega_{\text{e}}^2} \cos^2\theta V^2(r) \right]. \tag{2.44}$$

For large distances $r = |z - z'|$ between polaritons the bare van der Waals potential dominates, while for small distances r the correction term dominates, as it diverges like r^{-12}. We observe that the sign of the correction term can be tuned independently from the bare interaction by changing the sign of the single photon detuning Δ. This behavior is illustrated in Figure 2.7, where we show linear and double logarithmic plots of the potential (2.44) for negative as well as positive single photon detuning Δ. We can identify a length scale

$$r_0 = (|C_6 \Delta| \cos^2(\theta)/\Omega_e^2)^{1/6} = \cos^{2/3}(\theta) R_{\text{B}}, \tag{2.45}$$

where the second order correction becomes irrelevant for $r \gg r_0$ and dominating for $r \ll r_0$, respectively. Here R_{B} denotes the (off-)resonant blockade radius, defined in Eq. (2.21). In the case of an repulsive interaction potential $V(r)$ the interaction leads to a blockade, i.e., a vanishing two-photon amplitude for distances smaller R_{B}. Hence, the correction term is negligible in the limit of slow light, where $r_0 \ll R_{\text{B}}$. However, in the case of an attractive potential $V(r)$ Rydberg polaritons the correction term becomes important. Since the sign of the second order correction is only determined by the sign of the single-photon detuning Δ, as is the sign of the effective mass (2.40), the interaction between Rydberg polaritons is always a repulsive interaction at small distances, leading to a blockade

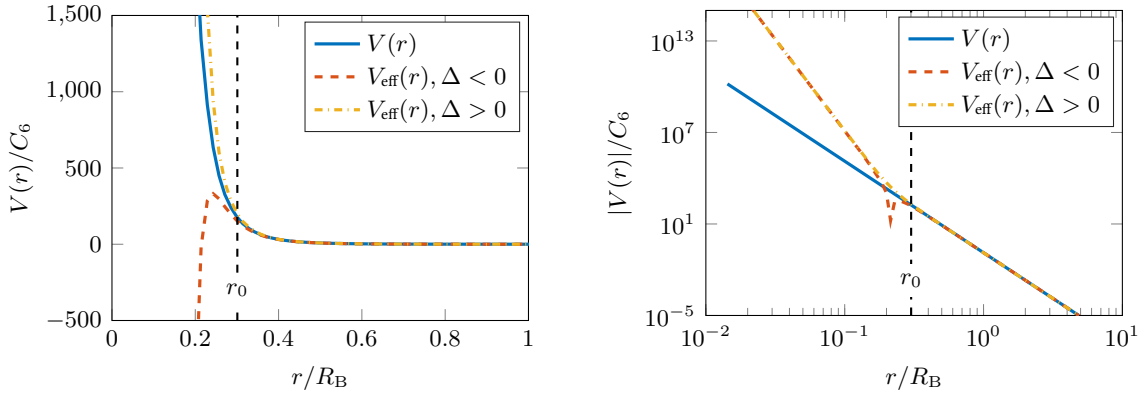

(a) Linear plot.

(b) Double logarithmic plot.

Figure 2.7: Illustration of the effective two-body interaction potential $V_\mathrm{eff}(r)$ defined in Eq. (2.44). (a) Potential with linear axis scaling and (b) the absolute value of the potential in double-logarithmic axis scaling. The red dotted and yellow dash-dotted lines show the effective potential for negative and positive detuning, respectively and positive van der Waals interaction strength C_6.

of polaritons.

2.3.2 Dissipative dynamics

The dissipative dynamics is described by the remaining terms in Eq. (2.35). These terms are given in Lindblad form [9], see also Section 1.3. In particular the dissipative terms are proportional to the decay rate γ of the intermediate atomic state which is the only decay process in the system. As the free Rydberg polaritons propagate lossless, cf. (1.14), all dissipative channels in the master equation originate from coupling to bright polaritons, which are subject to decay. This coupling is either induced by interaction or non-adiabatic coupling and get generated by the operators $\hat{L}$ and the higher order interaction processes. Therefore, the dissipative terms in the master equation have a structure similar to the unitary, which we discussed in the previous section, but generate dissipative time evolution. We proceed as with the unitary terms and consider the different processes separately.

Imaginary mass term

The term generated by the operator $\hat{L}_2$ is in Lindblad-form given by

$$\mathcal{L}\rho = \frac{\gamma}{\Omega_\mathrm{eff}^2} c^2 \sin^2\theta \cos^2\theta \int \mathrm{d}z \, \left[2\partial_z \hat{\Psi}(z) \rho \partial_z \hat{\Psi}^\dagger(z) - \left\{ \rho, \partial_z \hat{\Psi}^\dagger(z) \partial_z \hat{\Psi}(z) \right\} \right] . \tag{2.46}$$

This term can be considered as an imaginary mass term. This can be seen evaluating the adjoint equation for some operator. For instance, when only considering the dynamics generated by Eq. (2.46),

we find for the expectation value $\langle\hat{\Psi}^\dagger(x)\hat{\Psi}(x)\rangle$ the equation of motion

$$\frac{d}{dt}\langle\hat{\Psi}^\dagger(z)\hat{\Psi}(z')\rangle = v_\mathrm{g}L_\mathrm{abs}\sin^4\theta\left(\partial_z^2+\partial_{z'z'}\right)\langle\hat{\Psi}^\dagger(z)\hat{\Psi}(z')\rangle\,, \tag{2.47}$$

where $\partial_{xx}=\frac{\partial^2}{\partial x^2}$. This result can also be achieved by transforming the effective polariton mass (2.40) to a complex quantity as

$$m^{-1}\to\left(1+\mathrm{i}\frac{\gamma}{\Delta}\right)m^{-1}. \tag{2.48}$$

Note that including the imaginary part in the Hamiltonian makes it a non-hermitian Hamiltonian that has to be applied using a generalized von Neumann equation. This complex mass coincides with the complex mass derived in [49].

Nonlinear decay term

The operator $\hat{L}_1$ and the last term in the master equation (2.46) lead to non-linear losses. While the latter simply describes a two-excitation decay which leads to a loss of two excitations, the former term can be interpreted as a non-linear single-excitation decay. This non-linear loss term gets generated by the Lindblad operator $\hat{L}=\sqrt{\hat{\Gamma}(z)}\hat{\Psi}(z)$, where $\hat{\Gamma}$ denotes an *operator valued loss rate* given by

$$\hat{\Gamma}(z)=\frac{\gamma\cos^2\theta\sin^6\theta}{\Omega_\mathrm{e}^2}\left[\int\mathrm{d}z'\,V(z-z')\hat{\Psi}^\dagger(z')\Psi(z')\right]^2. \tag{2.49}$$

Note that it is not possible to simplify this loss mechanism by replacing $\hat{\Gamma}$ with its expectation value, i.e., performing a mean field approximation, since $V(r)$ diverges for $r\to 0$. Even if a cutoff would be introduced for the interaction potential the mean field expression $\hat{L}=\langle\hat{\Gamma}(z)\rangle\,\Psi(z)$ would describe a strong single-excitation loss process which is not physical.

2.3.3 Trajectory approach

In general the state of an open system is a mixed state, i.e., has to be described by a density matrix ρ. To analyze the time evolution of an observable $\hat{O}$, one has to evaluate

$$\partial_t\langle\hat{O}\rangle=\mathrm{tr}\{\rho\partial_t\hat{O}\}=\mathrm{tr}\{\hat{O}\partial_t\rho\}. \tag{2.50}$$

Note that the middle expression of (2.50) is in the Heisenberg picture of quantum mechanics while the rightmost expression is to be taken in the Schrödiger picture. The equality can easily be seen utilizing the invariance of the trace under cyclic permutations. The evaluation of (2.50) can be done using an adjoint equation, i.e., writing equations of motion for the expectation values leading to a coupled set of equations. For instance, this can be done for the single- and two-excitation density

matrices, $\rho_1(x,y) = \langle\hat{\Psi}^\dagger(x)\hat{\Psi}(y)\rangle$ and $\rho_2(x,y,y,x) = \langle\hat{\Psi}^\dagger(x)\hat{\Psi}^\dagger(y)\hat{\Psi}(y)\hat{\Psi}(x)\rangle$, respectively, see Appendix C. The master equation generates a set of coupled equations, as the decay leads to a coupling of two-photon observables to single-photon observables and so forth, leading to a hierarchy of equations, terminating at the total number of excitations that are considered. However, the specific form of $\hat{L}$ in the master equation leads to another hierarchy of equations, coupled by derivatives, that are difficult to solve.

Thus we choose a different route to investigate the master equation dynamics. As introduced in Section 1.3.3, the time evolution can be calculated using trajectories, i.e., considering wave functions evolving under a non-Hermitian Hamiltonian $\hat{\mathcal{H}}_{\text{eff}}$ with random projections due to the jump operators, for instance $\hat{L}$, and performing a stochastic average over these trajectories. Here these jumps correspond to projections of the two-polariton wave function onto the single-photon wave function, i.e., the loss of a polariton. In the off-resonant regime, where $|\Delta| \gg \gamma$, the time-scales on which these jumps occur are large compared to the time-scales governing the unitary time evolution. Consequently, we can find an approximate solution by neglecting the projections and considering only the non-Hermitian Hamiltonian. This allows us to consider only the wave function ψ_2 of two polaritons. We recall the definition

$$|\Psi_2(t)\rangle = \iint \mathrm{d}z\,\mathrm{d}z'\,\psi_2(z,z',t)\hat{\Psi}^\dagger(z)\hat{\Psi}^\dagger(z')\,|0\rangle\,, \tag{2.51}$$

with the two-excitation amplitude $\psi_2(z,z',t) = \langle 0|\hat{\Psi}(z)\hat{\Psi}(z')|\Psi_2(t)\rangle$.

Note that the norm of $\|\psi_2\|$ is not conserved when evolving under a non-Hermitian Hamiltonian, but gives the probability of remaining in the two-excitation subspace, i.e., the probability that no projection occurred.

2.4 Wave-function simulations of the Maxwell-Bloch equations

In this section we want to employ numerical methods to calculate the propagation of two photons in a gas of Rydberg atoms [8, 42]. The idea is to simulate the full Maxwell-Bloch equations to understand the propagation of photons inside the medium, especially under off-resonant driving conditions. The Maxwell-Bloch equations were the starting point for the derivation of the effective field theory of Rydberg polaritons which lead to the master equation in the previous section. Hence, we use the results in this section as a benchmark to validate the master equation. The simulation of the full Maxwell-Bloch equations is numerically challenging even with the restriction to one spatial dimension as one has to deal with the time evolution of strongly interacting particles propagating in continuous space and which are moreover subject to losses. Thus we have to restrict the simulations of the full equations to two particles and use approximations and simplifications of the problem to achieve further reduction of the complexity.

In the following we start with a brief introduction of the numerical methods. Then we simulate

how a pair of particles propagates through a boundary into a medium with Rydberg interactions and back into free space. Next we analyze the propagation inside the medium by making use of periodic boundary conditions and reducing the dimensionality and thus the computational complexity by considering the relative dynamics only.

2.4.1 Methods and observables

The full time-evolution of our model is described by the Maxwell-Bloch equations (1.13) for the operators $\hat{\mathcal{E}}, \hat{\sigma}_{\mathrm{ge}}, \hat{\sigma}_{\mathrm{gr}}$ and additional interaction processes between the coherences $\hat{\sigma}_{\mathrm{gr}}$. As these equations are not exactly solvable, one has to apply approximations and simplifications to get an solution and use numerical methods. We use wave-function methods to map the equations of motion of the operators to equations for complex valued functions describing the amplitudes and phases of the different wave-function components. Restricting ourselves to a certain number of excitations leads to a closed set of equations that can be integrated numerically. In general the state vector of a few-photon pulse with contributions from electrical field $\hat{\mathcal{E}}$ optical $\hat{\sigma}_{\mathrm{ge}}$ and atomic $\hat{\sigma}_{\mathrm{gr}}$ coherences is given by a superposition,

$$|\Psi(t)\rangle = |0\rangle + |\psi_1\rangle + |\psi_2\rangle + \dots \tag{2.52}$$

$$= |0\rangle + \int \mathrm{d}z_1 \sum_\alpha \psi_\alpha^{(1)}(z_1,t)\hat{O}_\alpha^\dagger(z_1)\,|0\rangle + \iint \mathrm{d}z_1\,\mathrm{d}z_2 \sum_{\alpha,\beta} \psi_{\alpha\beta}^{(2)}(z_1,z_2,t)\hat{O}_\alpha^\dagger(z_1)\hat{O}_\beta^\dagger(z_2)\,|0\rangle + \dots\,, \tag{2.53}$$

of vacuum, one-, two-, and higher number states. The sums over α, β run over all possible n-particle wave functions, i.e., the operators are $\hat{O}_\alpha \in \{\hat{\mathcal{E}}, \hat{\sigma}_{\mathrm{ge}}, \hat{\sigma}_{\mathrm{gr}}\}$ corresponding to excitations in the electrical field $\hat{\mathcal{E}}$, optical polarization $\hat{\sigma}_{\mathrm{ge}}$ and spin coherence $\hat{\sigma}_{\mathrm{gr}}$. The amplitudes

$$\begin{aligned} \psi_\alpha^{(1)} &= \langle\psi(t)|\hat{O}_\alpha^\dagger|0\rangle\,, \\ \psi_{\alpha\beta}^{(2)} &= \langle\psi(t)|\hat{O}_\alpha^\dagger\hat{O}_\beta^\dagger|0\rangle\,, \\ &\vdots \end{aligned} \tag{2.54}$$

give the probability of finding 1, 2, ... excitations $\hat{O}_\alpha$ or $\hat{O}_\beta$ at positions z_1 or z_1, z_2, respectively, and similar for higher number of particles. For simplicity we absorb the normalization of the wave function into the components $\psi^{(1)}, \psi^{(2)}, \dots, \psi^{(n)}$. In the following we consider only states of fixed excitation numbers. In particular we are interested in two-excitation states, as the vacuum state is trivial and the single-excitation state is not interesting due to the lack of interaction effects. Moreover, under off-resonant driving conditions dissipation is negligible, and thus the number of particles

should be almost conserved.

To solve the equations we introduce a discretization of the space coordinates,

$$\psi_2(z_1, z_2) \to \psi_2(z_{1,j}, z_{2,j}) \tag{2.55}$$

and use a combination of different methods to efficiently calculate the time propagation for a finite time step dt. We use a finite difference scheme to calculate the partial derivatives. To simulate the propagation of a two-photon pulse from free space into the medium, we use adaptive boundary conditions, using a nonuniform spatial grid to account for the EIT pulse compression [1].

2.4.2 Simulation of full Maxwell-Bloch equations

We start with the simulation of the full Maxwell-Bloch equations of two interacting photons. For a wave function with exactly two excitations they assume a Schrödinger-like form that can be written for the vector $\mathbf{\Psi}_2$ with components $\psi^{(2)}_{\alpha\beta}$

$$\mathrm{i}\frac{\partial}{\partial t}\mathbf{\Psi}_2(z_1, z_2, t) = \hat{\mathcal{H}}(z_1, z_2)\mathbf{\Psi}_2(z_1, z_2, t), \tag{2.56}$$

where the Hamiltonian $\hat{\mathcal{H}}$ is given by

$$\hat{\mathcal{H}}(z_1, z_2) = \hat{\mathcal{H}}_0(z_1) \otimes \hat{\mathcal{H}}_0(z_2) + V(z_1 - z_2)\hat{\mathrm{P}}_{\mathcal{SS}}. \tag{2.57}$$

Here, $\hat{\mathcal{H}}_0(z)$ is the real space representation of the matrix in Eq. (1.13) and $\hat{\mathrm{P}}_{\mathcal{SS}}$ denotes the projector onto the component $\langle\psi(t)|\hat{\sigma}_{\mathrm{gr}}\hat{\sigma}_{\mathrm{gr}}|0\rangle$ as the interaction only affects this component of two Rydberg excitations. To large energies we introduce a cutoff a into the van der Waals interaction potential

$$V_{\mathrm{eff}}(r) \to \frac{\sin^4\theta C_6}{r^6 + a^6}. \tag{2.58}$$

To verify that the cutoff has no influence onto the simulation results we performed benchmark simulations showing that the results are independent of the cutoff.

Propagation through boundary

To capture the physics when the photons propagate from free space, where they propagate with vacuum speed of light, into the medium, where they are much slower with the velocity $v_{\mathrm{g}} \ll c$ and the pulse experiences EIT compression as well as interaction due to the coupling to Rydberg atoms, we split the space into two regions inside the medium and in free space. This is illustrated in Figure 2.8. Using this method to calculate the time evolution for two-photons according to the Maxwell-Bloch equations we find that the pulse gets split into two parts, avoiding a region of small

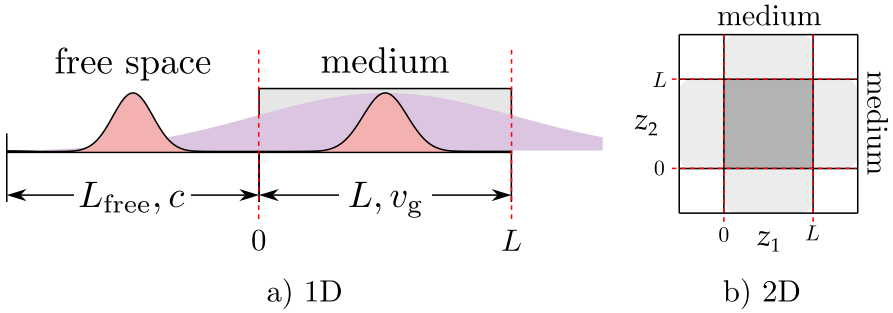

Figure 2.8: Illustration of the adaptive grid. As the pulse propagates in free space with vacuum speed of light c and in the medium under conditions of EIT with the group velocity $v_{\text{g}} \ll c$ and moreover gets spatially compressed, we split the space into two parts and discretize free space and the medium separately with different step size. (a) illustrates this in one spatial dimension and (b) for two spatial dimensions.

relative distance. In Figure 2.9 we show snapshots of the simulation for off-resonant and resonant EIT driving conditions. For both cases the figures show the formation of an avoided volume for small distances, which is the well-known effect of Rydberg photon blockade [8, 42] and allows us to compare resonant and off-resonant propagation. While in the resonant case the interaction leads to decay of polaritonic excitation and loss of amplitude, in the resonant case a much slower decay seems to be present and a repulsion of the two photons can be observed.

On the basis of the master equation we showed in the previous section that the dissipative terms play no role in the dynamics when the single photon detuning is large, but two photons inside a blockade distance propagate at the vacuum speed of light through the medium and thus escape from the wave packet. Moreover, polaritons interact repulsively inside which prevents photons from getting inside the blockade region.

Periodic boundary conditions

In the previous section we used adaptive boundary conditions to simulate the transition of a two-photon pulse from free space to a gas of Rydberg atoms. As this calculation is numerically challenging, we want to find simplifications that allow us to capture the important physics. As a first step we assume an atomic medium with periodic boundary conditions. In this case we can use a uniform grid for spatial discretization. This allows us to calculate the derivative propagator in the Fourier space, where it is diagonal. Using a Suzuki-Trotter decomposition and utilizing a Fast-Fourier-Transform implementation [63] allows to calculate the time evolution much faster and furthermore allows us to use a higher precision or simulate longer evolution times. A drawback of this method is that we have to make an ansatz for the initial state that is not an eigenstate and thus essentially have to perform a quench initially.

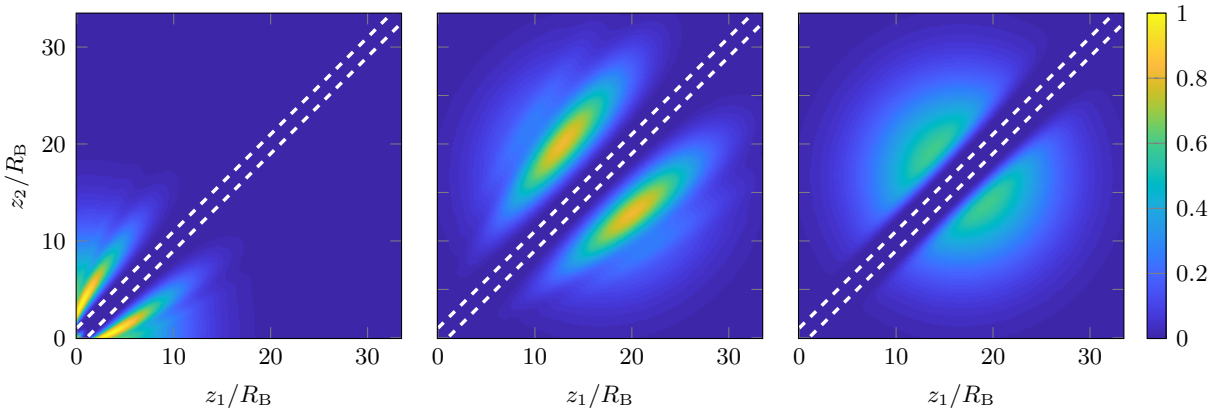

(a) $\Delta = 4\gamma,\ t/T = 0.1$ (b) $\Delta = 4\gamma,\ t/T = 0.5$ (c) $\Delta = 0,\ t/T = 0.5$

Figure 2.9: Electrical field component of Rydberg polariton propagating through a boundary at $z = 0$ into a gas of Rydberg atoms. Simulation of two-excitation wave equation using the full Maxwell Bloch equations, Eqs. (1.13) and interactions. (a) and (b) show snapshots of $|\mathcal{EE}|^2$ the propagation of a two-photon pulse under off-resonant EIT conditions and (c) the resonant case. The propagation time t is given in units of the time $T = L/v_\mathrm{g}$, where $t = 0$ denotes the time, when the center of the pulse is at $z_1 = z_2 = 0$ and L denotes the length of the medium. The parameters of the simulation are $g = 10\gamma,\ \Omega = 0.5\gamma$. The dashed lines indicate the blockade distance $|z_1 - z_2| = R_\mathrm{B}$. The color scale of the figure is set to the maximal value of $|\mathcal{EE}|^2$ in (a).

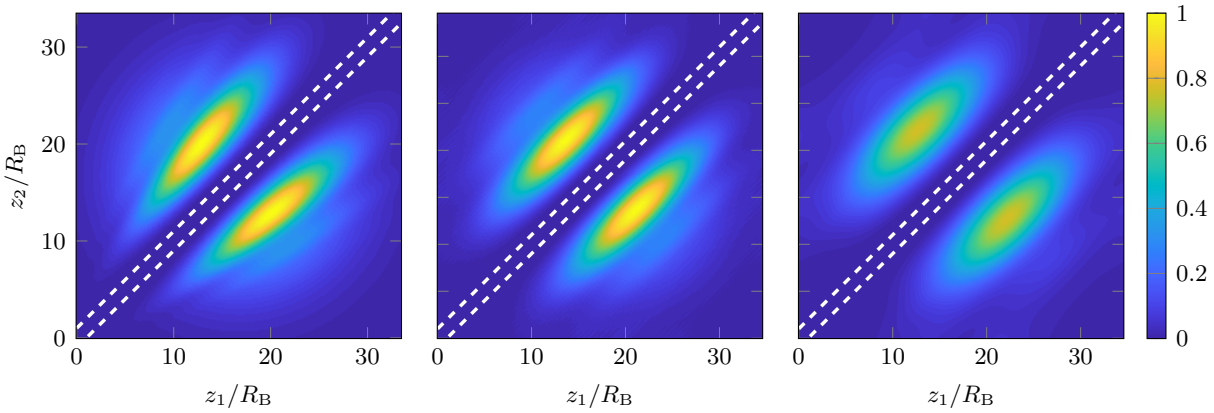

(a) w/ boundary, $t = 0.5T$ (b) inside medium, $t = 0.5T$ (c) inside medium, $t = T$

Figure 2.10: Electrical field component of Rydberg polariton propagating in a gas of Rydberg atoms. Simulation of two-excitation wave equation equation under off-resonant EIT-conditions using the full Maxwell-Bloch equations, Eqs. (1.13). (a) shows the result of the previous figure after propagation through boundary as comparison for (b) where we quench a non-interacting Rydberg polariton pulse inside the medium at $t = 0$ and calculate the propagation inside the medium with periodic boundary conditions. This allows us to extend the time evolution to larger times as shown in (c). The propagation time t is given in units of the time $T = L/v_\mathrm{g}$, where $t = 0$ denotes the time, when the center of the pulse is at $z_1 = z_2 = 0$ and L denotes the length of the medium. The parameters of the simulation are $\Delta = 4\gamma$, $g = 10\gamma$, $\Omega = 0.5\gamma$. The dashed lines indicate the blockade distance $|z_1 - z_2| = R_\mathrm{B}$. The color scale of the figure is set to the maximal value of $|\mathcal{EE}|^2$ in (a).

In Figure 2.10 we compare the result of the adaptive boundary calculation (a) with a simulation of a two-polariton pulse inside the medium with periodic boundary conditions (b). For these simulations we choose initially a non-interacting two-polariton wave packet with a Gaussian shape and perform an interaction quench. As can be seen by comparing the two methods, they yield a very good agreement. The main difference is that the "full" simulation shows an increasing repulsion with increasing center-of-mass coordinate $R = (z_1 + z_2)/2$, i.e., along the anti-diagonal axis. This is due to the fact that the parts with larger R are for a longer time inside the medium. In contrast to this, for the simulation inside the medium with periodic boundary conditions all parts are propagating in the medium for the same amount of time.

The periodic boundary conditions allow us to simulate larger time scales which is shown in Figure 2.10(c), where we show a snapshot of the electrical field component after twice as long propagation time.

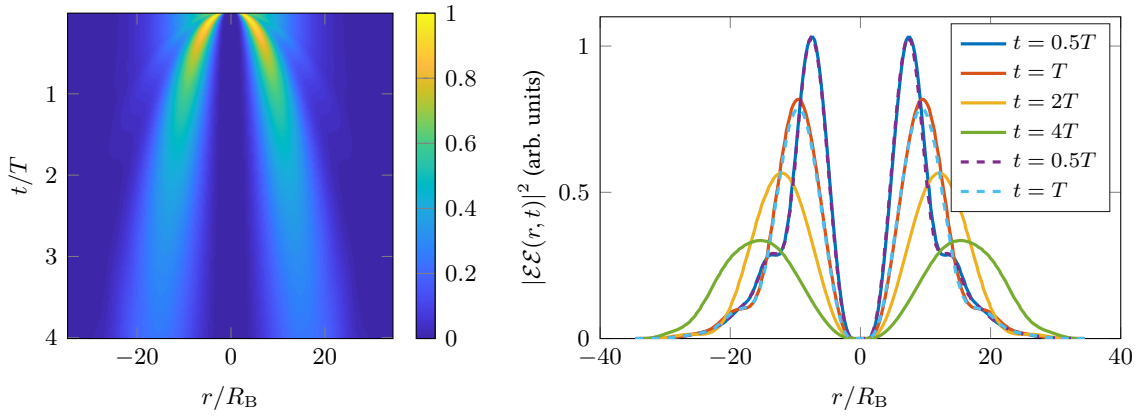

(a) (b)

Figure 2.11: Simulation of Rydberg polariton propagation in a gas of Rydberg atoms using full Maxwell-Bloch equations. (a) Time evolution of the two-photon wave function $\psi_2(r, K = 0, t)$ in the relative coordinate $r = z_1 - z_2$ up to a time of $t = 4T$, where $T = L/v_g$. Shown is the component $|\mathcal{E}\mathcal{E}(r,t)|^2$ in arbitrary units. (b) Cross section of two-excitation wave equation. Simulation of the full Maxwell-Bloch equations. The solid lines show $|\mathcal{E}\mathcal{E}(r,t)|^2$ for fixed times $t/T = 0.5, 1, 2, 4$ calculated using only relative time evolution, i.e., horizontal cross-sections of (a). The dashed lines show for times $t/T = 0.5, 1$ cross-sections along the line $x + y = 0$ of the simulation in both coordinates z_1, z_2 using periodic boundary conditions, which are cross-sections of the simulations shown in Figure 2.10(b)-(c). The plots are normalized to the maximal value at $t = 0$. Parameters of the simulations are as in Figure 2.10.

2.4.3 Relative dynamics

Due to its symmetry we expect the interaction between two excitation solely to affect the dynamics in the relative coordinate $r = z_1 - z_2$ of the wave packet. This matches the behavior seen in the simulation in the previous section which gives subsequently rise to a further possibility to reduce the complexity of the numerical simulation. Namely, we transform to relative and center-of-mass coordinates $r = z_1 - z_2$ and $R = \frac{1}{2}(z_1 + z_2)$, respectively. We perform a Fourier transform from R to K and assume that only $K = 0$ has a relevant contribution to the dynamics. Then the problem is reduced to a one-dimensional equation of motion of the wave function $\psi_2(r, K = 0, t)$, which is a computationally much simpler problem. In Figure 2.11(a) we show the dynamics in the relative coordinate only and in (b) we compare these results to cross sections of the full two-dimensional simulations in coordinates z_1, z_2.

2.5 Effective Hamiltonian

In the case of large single-photon detuning $|\Delta| \gg \gamma$ as simulated in the previous section the fundamental physics is governed by an interplay of repulsive interaction and a kinetic energy with an almost real mass, i.e., we expect a unitary time evolution. The simulation of two-photon wave packets using Maxwell-Bloch equations confirms this expectation mainly, although some small remaining decay can be observed.

In this case the decay processes in the master equation can be neglected, leading to a unitary time evolution governed by an effective Hamiltonian for the Rydberg polaritons. In leading order in $\cos(\theta)$ the Hamiltonian simplifies to

$$\hat{\mathcal{H}} = -\int \mathrm{d}z\, \hat{\Psi}^\dagger(z) \frac{\partial_z^2}{2m} \hat{\Psi}(z) + \frac{1}{2} \iint \mathrm{d}z\, \mathrm{d}z'\, V_{\text{eff}}(z - z') \hat{\Psi}^\dagger(z) \hat{\Psi}^\dagger(z') \hat{\Psi}(z') \hat{\Psi}(z), \tag{2.59}$$

in a frame co-moving with the group velocity v_g.

We can calculate eigenstates of this Hamiltonian by using again a discretization of the space coordinates and numerical exact diagonalization methods. We take a box of length L corresponding to the medium length used in the propagation simulations and impose open boundary conditions. We find the spectrum and lowest energy eigenstate shown in Figure 2.12, where we plotted a symmetric superposition $|gs\rangle = (|\psi_0\rangle + \mathrm{i}\,|\psi_1\rangle)/\sqrt{2}$ of the two degenerate ground states $|\psi_0\rangle$ and $|\psi_1\rangle$. In (c) we compare a cross section of this state to the ground state calculated for the relative coordinate only, i.e., for numerically only one dimension, where we find a disagreement between the spatial shapes of these two states.

However, we find that the eigenstate calculated for relative coordinate restricted to a box of half the size agrees very well with a cross-section of the time evolved state from Figure 2.10(c).

From this result we conclude that the wave function of two Rydberg polaritons evolves into state close to the ground state of the effective Hamiltonian.

2.6 Conclusion

In this chapter we investigated the propagation of photons under conditions of electromagnetically induced transparency in a gas of Rydberg atoms. We showed that the dimensionality of the model can be reduced from three to one if the transverse beam diameter of the probe field is smaller than the Rydberg blockade radius. We showed that under paraxial propagation conditions and for sufficiently small densities of excitations the system can be described by an effective field theory of a single species of quasiparticles called Rydberg polaritons. This theory is in general an open system that can be described by a master equation. We employed numerical wave-function simulations to find the state of two Rydberg polaritons inside the medium and to compare the time evolution described by

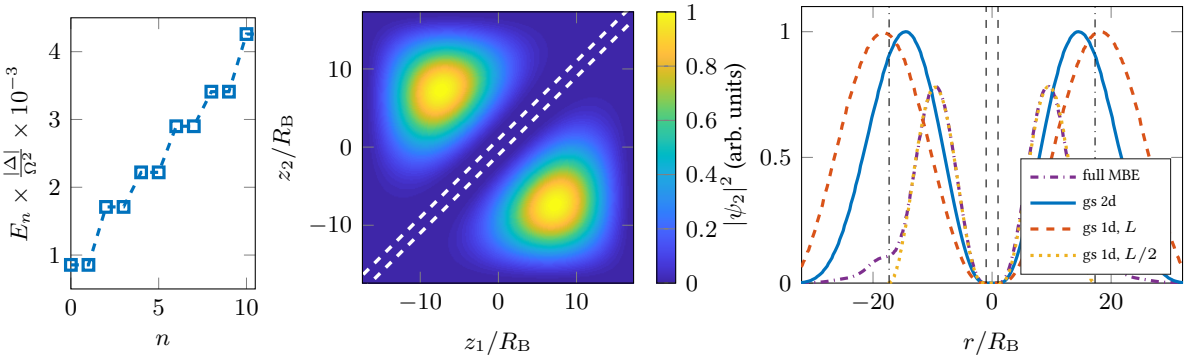

(a) Spectrum (b) Ground state (c) Cross section, normalized

Figure 2.12: Numerical diagonalization of effective Hamiltonian (2.59). We use numerical diagonalization to calculate the eigenstate of the Hamiltonian $\hat{\mathcal{H}}$ for two Rydberg polaritons on a discretized spatial grid with open boundary conditions. (a) shows the numerical spectrum we find for $\Delta = -4\gamma$, $g\sqrt{n} = 10\gamma$, $\Omega = 0.5\gamma$ and a calculation in two dimensions as shown in (b) where we plot a symmetric superposition of the two degenerate ground states. (c) shows a cross section of (b) along the axis $z_1 + z_2 = 0$ (solid blue line) compared to a ground state calculated in one dimension along the relative coordinate $r = z_2 - z_1$ (dashed red line) using the same medium length as the propagation calculations above. Both curves are normalized to 1. The dash-dotted violet line shows the cross section of Figure 2.10(c) of a polariton pulse propagating inside the medium for a time $t = L/v_\mathrm{g}$ after an initial interaction quench. This cross section is compared to a rescaled eigenstate calculated inside a one-dimensional box of length $L/2$ (dotted yellow line).

the effective field theory with a simulation of the full paraxial Maxwell-Bloch equations. We showed that under off-resonant driving conditions and for sufficiently large inter-particle separation the Rydberg polaritons behave like massive Schrödinger particles with repulsive interactions. For shorter distance there is a coupling of Rydberg polaritons to decaying and fast propagating bright polaritons. Correspondingly the dissipative time evolution reduces to a unitary time evolution described by an effective Hamiltonian. We used numerical exact diagonalization to calculate the two-excitation ground-state of this effective Hamiltonian and found very good agreement with the two-excitation state from the wave-function simulation. This result allows to analyze many-body physics of Rydberg polaritons described by the effective Hamiltonian. This will be the subject of the following chapter. Under off-resonant driving conditions with finite single-photon detuning also bound two-particle states exist. Since, these states cannot be excited for large blockade distances as considered in the current chapter but will be considered in Chapter 4.

Chapter 3

Many-body physics of Rydberg polaritons

Photons propagating in a gas of Rydberg atoms under conditions of electromagnetically induced transparency form massive quasi-particles, termed Rydberg polaritons, interacting with a van der Waals-type interaction potential. Under certain conditions the dimensionality of this system effectively reduces to one. In the case of off-resonant driving conditions, i.e., with a single-photon detuning that is large compared to the atomic decay rate, the Rydberg polaritons behave like massive Schrödinger particles with a unitary time evolution described by an effective Hamiltonian. The mass and the interaction strength are independently tunable parameters. In the case of repulsive interactions the polaritons repel each other leading to an avoided volume. In the previous chapter we showed that a pair of photons propagating from free space into a gas of Rydberg atoms forms a state that has a large overlap with a two-excitation ground state of the effective Hamiltonian.

In the present chapter we want to generalize these results to many particles and larger length scales. Here the properties and results of our model suggest that the setup can be used to convert an initial wave-packet of photons into a train of single photons. As the time evolution inside the medium is a unitary process with repulsive interactions, the photonic state may build long-range correlations, leading to the formation of a quasi-crystalline state, a so-called Wigner crystal. This state has been predicted for electrons a long time ago [73]. Such a state has potential applications in all-optical (quantum) communication and information. For instance, a regular train of photons can provide high bit rates for quantum repeater protocols and multiplexing of photons. Note that this is opposed to the dissipative case where an initial wave-packet evolves into a superposition of photon states with different particle numbers [42].

In the following, we want to address these questions and calculate the ground state in the many-particle case [74],[Otterb2013] and analyze its properties and correlation length in terms of a Luttinger liquid theory. We investigate the possibilities to reach a regime of strongly interacting Rydberg polaritons. This regime turns out to be inaccessible under stationary driving conditions. However, this can be overcome by changing the EIT driving conditions in time, i.e., performing a storage of polaritons into a stationary spin wave [3, 75, 76]. Using a time-dependent Luttinger liquid theory [77, 78] allows us to calculate the correlation functions during this time-dependent protocol.

The results presented in the following are summarized in references [Otterb2013], which was a collaboration of Johannes Otterbach, Razmik Unanyan, Michael Fleischhauer and myself and [Moos2015], which was a collaboration of Razmik Unanyan, Michael Fleischhauer and myself with contributions by Michael Höning. The density-matrix renormalization-group simulations used in the chapter and as well as the publications were provided by Dominik Muth, see also [74].

3.1 Wigner crystal of Rydberg polaritons

In the case of large single-photon detuning the physics of Rydberg polaritons is described by the Hamiltonian (2.59) in a co-moving frame,

$$\hat{\mathcal{H}} = -\int \mathrm{d}z\, \hat{\Psi}^\dagger(z)\frac{\partial_z^2}{2m}\hat{\Psi}(z) + \frac{1}{2}\iint \mathrm{d}z\, \mathrm{d}z'\, V_{\text{eff}}(z-z')\hat{\Psi}^\dagger(z)\hat{\Psi}^\dagger(z')\hat{\Psi}(z')\hat{\Psi}(z),$$

with a real mass m and a repulsive interaction potential V_{eff}. In the following we investigate many body properties of this Hamiltonian.

3.1.1 Many-body ground state

We are interested in the many body ground state of the Hamiltonian (2.59). For sufficiently small group velocity and small excitation densities, the effective potential reduces to a van der Waals potential, which we modify by introducing a cutoff

$$V_{\text{eff}}(r) \approx \frac{\sin^4\theta C_6}{r^6} \to \frac{\sin^4\theta C_6}{a^6 + r^6}, \tag{3.1}$$

i.e., a screening of the short distance interaction at the length a to account for a potential regularization at short distances [42]. This screening is physically always present, e.g., in our model due to the finite distances of Rydberg atoms in a dilute gas. However, for sufficiently strong interactions the results are independent of the cutoff, cf. Figure 3.2, and thus we neglect a in the remainder of this chapter. Then the Hamiltonian can be described by a single, dimensionless parameter Θ, given by the interaction strength at average distance $1/\rho_0$ between excitations compared to the Fermi energy generalized to the bosonic system, [74].

$$\Theta = \frac{1}{2\pi}\rho_0^4 m \sin^4\theta C_6. \tag{3.2}$$

Ground states of bosonic systems with polynomially decaying interactions $\sim r^{-\beta}$ can numerically be calculated. In [74] the author employed the density matrix renormalization group (DMRG) method [79] to calculate ground states of van der Waals-type interacting bosons for periodic as well as open boundary conditions. In Figure 3.1 we show first-order and normalized density-density correlation

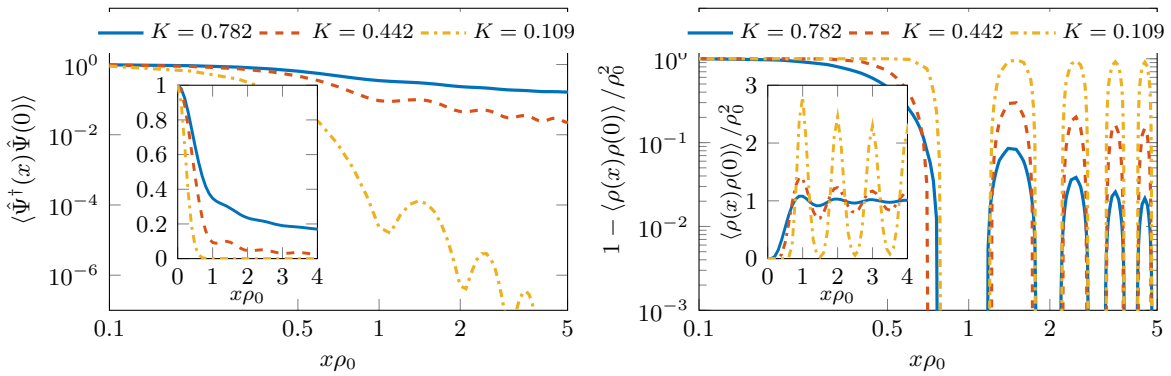

(a) First order correlation function.

(b) Second order correlation function.

Figure 3.1: First and second order correlation function calculated by DMRG. Shown are results taken from [74],[Otterb2013] for 10 particles on 100 lattice sites with periodic boundary conditions for different interaction strengths. (a) First order correlation function and (b) normalized second order correlation function. The main figures show double logarithmic plots of the correlation function and the deviation of the correlation function from one, respectively. The insets show linear plots of the correlation functions. See also Figure 3.3.

functions in double-logarithmic and linear representation taken from [Otterb2013]. The correlation functions were calculated using DMRG on a discretized lattice with 10 particles on 100 sites and periodic boundary conditions. The Figure contains results for three different interaction strengths Θ, corresponding to a parameter K as shown in Figure 3.2. We observe that for decreasing K the density-density correlations $\langle\rho(x)\rho(0)\rangle$ develop pronounced peaks at distances that are multiples of the inverse density ρ_0^{-1}, indicating the formation of a charge density wave. Note that the correlation function around $x = 0$ is more suppressed than for free fermions, which is the strongest possible for point-like interactions [80, 81].

3.1.2 Luttinger liquid approach

To explain the structure of the correlation functions in Figure 3.1 we use Luttinger liquid theory [10], see also Section 1.4. This approach allows for a semi-analytical treatment of one-dimensional interacting models in the limit of low energy and can also be applied to bosons with polynomially decaying interactions [82]. In particular, Luttinger liquid theory provides means to generalize the DMRG results and extract a correlation length.

To this end we assume a fixed excitation density ρ_0 and follow the standard Luttinger liquid approach to construct an effective low-energy Hamiltonian,

$$\hat{\mathcal{H}}_{\mathrm{LL}} = \frac{1}{2\pi}\int \mathrm{d}z\, v_{\mathrm{s}} K \left[\nabla\hat{\theta}(z)\right]^2 + \frac{v_{\mathrm{s}}}{K}\left[\nabla\hat{\phi}(z)\right]^2 . \tag{3.3}$$

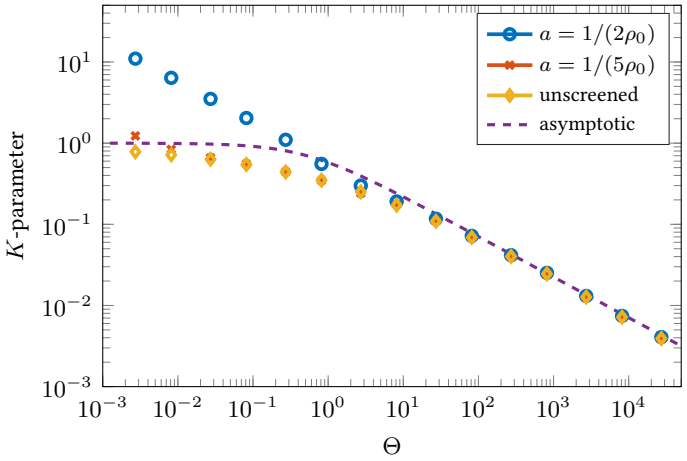

Figure 3.2: DMRG results by [74],[Otterb2013] for 10 particles on 100 lattice sites with periodic boundary conditions. Luttinger K parameter as function of Θ from (3.2) extracted from DMRG calculations for different short-distance cutoffs a of the interaction potential, the unscreened interaction potential ($a = 0$) and the formula (3.8), [83], for comparison.

Here, $\hat{\phi}$ and $\hat{\Pi} = \frac{1}{\pi}\nabla\hat{\theta}$ are canonically conjugate fields with $[\hat{\phi}(x), \hat{\Pi}(y)] = \mathrm{i}\delta(x-y)$. The Luttinger liquid is determined by two constants, the speed of sound v_s and the dimensionless Luttinger parameter K. The latter constant universally governs the asymptotic behavior of the first order and density-density correlation functions, which are in leading order power laws with exponents $-1/2K$ and $-2K$, respectively. Thus, for $K \gg 1$ the dominant long-range correlations are superfluid order, while for $K \ll 1$ a charge-density wave dominates, where $K = 1/2$ marks the crossover point. This expected behavior is matched by the results in the Figures 3.1, as can be directly observed from the logarithmic representations.

We can extract the K-parameter from the DMRG simulation. To this end we note that the ratio

$$K/v_\mathrm{s} = \pi\rho^2\chi, \tag{3.4}$$

can be determined from the compressibility $\chi^{-1} = \rho^2\frac{\partial\mu}{\partial\rho}$ [10]. Furthermore, for Galilean invariant systems the relation

$$v_\mathrm{s}K = \frac{\pi\rho}{m} \tag{3.5}$$

holds [35]. Combining both relations allows to determine the K parameter, as a function of Θ from (3.2), the single free parameter of our microscopic model. In Figure 3.2 we show the resulting relation for different screening lengths a and the unscreened case. Using the independently determined value for K, we can determine the agreement of the correlation functions with the Luttinger liquid theory. To this end we use the formulas given in [34] for the correlation functions of a Luttinger liquid constrained to a box of length L with periodic boundary conditions. Including higher harmonics the

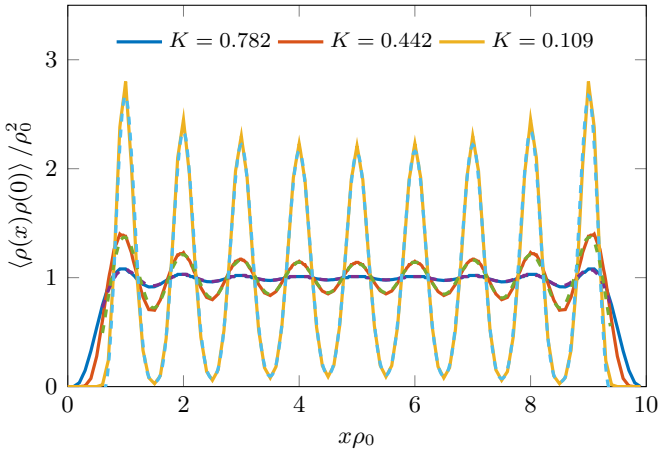

Figure 3.3: DMRG results by [74],[Otterb2013] for 10 particles on 100 lattice sites with periodic boundary conditions. Solid lines: density-density correlation functions shown also in Figure 3.1(b) for different interaction strengths. Dashed lines: fits of the density-density correlation functions by Eq. (3.7). Note that K is not a fit parameter but extracted from the DMRG calculation as described in the main text.

first order correlation function is given by the expression

$$\langle\hat{\Psi}^\dagger(x)\hat{\Psi}(0)\rangle = \rho_0 \frac{1}{[\rho_0 d(x,L)]^{1/2K}} \left\{ B_0 + \sum_{n=1}^{\infty} B_{2n} \frac{1}{[\rho_0 d(x,L)]^{2m^2K}} \cos(2\pi n \rho_0 x) \right\} \tag{3.6}$$

and the density-density correlation function by

$$\langle\rho(x)\rho(0)\rangle = \rho_0^2 \left\{ 1 - \frac{K}{2\pi^2} \left[\frac{1}{\rho_0 d(x,L)} \right]^2 + \sum_{n=1}^{\infty} A_{2n} [\rho_0 d(x,L)]^{-2n^2K} \cos(2\pi n \rho_0 x) \right\} \tag{3.7}$$

where $d(x,L) = L|\sin(\pi x/L)|/\pi$. We fit the formula (3.7) to the density-density correlation functions obtained by DMRG with the non-universal coefficients A_{2n} as fit parameters. Additionally, we restrict the fit to a domain $0.5 \leq x\rho_0 \leq L\rho_0 - 0.5$, as the smaller (and larger) x correspond to high energy contributions that are not well described by Luttinger liquid theory. In Figure 3.3 the density-density correlation functions obtained by DMRG are displayed together with the corresponding fitting results. The coefficients A_{2n} obtained by the fitting are displayed in Table 3.1. We recognize a very good agreement between numerical results and the fitted Luttinger liquid correlation function, proving that the low-energy physics of the Rydberg polariton model (2.59) is well described by Luttinger liquid theory (3.3). Moreover, the fitting results show that for weak interactions the density correlations are determined solely by the second harmonic with coefficient A_2, while for the stronger interacting case with $K = 0.109$ the fourth and sixth harmonic become increasingly important. However, as they fall

K	A_2	A_4	A_6
0.782	0.1011	0	2.59×10^{-6}
0.442	0.3639	0	5.2×10^{-5}
0.109	1.3116	0.3485	0.0317

Table 3.1: Coefficients A_{2n} of the Luttinger harmonics in (3.7) extracted from a fit of the DMRG density correlation functions on the interval $0.5 \leq x\rho_0 \leq L\rho_0 - 0.5$.

.

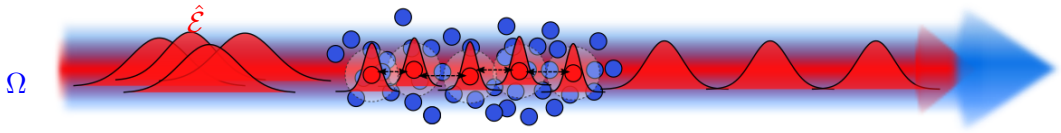

(i) input field (ii) Rydberg medium (iii) correlated photon train

Figure 3.4: Idea sketch: creation of a regular train of photons.

off with much larger exponents $-2m^2K$, the second harmonic remains the dominant contribution for larger distances. We note that the first-order correlation functions can be fitted analogously with comparable goodness of the fit, but are of minor interest for the following, as they decay very quickly for $K \gg 1$.

3.1.3 Strongly interacting regime under stationary EIT conditions

We turn now to our microscopic model of propagating Rydberg polaritons. We estimate the driving conditions needed to reach the strongly interacting regime, i.e., $K \ll 1$, under stationary conditions of EIT.

In the case of the unscreened van der Waals interaction potential an approximate formula for the K parameter has been given by [83],

$$K = \frac{1}{\sqrt{1 + \frac{\pi^4}{45}\Theta}}, \tag{3.8}$$

which is asymptotically correct in the case of small and large interaction strengths, as can also be observed from Figure 3.2. Using the definition of the effective mass (2.40) and the blockade radius (2.21) we can rewrite the definition (3.2) of Θ in terms of system parameters,

$$\Theta \approx \frac{1}{4\pi}(\rho_0 R_\mathrm{B})^4 \left(\frac{\gamma}{\Delta}\right)^2 d_\mathrm{B}^2, \tag{3.9}$$

where we assumed slow light, i.e., $v_\mathrm{g} \ll c$ and $d_\mathrm{B} = R_\mathrm{B}/L_\mathrm{abs}$ denotes the optical depth per blockade

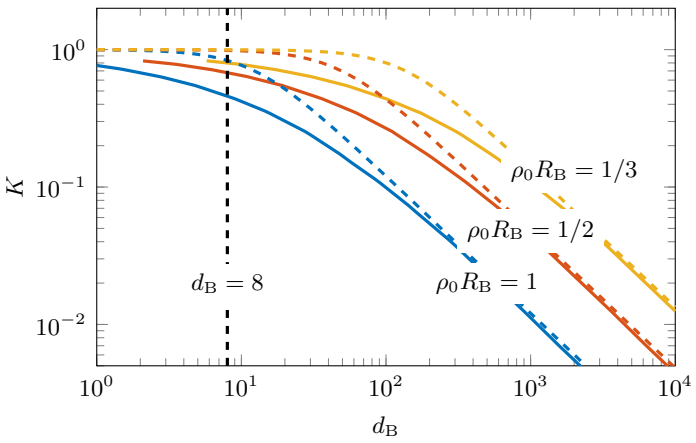

Figure 3.5: Log-log plot of Luttinger parameter K as a function of optical depth per blockade d_B. Shown for $|\Delta|/\gamma = 5$ and three different excitation densities $\rho_0 R_\mathrm{B} = 1, \frac{1}{2}, \frac{1}{3}$. *Solid lines:* interpolation of the DMRG results from [Otterb2013] presented in Figure 3.2. *Dashed lines:* Corresponding analytical approximation according to Eq. (3.10).

radius. Approximating Eq. (3.8) in the case of strong interactions and inserting the expression (3.9) yields the relation

$$K \approx 2.410 \frac{|\Delta|}{\gamma} \frac{1}{(\rho_0 R_\mathrm{B})^2} \frac{1}{d_\mathrm{B}}. \tag{3.10}$$

Here, $\rho_0 R_\mathrm{B}$ compares the excitation density to the blockade radius. In a stationary setup there can at most a single excitation exist per blockade radius, thus the density is limited by

$$\rho_0 R_\mathrm{B} \leq 1. \tag{3.11}$$

For larger densities excitations will be converted to bright state polaritons and subsequently decay or propagate out of the medium. Moreover, to realize the unitary model we require $|\Delta|/\gamma \gg 1$. The remaining free parameter in Eq. (3.10) is the optical depth per blockade. In Figure 3.5 we display the approximate relation (3.8) as well as the exact result obtained from interpolating the DMRG results shown in Figure 3.2 for different values of $\rho_0 R_\mathrm{B}$. and $\Delta/\gamma = 5$. We find that even for large excitation densities ($\rho_0 R_\mathrm{B} \approx 1$) the optical depth per blockade required for reaching the strongly interacting regime ($K \ll 1$) is orders of magnitude larger than experimentally feasible values that are on the order of 10 [8]. Furthermore, changing the optical depth per blockade d_B by changing the blockade radius while keeping $\rho_0 R_\mathrm{B}$ fixed requires smaller excitation densities with increasing d_B.

An typical experimental setup, see e.g. [8], uses a Rydberg medium of a certain, finite length L on the order of a few 10 microns. Condition (3.11) then limits the number of excitations in the medium to $N \leq \lceil L/R_\mathrm{B} \rceil$. Thus, for sufficiently large d_B, the maximal number of excitations in a finite system reduces to a single excitation, when the blockade radius R_B becomes larger L. Hence, it is impossible

to reach a regime of arbitrary large interactions under stationary driving conditions. We remark, that a charge density wave could still be observed for not too strong interactions, as its amplitude can become quite large in finite systems [84]. An alternative may also be given by exciting Rydberg atoms in hollow core fibers, as has recently been realized [52, 53], see also [81].

3.2 Dynamical storage of Rydberg polaritons

We have shown that a stationary slow-light setup of polaritons propagating in a gas of Rydberg atoms, the interactions between the polaritons can lead to strong, long-range density-density correlations corresponding to a Wigner crystal of dark-state polaritons, i.e., a train of photons moving with the slow-light group velocity. However, the limit of long-range correlations is attained only for diverging blockade distance, which makes it impossible to create such a state in a finite system under stationary driving conditions.

In the following section we propose and investigate a possible solution to this problem by using a time-dependent protocol, i.e., dynamically changing the parameters from an initially weakly interacting to the strongly interacting regime. This protocol corresponds to a dynamical slowing down of polaritons or light storage [3, 75, 76] inside the medium by turning off the control field and thereby turning propagating polaritons into a stationary spin-wave. During storage the dimensionless interaction strength is dynamically increased, leading to a divergent blockade distance. We show that despite this fact a storage of Rydberg polaritons is possible and confirm that by numerical simulations.

3.2.1 Frequency pulling

Storing light in an EIT setup is performed by decreasing the control field strength Ω and thus the group velocity, the propagation speed of the polaritons. During that process the EIT transmission spectrum $T(\omega)$, see Eq. (1.10), becomes smaller. Nevertheless, storage of polariton works as in a dynamical protocol the spectrum $S(z, \omega)$ of a polariton pulse becomes narrower and thus stays inside the transparency window [1], as opposed to a spatial change of the group velocity. The picture seems to change, when taking interactions into account. The interaction energy between two Rydberg polaritons can be interpreted as a shift of the atomic levels, i.e., a space-dependent two-photon detuning δ, or, a shift of the pulse spectrum relative to the atomic resonance. Under stationary conditions, a finite two-photon detuning is allowed, if the shifted pulse spectrum fits inside the transmission spectrum. If the transmission spectrum tends to zero, however, this is no longer the case and the pulse gets absorbed or decoupled from the medium. As has been shown [20], this argument is too naive and the storage of Rydberg polaritons is possible despite the interactions. This can be seen as follows.

Let us consider the time evolution of a dark-state polariton pulse during storage. We assume that

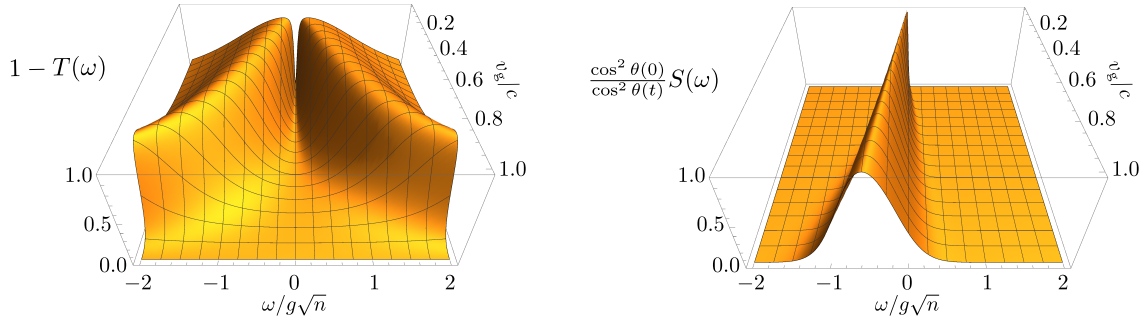

Figure 3.6: EIT transmission spectrum and normalized pulse spectrum during time-dependent slowdown of a light pulse.

initially the pulse propagates with a fixed two-photon detuning $\delta_0 = \omega_{\rm p}(0) + \omega_{\rm c} - \omega_{\rm rg}$. As has been shown in [20], this small two-photon detuning leads to a time-dependent phase shift of the dark-state polariton during storage,

$$\hat{\Psi}(z,t) = \hat{\Psi}\left(z - c\int_0^t \mathrm{d}\tau\, \cos^2\theta(\tau), 0\right) \exp\left\{\mathrm{i}\delta_0 \int_0^t \mathrm{d}\tau\, \sin^2\theta(\tau)\right\}. \tag{3.12}$$

If the mixing angle only changes slowly this causes a time-dependent modification of the spectrum $S(z,\omega)$ of the probe light field $\hat{\mathcal{E}}(z,t) = \cos\theta(t)\hat{\Psi}(z,t)$, that is given by

$$S(z,\omega) = \int_{-\infty}^{\infty} \mathrm{d}\tau\, e^{-\mathrm{i}\omega\tau} \langle \hat{\mathcal{E}}^\dagger(z,t)\hat{\mathcal{E}}(z,t-\tau)\rangle \tag{3.13}$$

$$= \frac{\cos^2\theta(t)}{\cos^2\theta(0)} S\left(0, \frac{1}{\cos^2\theta(t)}[\omega + \delta_0 \sin^2\theta(t)]\right). \tag{3.14}$$

The equation shows two effects, that are illustrated in Figure 3.6. First, there is a spectral narrowing of the pulse spectrum S proportional to $\cos^2\theta(t)$ which corresponds to the narrowing of the EIT transmission spectrum T during light storage and therefore guarantees that the spectral width of the pulse stays inside the EIT window at all times, if it did so initially [3]. Secondly and most importantly for the storage of interacting polaritons, there is a pulling of the central frequency of the pulse spectrum, i.e., the two-photon detuning $\delta(t)$ is shifted towards two-photon resonance,

$$\delta(t) = \omega_{\rm p}(t) + \omega_{\rm c} - \omega_{\rm rg} = \delta_0 \cos^2\theta(t) \to 0. \tag{3.15}$$

These effects have been observed experimentally [85]. It can be concluded that the two-photon linewidth of EIT light storage is determined by the collective Rabi frequency $\Omega_{\rm eff}$ by

$$\delta_{2,\rm ph}(t) = \frac{\Omega_{\rm eff}^2(t)}{|\Gamma|}, \tag{3.16}$$

rather than by the control field Rabi frequency $\Omega(t)$. As a consequence, the minimal distance of Rydberg polaritons is determined by (3.16) leading to the critical distance a_c,

$$a_\mathrm{c} = \max\left\{ R_\mathrm{B}(0) = \sqrt[6]{\frac{|C_6\Gamma|}{\Omega^2(0)}}, \sqrt[6]{\frac{|C_6\Gamma|}{\Omega^2_\mathrm{eff}(t)}} \right\}. \tag{3.17}$$

This length is bounded in a dynamical light storage protocol as opposed to the instantaneous blockade distance $R_\mathrm{B}(t)$. We note that in the case of slow light $\Omega_0 \leq \Omega_\mathrm{eff}(t)$ holds at all times and consequently we get $a_\mathrm{c} = R_\mathrm{B}(0)$. We conclude that the minimal distance of Rydberg polaritons does not diverge in a light storage protocol, making it possible to reach the strongly interacting regime with a finite number of excitations – at least dynamically.

3.2.2 Wave function simulation of storage

The result we derived above can be verified numerically, using two-excitation wave function simulations as introduced in Section 2.4. The two-excitation wave function is defined as in the previous chapter. As we have shown in Section 2.1, the relative and center-of-mass dynamics are decoupled, such that it is sufficient to simulate only the evolution in the relative coordinate r for center-of-mass coordinate $R = 0$. This can efficiently be done by using the split-operator approach with a time-dependent control field $\Omega(t)$. Specifically, we use a Gaussian protocol

$$\Omega(t) = \Omega_0 \exp\{-(t/\tau)^2\} \quad \Rightarrow \quad v_\mathrm{g}(t) \approx v_\mathrm{g}(0) \exp\{-2(t/\tau)^2\}, \tag{3.18}$$

where we assumed $\Omega_0^2 \ll g^2 n$. In Figure 3.7(a) we show the time-dependence of Ω and the time-dependence of the instantaneous blockade distance $R_\mathrm{B}(t) \propto \Omega(t)^{-1/3}$. We choose initial conditions of $\Omega_0 = 0.5\gamma$, $g\sqrt{n} = 10\gamma$ and a detuning of $\Delta = 4\gamma$. We determine the switching time τ by the condition $\int \mathrm{d}s\, v_\mathrm{g}(s) = L$, with L being the medium length, i.e.,

$$\tau = \frac{2L}{\sqrt{\pi} v_\mathrm{g}(0)}. \tag{3.19}$$

We calculate the simulation up to a time of $t = 3\tau$, as $v_\mathrm{g}(3\tau)$ is sufficiently small compared to $v_\mathrm{g}(0)$ and only small changes happen in the time evolution for larger times. The time evolution of the components $\mathcal{EE} = \langle 0|\hat{\Psi}(r/2)\hat{\Psi}(-r/2)|\Psi_2\rangle$ in relative coordinates and analogously defined $\mathcal{SS}$ of the wave function are displayed in Figure 3.7(b) and 3.7(c), where we plot the intensities $|\mathcal{EE}|^2$ normalized by $\cos^4\theta(0)$ and $|\mathcal{SS}|^2$ normalized by $\sin^4\theta \approx 1$. We observe that initially the wave-packet begins to spread as in the time-independent propagation, cf. Figure 2.11, but then the dispersion stops and the amplitude of the electrical field component gets shifted to the spin component. Note that the latter is only a small effect, since the initial state already is a slow light pulse. This is illustrated better in

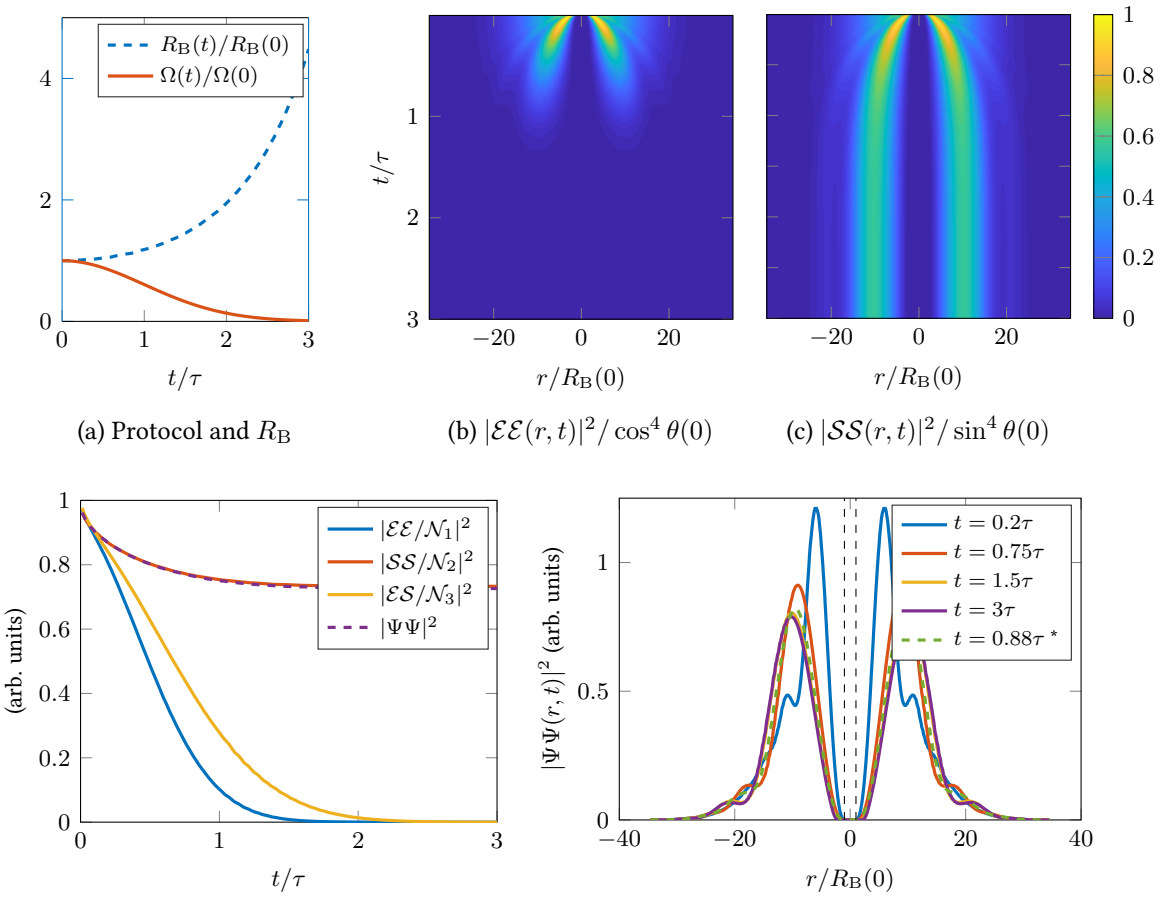

(a) Protocol and R_B (b) $|\mathcal{EE}(r,t)|^2/\cos^4\theta(0)$ (c) $|\mathcal{SS}(r,t)|^2/\sin^4\theta(0)$

(d) Occupation (e) Cross section

Figure 3.7: Simulation of storage of two-photon wave function propagating in a gas of Rydberg atoms using full Maxwell-Bloch equations, restricted to relative coordinate. In (a) the protocol for the simulation is displayed, namely $\Omega(t)/\Omega(0)$ and the diverging instantaneous blockade radius $R_B(t)/R_B(0) \propto \Omega(t)^{-1/3}$. (b) and (c) show the time evolution of the electric-field $\mathcal{EE}$ and spin component $\mathcal{SS}$ of the wave function, respectively. Shown is the amplitude squared normalized by $\cos^4\theta(0)$ and $\sin^4\theta(0)$ to make them comparable. (c) Shows the total amplitude squared integrated over r of the components $\mathcal{EE}, \mathcal{ES}$ and $\mathcal{SS}$ normalized by $\mathcal{N}_1 = \cos^2\theta(0), \mathcal{N}_2 = \cos\theta(0)\sin\theta(0)$, and $\mathcal{N}_3 = \sin^2\theta(0)$ as well as the integrated amplitude squared of the two-excitation Rydberg polariton, $\Psi\Psi$. Finally, (d) shows cross section of the polariton wave function for different times during the storage protocol (solid lines) and for comparison the cross section of a wave function propagating under stationary EIT conditions (dashed line), cf. Figure 2.11. The times are chosen such that the traveled distances of the propagating pulse and the stored pulse are equal. The vertical dashed lines indicate the blockade radius $\pm R_B$. Parameters of the simulation were $g\sqrt{n} = 10\gamma$, $\Omega(0) = 0.5\gamma$ and $\Delta = 4\gamma$. The characteristic storage time τ was chosen as in Eq. (3.19).

Figure 3.7(d), where we show the integrated intensities of the components $\mathcal{EE}$, $\mathcal{ES}$ and $\mathcal{SS}$ normalized by appropriate combinations of $\cos\theta(0)$ and $\sin\theta(0)$ as well as the combination of the three into the dark polariton $\Psi\Psi$, where the two-polariton amplitude is given by

$$\Psi\Psi(r,t) = \cos^2\theta(t)\mathcal{EE}(r,t) - \sin\theta(t)\cos\theta(t)[\mathcal{ES}(r,t) + \mathcal{SE}(r,t)] + \sin^2\theta(t)\mathcal{SS}(r,t). \quad (3.20)$$

We observe that the intensities containing electric field components are quickly turned to zero, while the spin-component is initially decaying and then saturates. The integrated intensity of the dark-state wave function is in very good agreement given by the spin amplitude as expected in the case of slow light.

Figure 3.7(e) finally shows snapshots of the relative wave function at different times during storage in comparison to the wave function propagating under stationary EIT conditions, taken from Figure 2.11. Specifically, we choose the propagating time of the latter such that the distance the wave packet travels during propagation is equal to the distance the stored wave packet travels. We observe that the wave function during storage evolves into a time-independent state with a shape similar to the propagating pulse. This confirms our result of the previous section, that the relevant length scale governing the avoided volume during storage is given by the initial blockade radius $R_{\mathrm{B}}(0)$. Therefore it is feasible to store a pulse of interacting Rydberg polaritons.

3.3 Time-dependent Luttinger liquid

As we have seen in the previous section the minimal distance of Rydberg polaritons stays finite during a light storage protocol. Thus, a pulse of Rydberg polaritons gets turned into a stationary density-wave of atomic Rydberg excitations during storage. As in a dynamical protocol the mass and consequently the dimensionless interaction strength get increased this hints to the possibility of reaching the strongly interacting regime with a dynamical protocol.

To investigate this, we will calculate the correlation functions during and after an storage protocol in this section. Therefore we employ a time-dependent Luttinger liquid theory [78, 86, 87]. An important field of research is non-equilibrium dynamics of closed interacting quantum systems [88]. Recently, Luttinger liquid theory has been applied to study the time evolution of closed quantum systems and specifically their correlation functions during and after quenches. In particular, sudden as well as finite time quenches have been investigated [77, 86, 89–91]. While the former case is always diabatic, i.e., brings the system out of equilibrium, a smooth or finite-time quench can in general be adiabatic, if it is slow compared to the slowest time scale in the system. However, this limit cannot be reached for a Luttinger liquid, as the system is gapless. Here, a smooth quench leads to a crossover in the system between adiabatic and diabatic regimes [77]. As we will show in the following this makes it possible to create sufficiently long-range correlations in a system of finite length, i.e., a

charge-density wave correlated on a length scale on the order of a typical sized atomic cloud in an experimental setup.

Let us now calculate the time evolution of the density-density correlation functions (1.54). To this end we assume a Galilean invariant system which is described by a Luttinger Hamiltonian (3.3). The system is initially in its ground state, which, for instance, can for interacting Rydberg polaritons be prepared under stationary slow light conditions. In the time-independent case the Hamiltonian can simply be diagonalized by rescaling the Luttinger liquid fields $\hat{\phi}, \hat{\theta}$ [10]. In the time-dependent case this is no longer the case, and a more sophisticated approach involving numerical simulations is needed in general.

3.3.1 Time-independent case

Let us first discuss the time-independent case. We introduce standard bosonic operators $[\hat{b}_p, \hat{b}_q^\dagger] = \delta_{p,q}$, transforming the Luttinger liquid fields $\hat{\phi}, \hat{\theta}$ in the thermodynamic limit $L \to \infty$ as

$$\hat{\phi}(x) = -\mathrm{i}\frac{\pi}{L}\sum_{p\neq 0}\left(\frac{L|p|}{2\pi}\right)^{1/2}\frac{1}{p}e^{-\alpha|p|-\mathrm{i}px}(\hat{b}_p^\dagger + \hat{b}_{-p}) \tag{3.21}$$

$$\hat{\theta}(x) = +\mathrm{i}\frac{\pi}{L}\sum_{p\neq 0}\left(\frac{L|p|}{2\pi}\right)^{1/2}\frac{1}{|p|}e^{-\alpha|p|-\mathrm{i}px}(\hat{b}_p^\dagger - \hat{b}_{-p}) \tag{3.22}$$

with α being a short-distance cutoff. If the system is not in the thermodynamic limit, topological excitations are important and additional terms have to be taken into account [10]. The Luttinger Hamiltonian (3.3) transforms into [10]

$$\hat{\mathcal{H}}_{\mathrm{LL}} = \frac{v_\mathrm{s}}{2}\sum_{p\neq 0}|p|\left[w\hat{b}_p^\dagger\hat{b}_p - \frac{g}{2}\left(\hat{b}_p^\dagger\hat{b}_{-p}^\dagger + \hat{b}_{-p}\hat{b}_p\right)\right], \tag{3.23}$$

where the coefficients are $w, g = K \pm K^{-1}$, respectively. This Hamiltonian can be diagonalized by a Bogoliubov transformation,

$$\begin{pmatrix}\hat{b}_p\\ \hat{b}_{-p}^\dagger\end{pmatrix} = \begin{pmatrix}\cosh\zeta & \sinh\zeta\\ \sinh\zeta & \cosh\zeta\end{pmatrix}\begin{pmatrix}\hat{\gamma}_p\\ \hat{\gamma}_{-p}^\dagger\end{pmatrix}, \tag{3.24}$$

where $e^{2\zeta} = K$. The resulting Hamiltonian expressed in terms of the new variables is

$$\hat{\mathcal{H}} = v_\mathrm{s}\sum_{p\neq 0}|p|\hat{\gamma}_p^\dagger\hat{\gamma}_p \tag{3.25}$$

corresponding to free bosons with linear dispersion. The only nonvanishing correlation function in a thermal state at temperature T reads

$$\langle \hat{\gamma}_p \hat{\gamma}_q^\dagger \rangle = \delta_{p,q} \coth(v_\mathrm{s}|p|/2T), \tag{3.26}$$

where we set $k_\mathrm{B} = 1$. Note that, in the limit $T \to 0$ the coth-factor becomes unity.

We are interested in density-density correlations $\langle \rho(x)\rho(0)\rangle$. In leading order they are describe by a charge-density wave, given by a spatial oscillation period given by the inverse of the density ρ_0 multiplied by a function $e^{-G_{\phi\phi}(z)}$ determining the spatial behavior of the amplitude. In the ground-state this is a power law like decay. Following (1.52), we find,

$$\begin{aligned} G_{\phi\phi}(z) = \langle [\phi(x) - \phi(0)]^2 \rangle &= \frac{2\pi}{L} \sum_{p>0} e^{-\alpha p} \frac{1 - \cos px}{p} \langle (\hat{b}_p^\dagger + \hat{b}_{-p})(\hat{b}_{-p}^\dagger + \hat{b}_p)\rangle \\ &\to \int_0^\infty \mathrm{d}p\, p^{-1} e^{-\alpha p}(1 - \cos px) \langle (\hat{b}_p^\dagger + \hat{b}_{-p})(\hat{b}_{-p}^\dagger + \hat{b}_p)\rangle \end{aligned} \tag{3.27}$$

in the thermodynamic limit [10]. Hence, the spatial envelope of the density correlations is determined by phase correlations. Consequently, to to determine the correlation function (3.27) we need to find $\langle (\hat{b}_p^\dagger + \hat{b}_{-p})(\hat{b}_{-p}^\dagger + \hat{b}_p)\rangle$. With Eq. (3.26) we find

$$\langle (\hat{b}_p^\dagger + \hat{b}_{-p})(\hat{b}_{-p}^\dagger + \hat{b}_p)\rangle = K \coth(v_\mathrm{s}|p|/2T) \tag{3.28}$$

for the correlation functions of a thermal state.

3.3.2 Time-dependent case

Now we turn to the case of an explicit time dependence of the system parameters, which translates into a time-dependent speed of sound v_s and Luttinger K parameter

$$v_\mathrm{s} \to v_\mathrm{s}(t), \quad K \to K(t). \tag{3.29}$$

We assume that the time variation is sufficiently slowly, such that the Luttinger-liquid approximation still holds and, furthermore, non-adiabatic corrections of the underlying polariton model are negligible, cf. Section 3.5 for an estimation. In this case the system can still be described by Hamiltonian, Eq. (3.23), where the total energy scale of as well as the ratio between particle-number conserving and non-conserving terms become time-dependent

$$\hat{\mathcal{H}}_\mathrm{LL} = \frac{v_\mathrm{s}(t)}{2} \sum_{p\neq 0} |p| \left[w(t) \hat{b}_p^\dagger \hat{b}_p - \frac{g(t)}{2} \left(\hat{b}_p^\dagger \hat{b}_{-p}^\dagger + \hat{b}_{-p} \hat{b}_p \right) \right], \tag{3.30}$$

with $w(t), g(t) = K(t) \pm K(t)^{-1}$. The Heisenberg equations of motion for the bosonic modes $\hat{b}, \hat{b}^\dagger$ under this Hamiltonian are given by

$$\mathrm{i}\frac{d}{dt}\begin{pmatrix}\hat{b}_p\\ \hat{b}^\dagger_{-p}\end{pmatrix} = \frac{v_\mathrm{s}(t)|p|}{2}\begin{pmatrix}w(t) & -g(t)\\ g(t) & -w(t)\end{pmatrix}\begin{pmatrix}\hat{b}_p\\ \hat{b}^\dagger_{-p}\end{pmatrix} =: M_p(t)\begin{pmatrix}\hat{b}_p\\ \hat{b}^\dagger_{-p}\end{pmatrix}, \tag{3.31}$$

where we introduced the time-dependent coupling Matrix M_p. These are differential equations coupling modes with momenta $\pm p$. To solve these equations we perform a time-dependent Bogoliubov transformation [92]

$$\hat{b}_p = u_p(t)\hat{b}_p(0) + v_p^*(t)\hat{b}^\dagger_{-p}(0), \tag{3.32}$$

$$\hat{b}^\dagger_p = u_p^*(t)\hat{b}^\dagger_p(0) + v_p(t)\hat{b}_{-p}(0), \tag{3.33}$$

which maps the time dependence of the operators to the coefficients, for which we introduce the notation $\mathbf{R}_p = (u_p(t), v_p(t))^t$. In this way, the Heisenberg equations of motion get mapped to coupled differential equations for $\mathbf{R}$, that can be written in the form

$$\mathrm{i}\partial_t \mathbf{R}_p(t) = M_p(t)\mathbf{R}_p(t), \quad \mathbf{R}_p(0) = (1,0)^T. \tag{3.34}$$

In general these equations cannot be solved analytically, since diagonalizing the time-dependent matrix $M_p(t)$ always creates non-adiabatic corrections that are off-diagonal, i.e., the transformed equations will again be coupled. Let us consider the matrix S_p such that $S_p^{-1}M_pS_p$ is diagonal and use this to transform the equations of motion, where the transformed equations of motion for $\mathbf{R}_p^{(1)} = S_p^{-1}\mathbf{R}_p$ are given by

$$\mathrm{i}\frac{d}{dt}\mathbf{R}_p^{(1)}(t) = S_p^{-1}(t)M_p(t)S_p(t)\mathbf{R}_p^{(1)}(t) + \dot{S}_p^{-1}(t)S_p(t)\mathbf{R}_p^{(1)}(t), \tag{3.35}$$

with initial condition $\mathbf{R}_p^{(1)}(0) = S_p^{-1}(1,0)^T$. Thus, the diagonalization of the time-dependent matrix $M_p(t)$ does not diagonalize the equations of motion as a new off-diagonal coupling arises, proportional to $\dot{S}_p^{-1}S_p$. Consequently, the initial value problem (3.34) can in general only be solved numerically.

Assuming that a solution $\mathbf{R}_p(t)$ exists we can calculate the time dependent correlation function of the bosonic operators,

$$\begin{aligned}\langle[\hat{b}^\dagger_p(t) + \hat{b}_{-p}(t)][\hat{b}^\dagger_{-p}(t) + \hat{b}_p(t)]\rangle &= \Big\langle\big\{[u_p^*(t) + v_p^*(t)]\hat{b}^\dagger_p(0) + [u_p(t) + v_p(t)]\hat{b}_{-p}(0)\big\}\\ &\qquad\times\big\{[u_p^*(t) + v_p^*(t)]\hat{b}^\dagger_{-p}(0) + [u_p(t) + v_p(t)]\hat{b}_p(0)\big\}\Big\rangle\\ &= [u_p^*(t) + v_p^*(t)]^2\,\langle\hat{b}^\dagger_p(0)\hat{b}^\dagger_{-p}(0)\rangle + [u_p(t) + v_p(t)]^2\,\langle\hat{b}_{-p}(0)\hat{b}_p(0)\rangle\\ &\qquad + |u_p(t) + v_p(t)|^2\,\langle\hat{b}^\dagger_p(0)\hat{b}_p(0) + \hat{b}_{-p}(0)\hat{b}^\dagger_{-p}(0)\rangle\,.\end{aligned} \tag{3.36}$$

Making use of the correlation function (3.28) at $t = 0$ this can be simplified to

$$\langle[\hat{b}_p^\dagger(t) + \hat{b}_{-p}(t)][\hat{b}_{-p}^\dagger(t) + \hat{b}_p(t)]\rangle \\ = \coth(v_\mathrm{s}(0)|p|/2T) \times \left\{ K_0 \Re[u_p(t) + v_p(t)]^2 + \frac{1}{K_0} \Im[u_p(t) + v_p(t)]^2 \right\}, \quad (3.37)$$

where $K_0 = K(t = 0)$.

We note that a correction $\dot{S}_p^{-1} S_p$ in Eq. (3.35) appears that again is an off-diagonal matrix proportional to $\dot{K}/K$. For sufficiently small $\dot{K}(t)$, one can find a perturbative solution which reflects the gaplessness of the Luttinger liquid. Comparing the off-diagonal terms to the difference of the diagonal terms we find that the off-diagonal coupling can be neglected, if

$$|v_\mathrm{s}(t)p| \gg \left| \frac{1}{4} \frac{\dot{K}(t)}{K(t)} \right|. \quad (3.38)$$

To be fully adiabatic this condition has to be fulfilled at all times and for all relevant momentum modes p. However, this is impossible to achieve for small momenta p, since the Luttinger model is gapless. Consequently, a dynamical protocol cannot be used to transform a ground state of weakly interacting Rydberg polaritons adiabatically to the strongly interacting regime.

Nevertheless we can assume that the time scale on which $K(t)$ changes is bounded, giving rise to a critical momentum p_c, such that all momentum modes with $|p| > p_\mathrm{c}$ obey (3.38) at all times. Then we expect a crossover between modes with p being larger and smaller p_c from an adiabatic following ($p \ll p_c$) of the storage protocol to a diabatic following, i.e., a sudden quench ($p \gg p_c$). The momentum scales are related to length scales of the correlation functions. Large momenta correspond to small distances and small momenta to large distances. That means, the crossover momentum scale p_c can be related to a crossover length scale $L_\mathrm{c} \sim 1/p_\mathrm{c}$.

From this simple argument we conclude that correlation functions can adiabatically follow a sufficiently slow quench over a finite distance, while correlation functions on large scales always exhibit diabatic behavior. Consequently, true long-range order cannot be obtained in a Luttinger liquid model.

3.4 Reaching the strongly interacting regime

In the Luttinger model true long-range order can not be achieved, due to the gaplessness of the model, but very slowly decaying correlation functions can be achieved by a slow quench. However, so far we neglected the fact that we employed the Luttinger model in a moving frame and the underlying microscopic model is propagating in space. As experimental realizations require a finite medium length L, the characteristic storage time has to be restricted such that the Rydberg polaritons get

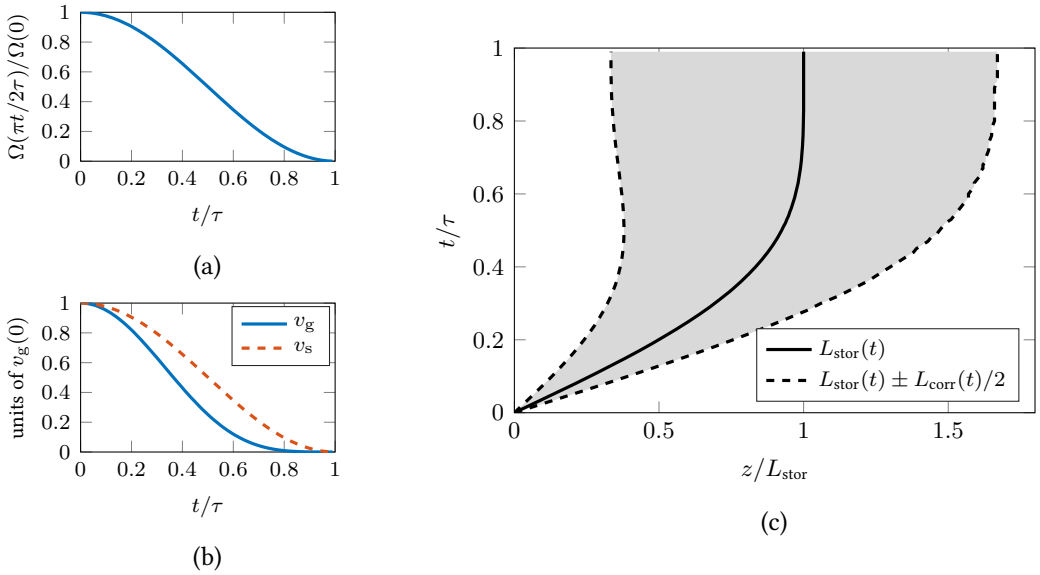

Figure 3.8: Pulse propagation and spreading of correlations during storage. (a) The time dependent control field $\Omega(t) \propto \cos^2(\pi t/2\tau)$ defines the protocol. (b) Group velocity $v_g(t)$ and speed of sound $v_s(t)$ during the protocol in units of $v_g(0)$. (c) Light-cone like spreading of correlations of a propagating pulse during storage. We set $v_s(0) = v_g(0) = 0.01c$ for the initial velocities[2].

stored before leaving the medium. This condition can be put in the form

$$L_{\text{stor}} = \int_0^\infty \mathrm{d}s\, v_g(s) < L, \tag{3.39}$$

where L_{stor} denotes the distance a pulse travels inside the medium during the storage. This condition sets a limit on the characteristic storage time, and thus the question arises, if long-range correlations inside the medium can be achieved. As the correlations propagate with the speed of sound v_s we can analogously to (3.39) define a correlation length during storage by

$$L_{\text{corr}} = \int_0^\infty \mathrm{d}s\, v_s(s). \tag{3.40}$$

Then states with long-range correlations are experimentally accessible, if $L_{\text{corr}} > L$, or, alternatively, $L_{\text{corr}} \gg L_{\text{stor}}$. That is the case, if the speed of sound is large compared to the group velocity. To answer the question if this holds true, we note that in any Galilean invariant system[1] the speed of sound is determined by the relation $v_s = \pi\rho_0/(mK)$ where the mass m and the Luttinger parameter K are both time-dependent. The mass is inverse proportional to the group velocity, cf. Eq. (2.40) and

[1] And approximately for the bulk of sufficiently large finite systems.

furthermore K is a unique function of m, which in the strongly interacting limit can be approximated by $K(t) \propto [m(t)]^{-1/2}$, which can be derived from Eq. (3.8) together with (3.2). Combining these relations, we can determine the time-dependence of the speed of sound by

$$v_{\mathrm{s}}(t) = v_{\mathrm{s}}(0) \times \sqrt{\frac{v_{\mathrm{g}}(t)}{v_{\mathrm{g}}(0)}}. \tag{3.41}$$

In the case of slow light we can assume $v_{\mathrm{s}}(0) \approx v_{\mathrm{g}}(0)$ for the initial velocities[2]. Thus the speed of sound tends slower to zero as the group velocity during storage, allowing correlations to spread faster as the pulse propagates and consequently allows to create a correlated state during storage of a pulse of Rydberg polaritons. This is illustrated in Figure 3.8 for a storage protocol $\Omega(t) \propto \cos^2(\pi t/2\tau)$, (a) shows the protocol, (b) the time-dependence of the velocities and (c) illustrates the spreading of correlations of a propagating pulse.

Note, that the approximate relation $K \propto 1/\sqrt{m}$ overestimates the Luttinger parameter and subsequently underestimates the speed of sound, i.e., the result is further improved when taking the correct relation.

3.4.1 An exactly solvable case

As argued in the previous section, the equations of motion, Eq. (3.31), for the bosonic modes of the Luttinger model can, in general, not be solved analytically for time-dependent parameters. Moreover, we showed that no perturbative solution exists for arbitrary momenta, as the Luttinger Hamiltonian is gapless. One possible way to solve the equations of motion is in using numerical methods, which we will employ in the next section. The form of the transformed Equations of motion (3.35), however, gives rise to another, analytical way to solve the equations, which we will discuss now.

We want to solve an initial value problem (IVP) with a system of linear differential equation given in vector-matrix form by

$$\mathrm{i}\frac{d}{dt}\mathbf{R}^{(0)}(t) = M_p^{(0)}(t)\mathbf{R}^{(0)}(t), \quad \mathbf{R}^{(0)}(0) = \mathbf{R}_0. \tag{3.42}$$

We try to find a solution of this IVP by performing a series of n linear transformations, where $S^{(n)}$ denotes the nth transformation matrix as follows. First, starting from the original problem (3.42), we find the matrix $S^{(1)}(t)$, such that

$$D^{(1)}(t) = [S^{(1)}(t)]^{-1} M_p^{(0)}(t) S^{(1)}(t) = \text{diag}. \tag{3.43}$$

[2]This assumption is reasonable, as under the assumption of $v_{\mathrm{g}}(0) \ll c$ the ratio of both velocities is given by $v_{\mathrm{s}}(0)/v_{\mathrm{g}}(0) = \sqrt{\pi^5/45}(\rho_0 R_{\mathrm{B}})^3$ with $\rho_0 R_{\mathrm{B}} \leq 1$.

is a diagonal matrix. Applying this transformation to the IVP by multiplying with $[S^{(1)}]^{-1}$ and inserting $\mathbb{1}$s yields

$$\mathrm{i}[S^{(1)}(t)]^{-1}\frac{d}{dt}\left[S^{(1)}(t)[S^{(1)}]^{-1}\mathbf{R}^{(0)}(t)\right] = [S^{(1)}(t)]^{-1}M_p^{(0)}(t)S^{(1)}(t)\mathbf{R}^{(0)}(t), \quad \mathbf{R}^{(0)}(0) = \mathbf{R}_0$$

This can be rearranged to

$$\begin{aligned}\mathrm{i}\frac{d}{dt}\mathbf{R}^{(1)}(t) &= \left\{D^{(1)}(t) - \mathrm{i}[S^{(1)}(t)]^{-1}\partial_t S^{(1)}(t)\right\}\mathbf{R}^{(1)}(t) \\ &=: M_p^{(1)}(t)\mathbf{R}^{(1)}(t), \quad R^{(1)}(0) = [S^{(1)}(0)]^{-1}\mathbf{R}_0. \end{aligned} \tag{3.44}$$

We observe that the diagonalization of the time-dependent matrix $M_p^{(1)}(t)$ requires a second time-dependent diagonalization matrix $S(t)$ and this leads subsequently to new off-diagonal couplings in the differential equation. An exact diagonalization of the differential equation can thus not be achieved in general. Neglecting these second order coupling corresponds to a so-called super-adiabatic approximation [93].

To get a better approximation we can iterate the above procedure n times which has been investigated [93] and leads to a transformed initial value problem of

$$\mathrm{i}\frac{d}{dt}\mathbf{R}^{(n)}(t) = M_p^{(n)}(t)\mathbf{R}^{(n)}(t), \qquad \mathbf{R}^{(n)}(0) = [S^{(n)}(0)]^{-1}\cdots[S^{(1)}(0)]^{-1}\mathbf{R}_0. \tag{3.45}$$

Dropping now the off-diagonal corrections of nth order gives a higher order adiabatic approximation.

Typically one finds, that the accuracy of the deviation of the nth order adiabatic solution from the exact solution first decreases with n but at a certain n this behavior changes and the further iterations make the approximation again worse. However, there exist special cases where the equations get diagonalized by n iterations and thus an exact solution can be found. Such a super-adiabatic solution can also be found for Eq. (3.31) as follows. We repeat the diagonalization procedure with Eq. (3.35) by calculating the Matrix $S_p^{(1)}(t)$ that diagonalizes the Matrix $M_p^{(1)}(t)$. This step again preserves the structure of the equations of motion, i.e., results in an equation with the same form as the original equation, with off-diagonal coupling by the matrix

$$\left[\dot{S}_p^{(1)}\right]^{-1} S_p^{(1)} = \frac{\mathrm{d}}{\mathrm{d}t}\left[\frac{\partial_t K(t)}{K(t)v_\mathrm{s}(t)}\right]\begin{pmatrix}0 & 1\\ -1 & 0\end{pmatrix}. \tag{3.46}$$

Expressing the speed of sound by $v_\mathrm{s} = \pi\rho_0/mK$ and employing the unique relation of Luttinger parameter K and effective polariton mass m, cf. Figure 3.2, we can find a special time-dependence of $K(t)$, such that expression (3.46) vanishes at all times. With the approximation for small K, where

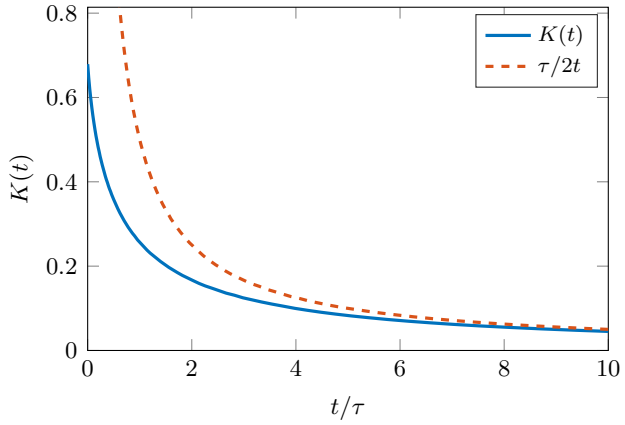

Figure 3.9: Blue, solid line: function $K(t)$ for the super-adiabatic protocol, Eq. (3.47) for $K_0 = 0.679$; red, dashed line: asymptote for large t.

$v_s(t) \propto K(t)$, this yields a differential equation for $K(t)$ that has the solution

$$K(t) = e^{-\operatorname{acosh}(t/\tau + C)}, \tag{3.47}$$

where $C = \frac{1}{2}(K_0 + 1/K_0)$ and τ is the characteristic time of the smooth quench. In the limit of large time, $t \gg \tau$, the leading order term is given by $K(t) \approx \tau/2t$, as indicated by the dashed line in Figure 3.9. Note that it is a very slow decay, thus it takes long times to reach the limit of $K \ll 1$. For the time-dependence (3.47) of the Luttinger parameter, the off-diagonal couplings, Eq. (3.46) vanish, i.e., a second iteration of the diagonalization transformation diagonalizes the Eqs. (3.35) and they can be solved analytically. This corresponds to exact super-adiabaticity.

Before we discuss this solution in detail, let us calculate the crossover and correlation lengths L_c and L_{corr}, respectively, to get some insight into the solution. As by construction for the special solution (3.47) the derivative in Eq. (3.46) vanishes at all times, the critical momentum p_c becomes a constant of time, given by

$$p_c = \left| \frac{\dot{K}(t)}{K(t) v_s(t)} \right| = \frac{\eta}{\tau} = \text{const.}, \tag{3.48}$$

where $\eta^{-1} = \frac{1}{2}(\rho_0 R_B)^5 d_B \frac{\gamma}{\Delta} v_g(0)$ is defined by the relation $\eta v_s = (K\Theta)^{-1}$, cf. Eq. (3.5). The inverse of momentum scale p_c defines the crossover length between adiabatic and diabatic correlations,

$$L_c = \frac{1}{p_c} = \frac{1}{2}(\rho_0 R_B)^5 v_g d_B \frac{\gamma}{\Delta} \tau, \tag{3.49}$$

where the constants R_B, v_g, d_B on the right-hand side have to be taken at the initial time. The crossover length is proportional to the characteristic quench time τ, the initial group velocity v_g and

the optical depth per blockade d_{B}. It is very sensitive to the initial excitation density per blockade $\rho_0 R_{\mathrm{B}}$. This length scale appears in the exact super-adiabatic solution of the equations of motion, which assumes the form

$$\mathbf{R}_p(t) = \begin{pmatrix} e^{-\mathrm{i}\xi(t)/L_{\mathrm{c}}} & 0 \\ 0 & e^{\mathrm{i}\xi(t)/L_{\mathrm{c}}} \end{pmatrix} \mathbf{R}_p^{(2)}(0), \tag{3.50}$$

where $\xi(t) = \frac{1}{2L_{\mathrm{corr}}(t)}\sqrt{p^2 L_{\mathrm{c}}^2 - 1}$ and $\mathbf{R}_p^{(2)}(0) = \left[S_p^{(1)}\right]^{-1} S_p^{-1}\mathbf{R}_p(0)$. We observe that for increasing p at the critical momentum scale $p = p_{\mathrm{c}}$ the square root changes from an imaginary to a real, positive quantity, i.e., the character of the solution changes qualitatively. How this affects the correlation functions, we will analyze in the following paragraph. The correlation length is defined by the integral (3.40), which can be calculated for the time dependence (3.47), yielding

$$L_{\mathrm{corr}}(t) = \int_0^t \mathrm{d}s\, v_{\mathrm{s}}(s) = \frac{L_{\mathrm{c}}}{2} \ln\left(\frac{K(0)}{K(t)}\right). \tag{3.51}$$

L_{corr} denotes the maximal distance, where correlations can built up during storage. This length is given by $L_{\mathrm{c}}/2$ times logarithmic corrections and diverges logarithmically for $K(t) \to 0$. For large times the K-parameter vanishes like $K(t) \propto \tau/2t$, thus in this special protocol it takes very long times to reach small K parameters.

3.4.2 Correlation functions in the super-adiabatic case

With the super-adiabatic solution derived in the previous section it is now straightforward to invert the transformations and obtain the time evolution of the operators $\hat{b}_p^\dagger(t)$ and $\hat{b}_p(t)$ and then correlation functions of these. In Chapter 2 we performed numerical simulations of two polaritons propagating under stationary slow light conditions in the weakly interacting regime and found that after an initial transient they evolve into a state close to the two-polariton ground state, see Figure 2.12(c). Thus it is reasonable to assume that the initial state of the many-body model is close to the many-body ground state or a low-temperature thermal state and we choose such a state for the calculations of the time-dependent Luttinger model as initial state. The initial LL-Hamiltonian for $t \leq 0$ is time-independent, and can be diagonalized by a rescaling of the parameters [10], or by a Bogoliubov transformation [92]. The p-dependent matrix generating the Bogoliubov transformation is equal to $S = S_p(0)$, we introduced in Eq. (3.35). The resulting diagonal Hamiltonian reads

$$\hat{\mathcal{H}} = v_{\mathrm{s}}(0) \sum_{p\neq 0} |p| \hat{\gamma}_p^\dagger \hat{\gamma}_p. \tag{3.52}$$

To begin with, let us consider the case of zero Temperature, $T = 0$. In this case the correlations functions in the operators $\hat{\gamma}_p^\dagger, \hat{\gamma}_p$ are given by

$$\langle \hat{\gamma}_p \hat{\gamma}_q^\dagger \rangle = \delta_{p,q}. \tag{3.53}$$

After obtaining the corresponding initial state of the operators $\hat{b}_p^\dagger, \hat{b}_p$ we can calculate arbitrary time-dependent correlation functions during a light storage protocol with the solution (3.50). In particular, we can calculate the equal time density-density correlations, which are in Luttinger liquid theory of the universal form [10],

$$\langle \rho(z)\rho(0)\rangle = \rho_0^2 - \frac{K}{2\pi}\frac{1}{z^2} + A_2\rho_0^2 \cos(2\pi\rho_0 z) e^{-2G_{\Phi\Phi}(z)} + \ldots, \tag{3.54}$$

i.e., determined by the correlation function $G_{\phi\phi}(z,t) = \langle[\phi(z) - \phi(0)]^2\rangle$. This can be derived from (1.52), see also (3.27). For the time-independent ground state the density-density correlation function reduces to the expression (1.54). For the protocol (3.47) we can derive this time-dependent correlation function with Eq. (3.36) and (3.50), leading to

$$\begin{aligned} G_{\phi\phi}(z,t) &= \int \mathrm{d}p\, \frac{1-\cos(pz)}{p} \langle (\hat{b}_p^\dagger + \hat{b}_{-p})(\hat{b}_{-p}^\dagger + \hat{b}_p)\rangle \\ &= K(t) \int \mathrm{d}p\, \frac{e^{-\alpha p}}{p}[1-\cos(pz)] \left\{ 1 - \frac{\sin[2\xi(t)/L_\mathrm{c}]}{\sqrt{L_\mathrm{c}^2 p^2 - 1}} + \frac{1-\cos[2\xi(t)/L_\mathrm{c}]}{L_\mathrm{c}^2 p^2 - 1} \right\}, \end{aligned} \tag{3.55}$$

where we introduced the cutoff α to treat high-momentum divergences. For the integral (3.55) no closed expression exists, i.e., further integration can only be done numerically. However, for the limiting cases for small and large momentum modes p, compared to p_c, we can derive asymptotic results. These correspond to large and small distances z, respectively, as compared to L_c. Since the correlation length L_corr is growing logarithmically with K according to (3.51), i.e., only slowly, we assume that $L_\mathrm{c} \lessapprox L_\mathrm{corr}(t)$. In the regime $p \gg p_\mathrm{c}$ the terms $\cos(2\xi(t)/L_\mathrm{c})$ and analogously $\sin(2\xi(t)/L_\mathrm{c})$ oscillate quickly in p and thus average to zero in the integral. Within this approximation we find a closed expression for (3.55),

$$G_{\phi\phi}(z,t) = -K(t)\ln\Big(\frac{\alpha}{z}\Big) + \text{const.}, \tag{3.56}$$

in the limit of small α. The correlation function has the form of ground state correlation function with a power law in the density-density correlations, where the exponent is given by $2K(t)$. Hence, for distances $z \ll L_\mathrm{c}$ the correlations follow adiabatically the (moving-frame) ground state in the light storage protocol and become long-range for $K(t) \to 0$, indicating a quasi-crystalline order. However, in the regime of large distances $z \gg L_\mathrm{c}$, corresponding to momenta $p \ll p_\mathrm{c}$, the function

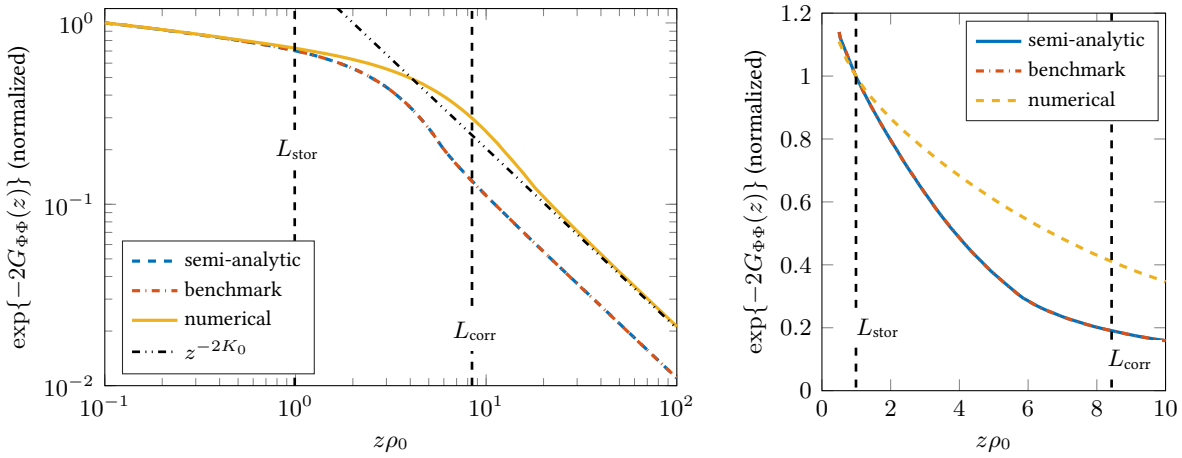

(a) Log-log (b) Linear

Figure 3.10: Spatial envelope $\exp\{-2G_{\Phi\Phi}(z, t_{\text{max}})\}$ of the density-density correlations after a smooth quench according to the storage protocol (3.47) with $K_0 = 0.5$, $\tau = 4/\rho_0 v_{\text{g}}(0)$ and a total time of $t_{\text{max}} = 24\rho_0 v_{\text{g}}(0)$. (a) Log-log representation normalized to the value at $z\rho_0 = 0.1$ and (b) linear representation normalized to the value at $z\rho_0 = 1$ show the semi-analytical solution (3.55) (blue, dashed line) compared to a numerical integration of the equations of motion with $\Theta(K)$ as in Eq. (3.8) as a benchmark (red, dash-dotted line) and $\Theta(K)$ obtained from interpolating the DMRG results displayed in Figure 3.5 (yellow solid line). The black dash-double-dotted line shows the initial spatial envelope of the density-density interactions given by a power law with exponent $-2K_0$. Finally, the vertical dashed lines indicate the length scales L_{stor} and L_{corr} obtained from integrating $v_{\text{g}}(t)$ and $v_{\text{s}}(t)$, respectively.

$\xi(t)$ becomes purely imaginary and can be approximated by $\mathrm{i}\ln(K(0)/K(t))$. Then the integral (3.55) has the same form as Eq. (3.56), but we have to replace $K(t) \to K(0)$. That means that for large distances the storage is diabatic, i.e., the initial correlation functions get frozen and decay spatially with the initial exponent $2K(0)$. This agrees with the crossover from an adiabatic to a diabatic regime which we expected in the previous section.

3.4.3 Numerical integration

A full expression for the density-density correlations after the storage can be obtained numerically by integrating Eq. (3.55). In Figure 3.10 we show the resulting curves in log-log and linear representation. For comparison we show a power law with the exponent of the initial correlations.

In the derivation of this semi-analytic result we obtained the relation between the Luttinger parameter K and the system parameters from Eq. (3.8), which allowed us to find the super-adiabatic solution (3.55). However, this relation is only asymptotically correct. As we have an exact relation available, obtained by interpolating the data points calculated by DMRG shown in Figure 3.2, we can

also calculate the correlation function using this relation. To this end, we integrate the initial value problem (3.34) numerically with a time-dependent Luttinger parameter K given by (3.47) and the speed of sound determined by Eq. (3.5) and the relation between mass and K obtained by DMRG, see Figure 3.2.

The resulting curves are shown in Figure 3.10. Both results show the expected crossover at a length scale L_{corr} from an adiabatic to a diabatic regime. For large distances the correlation function decays as a power law with the initial exponent $2K_0$. Note that this exponent is different for the numerical solution and the semi-analytical solution, which comes about due to the fact that for equal dimensionless interaction strength Θ_0 the relations yield different K_0, cf. Figure 3.2. Consequently, the numerically calculated correlation function exhibits slower decaying correlations. In the case of short distances an approximation by a power law with the adiabatic exponent K_f does not make much sense, as this behavior is only asymptotically assumed for $z \to 0$. We find that a much better fit can be obtained by a Gaussian function $e^{-z^2/2\sigma^2}$ with a FWHM[3] of σ which agrees well with the correlation functions almost up to a length of $z = L_{\text{corr}}$. Moreover, this fit allows to extract a correlation length, which will be considered in the following in greater detail.

In conclusion, this result shows that the strongly interacting regime can be reached with correlations up to a certain distance.

3.4.4 Thermal excitations

Now we want to consider corrections onto the final correlation functions of the created charge-density wave, when the initial state of Hamiltonian (3.52) exhibits thermal excitations. For a temperature T the correlations (3.53) get modified to (3.26),

$$\langle \hat{\gamma}_p \hat{\gamma}_q^\dagger \rangle = \delta_{p,q} \coth\big(v_{\text{s}}|p|/2T\big).$$

The argument of the $\coth$ defines a thermal length $L_T \sim \pi\rho_0/(mTK)$ marking a crossover from a power law decay of the spatial correlation function to an exponential decay [34].

Let us now derive the time evolution of this initial state under a polariton storage protocol. As we have shown numerically and used in the previous section, the initial state created under stationary propagation of a two-photon pulse into a Rydberg medium is close to the ground state. As the Rydberg polaritons can only be excited inside the EIT window, we can estimate the maximal allowed momentum fluctuations by

$$|k| \leq |k_{\text{max}}| = \frac{\Omega_{\text{eff}}^2}{c|\Gamma|}. \tag{3.57}$$

Excitations with a kinetic energy corresponding to $k > k_{\text{max}}$ couple to bright-state polariton degrees of freedom which are subject to losses, cf. Section 2.1.3, and thus quickly disappear. Hence, when

[3] Full width at half maximum

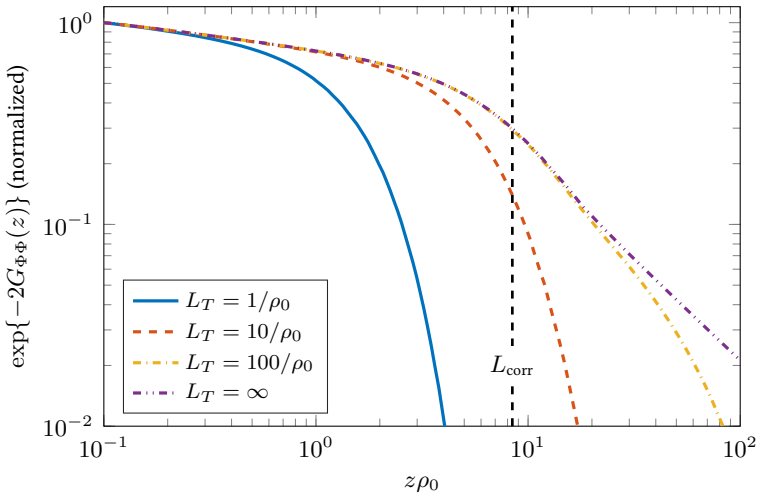

Figure 3.11: Log-log plot of the correlation function $e^{-2G_{\phi\phi}(z)}$ after storage of an initial state with initial excitations for different temperatures T characterized by the thermal length L_T. $L_T = \infty$ corresponds to the case $T = 0$, i.e., an initial ground state. The dashed vertical line indicates the correlation length L_{corr} obtained in the case $T = 0$ by integrating the sound velocity v_{s} in time.

modeling excitations of the initial state within the EIT window by a finite temperature T_0, we can estimate an upper bound for this temperature by $k_{\mathrm{B}}T_0 \leq \Omega_{\mathrm{eff}}^2(0)/(2m|\Gamma|c)$ corresponding to a thermal length scale [34] of

$$L_T \geq \frac{v_{\mathrm{s}}K}{\pi T} = 2\rho_0 R_{\mathrm{B}} \frac{|\Delta|}{\gamma} d_{\mathrm{B}}^{-1}, \tag{3.58}$$

where we set $k_{\mathrm{B}} = 1$. We take these thermal excitations into account in the initial correlation functions (3.26) of the time-dependent Luttinger model. Analog to the ground-state case we calculate the time evolution of the density-density correlations during storage. The resulting curve is displayed in Figure 3.11.

The behavior of the correlation function at small distances is again described by a Gaussian function which agrees very well with the numerically integrated correlation function up to large distances. For distances $z \gg L_T$ the correlation function crosses over to an exponentially decaying function similar to the initial state. However, the crossover point depends on the scale L_{c}. Therefore, the regime of adiabatic following may be extended beyond the initial thermal length scale L_T. To analyze this properly, we extract the crossover length scale in the finite temperature case, $L_{\mathrm{corr},T}$, by finding the value, where the correlations are decayed to $1/2$, i.e., where

$$G_{\phi\phi}(z = L_{\mathrm{corr},T}, t = t_{\mathrm{max}}) = \frac{1}{2}\log(2). \tag{3.59}$$

The length obtained by this is then compared to the correlation length L_{corr} in the absence of

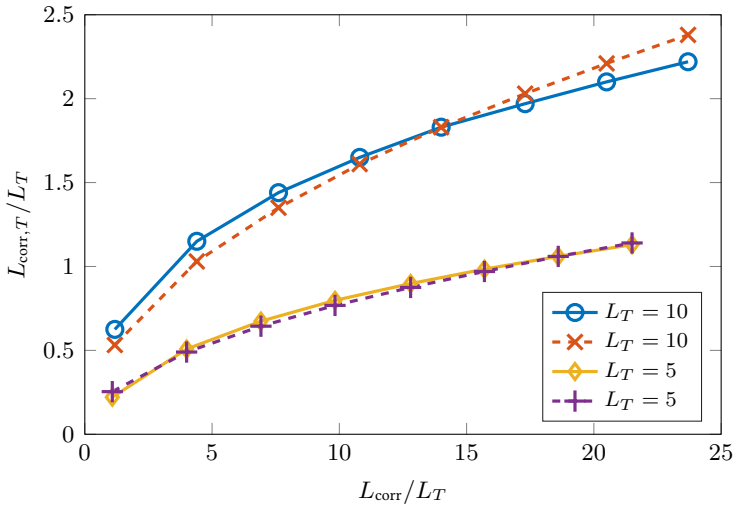

Figure 3.12: Plot of the correlation length after storage in the case of an initial state with thermal excitations $L_{\mathrm{corr},T}$ where the correlation function $e^{-2G_{\phi\phi}(z)}$ decayed to $1/2$ as function of the correlation length L_{corr} after storage in the absence of thermal excitations, obtained from integrating the sound velocity v_{s} over the storage protocol. Both axes are rescaled by the thermal excitation length. The blue circles (yellow diamonds) show the results obtained from numerically integrating the time evolution of the correlation function $G_{\phi\phi}(z)$ with an initial thermal length of $L_T = 10$ ($L_T = 5$). The red x's (violet crosses) connected by dashed lines are analytical curves $\propto \sqrt{L_{\mathrm{corr}}}$ according to Eq. (3.60). For obtaining these results a Lorentzian function has been used as protocol. The parameters are $L_T = 10$, $K_0 = 0.25$, $\Theta_0 = 1.99$ and $K(t_{\mathrm{max}}) = 0.018$ for the upper curves and $L_T = 5$, $K_0 = 0.5$, $\Theta_0 = 0.12$ and $K(t_{\mathrm{max}}) = 0.029$ for the lower curves. The lines connecting the points are a guide to the eye.

thermal excitations. To this end we performed storage with initial thermal excitations by numerically calculating the time evolution of $G_{\phi\phi}(z,t)$ during storage, according to a protocol with a Lorentzian shape, $\Omega(t) = \Omega(0)/(1+t^2/\tau^2)$. The storage is performed up to a maximal time $t_{\max}$. We change the maximal time $t_{\max}$ and the characteristic switching time τ such that the final Luttinger parameter $K(T)$ is constant for all runs. In this way, we obtain $L_{\mathrm{corr},T}$ for different values of L_{corr}. In Figure 3.12 we show the resulting curves for $L_T = 5, 10$, where both axes are rescaled by L_T. We find that $L_{\mathrm{corr},T}$ behaves in good agreement as a function $L_{\mathrm{corr},T} \propto \sqrt{L_{\mathrm{corr}}}$, see Figure 3.12. Specifically we find that the relation is given by

$$L_{\mathrm{corr},T} \approx \frac{1}{2\pi\alpha}\sqrt{L_{\mathrm{corr}} L_T}, \tag{3.60}$$

where $\alpha = K_0[\log(K_0/K_f)]^{1/4}$. Thus, the correlation length after storage is given by the geometrical mean of thermal length scale L_T and the correlation length L_{corr} attained in the absence of thermal excitations.

The result (3.60) is a remarkable result. It shows that by storage of Rydberg polaritons a Wigner crystal can be obtained with a finite correlation length larger twice the storage length L_{stor}, even if the initial state exhibits large thermal fluctuations.

3.5 Experimental feasibility

In this section we want to address limitations arising in an experimental realization of the proposed Rydberg polariton storage and their influence on the results.

Finite medium length. In experimental realizations only finite medium lengths are available. These are typically on the order of some $10\,\mu\mathrm{m}$ for typical quantum optical setups, cf. [8, 44, 45]. Thus the typical time scale τ of a photon storage protocol has to be limited such that the distance the polaritons travel during storage is less than the medium length, i.e., the pulse gets to a full halt inside the atomic medium. As the Rydberg polaritons travel with the group velocity v_{g}, the distance they propagate inside the medium is given by the integral (3.39), which in the case of the super-adiabatic protocol, Eq. (3.47), can be integrated analytically,

$$L_{\mathrm{stor}} = \int_0^\tau \mathrm{d}s\, v_{\mathrm{g}}(s) \leq v_{\mathrm{g}}(0)\Theta_0 K_0 \tau. \tag{3.61}$$

As for a finite system this length scale is ultimately limited by the system length, we compare L_{stor} to the correlation length L_{corr} in case of the super-adiabatic protocol. Taking the quotient of these two, the time scale τ cancels and we get the maximal correlation length that can be achieved for a given

storage length L_{stor} as

$$\frac{L_{\text{corr}}}{L_{\text{stor}}} = \frac{\pi^4}{45}\frac{\rho L_{\text{abs}}}{K_0}\frac{|\Delta|}{\gamma}\ln\left(\frac{K_0}{K_{\text{f}}}\right), \tag{3.62}$$

where the initial K_0 is also dependent on $\rho_0 R_{\text{B}}$ and d_{B}. An experimentally feasible K_0 can be read off Fig. 3.5. This shows that it is possible to get to the regime of strong correlations with a correlation length on the order of the medium length for sufficiently small final K_{f}.

Note that realizing Rydberg EIT inside hollow-core fibers [52, 53], allows for much longer one-dimensional atomic setups, relaxing these conditions.

Non-adiabaticity. Under continuous wave (*cw*) EIT conditions the validity of the model was guaranteed as long as the initial pulse width fitted inside the EIT window, defined by Eq. (1.12). In a dynamical setup, when using a time dependent control field, this condition has to be modified and additionally $\partial_t\theta(t) \ll \sin\theta\cos\theta\Omega_{\text{eff}}/|\Gamma|$. This restricts the characteristic switching times (denoted τ above) during which an input pulse can get stored, cf. (1.21). For the protocol (3.47) the nonadiabatic coupling $\propto \partial_t\theta$ is bounded by its value at $t = 0$. We find the condition

$$\tau \gg 2\frac{L_{\text{abs}}|\Gamma|}{c\gamma}\frac{K_0}{(K_0^2-1)^2}. \tag{3.63}$$

We combine this expression with Eq. (3.61), and set $L_{\text{stor}} = L/2$ leading to a lower bound on the total optical depth $d = L/L_{\text{abs}}$ of the system,

$$d \gg \frac{\cos^2\theta}{\pi}\frac{\gamma}{|\Gamma|}(\rho_0 R_{\text{B}})^4 d_{\text{B}}^2\frac{K_0^2}{(K_0^2-1)^2}. \tag{3.64}$$

Although this expression diverges for $K_0 \to 1$ it can easily be fulfilled for values $K_0 \lesssim 0.8$ and $d_{\text{B}} \approx 10$ which are reasonable initial values, cf. Figure 3.5, as $\cos^2\theta \ll 1$ under slow light conditions. Consequently the storage of Rydberg polaritons is always adiabatic in terms of the polariton model. This justifies the use of Luttinger liquid theory despite using an explicit time-dependence of the parameters.

3.6 Conclusion

In summary, we considered many-body properties of Rydberg polaritons propagating under conditions of EIT. Specifically, we considered the regime of off-resonant driving and strong repulsive interactions in terms of large optical depth per blockade, where the physics is described by the many-body Hamiltonian derived in the previous chapter. We considered many-body ground states of this model calculated using DMRG calculations with open boundary conditions (provided by D. Muth), showing strong density correlations. Particularly, we determined non-universal coefficients of the theoretical

density-density correlations of a Luttinger liquid by fitting the DMRG results and showed that the numerically obtained result is described by Luttinger liquid theory with a very good agreement. We showed that the regime of strong correlations is difficult to reach under stationary EIT conditions, as the experimentally accessible interaction strength, quantified by the ratio of interaction and kinetic energy Θ cannot be made sufficiently large while retaining sufficiently large excitation densities. However, this restriction can be overcome when dynamically changing the interaction strength. In this way it is possible to reach the strongly interacting regime by turning propagating polaritons into a stationary density wave of Rydberg excitations. We argued that a storage of Rydberg polaritons is possible, despite the space-dependent two-photon detuning induced by the interaction, which we confirmed for two polaritons using two-excitation wave-function simulations. Moreover, in a dynamical finite polariton excitation densities can be preserved.

We used a time-dependent Luttinger liquid theory to calculate the time-evolution of density-density correlations of the stored density wave. As the Luttinger liquid is a gapless theory, a fully adiabatic storage can intrinsically not be achieved. By finding a storage protocol allowing to construct an exact super-adiabatic solution of the time-dependent correlation functions, we could gain analytical insight. We showed that a strongly correlated density-wave of Rydberg excitations can be generated, with slowly decaying density-correlations that build up over a certain distance, marking a crossover to a diabatic regime exhibiting a power-law decay with initial the initial exponent. We confirmed this result by numerically solving the time evolution of the correlation functions. Furthermore we showed that even in the case of initial thermal excitations a finite-range Wigner crystal can be created and considered limitations. Finally, we considered limitations arising in experimental realizations of the proposed polariton storage and found that the protocol is feasible.

Releasing this state from the medium by turning the stored density wave back into a propagating pulse creates a Wigner crystal of photons correlated over a finite range, respectively time, that can be observed by interferometric methods, cf. [8].

Chapter 4

Bound states of Rydberg polaritons

In the previous section we considered dark-state polaritons propagating under conditions of electromagnetically induced transparency in a gas of Rydberg atoms. Specifically, we considered off-resonant driving conditions with a single-photon detuning Δ. We showed by numerical simulations that the $g^{(2)}$-function at small distances are strongly suppressed, see also [42]. These results have been confirmed by experiments in the group of V. Vuletic, see [8]. However, in a more recent publication they showed also bunching of photon pairs, [65], and even of three photons, [66, 94]. Naively, this seems to be contrary to the results we obtained in the previous section. However, the phenomenon can easily be explained by the existence of bound states of photons and the contribution of scattering states, as was done in [8, 95]. These publications investigated in particular the spectral properties of the system. We analyze the conditions for and the dynamics of the creation of the bunching phenomena and the dynamics at large times. To this end, we use a Green's function approach to analyze the interplay of two-photon bound states, i.e., photonic molecules, and the scattering continuum of two photons. We use numerical methods to simulate the full system and confirm the analytical results. We find that the scattering continuum leads to a robust phase shift which can be utilized to separate bound-state and scattering contributions by an interferometric detection scheme.

The results presented in this chapter are published in reference [Moos2017] as a collaboration with Razmik Unanyan and Michael Fleischhauer. In particular, I provided the numerical simulations and contributed to the analytical calculations.

4.1 Green's function approach

For strong interactions between Rydberg polaritons that lead to a large separation between these, the interactions can be treated as a perturbation of the free model, see [68]. However, this treatment does not capture the physics at short distances, particularly bound states and the associated bunching of polaritons, as has recently been shown to occur under certain conditions [65, 66, 95]. Instead of using perturbation theory, one has to consider the full scattering problem as was done in [95] (see also [67]).

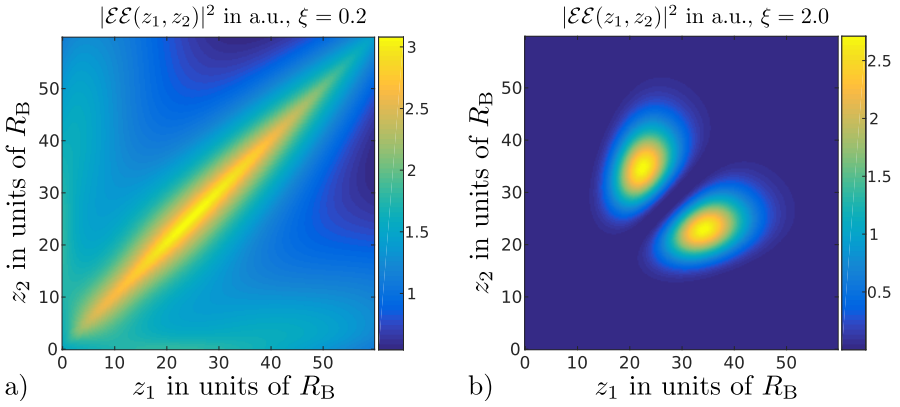

Figure 4.1: Time evolution of wave function for two excitations propagating inside a three-level medium, where we consider the propagation from free space into the medium, where the former is not displayed in the picture. Depending on the conditions two qualitatively different phenomena can be observed. a) Bunching for weak Rydberg interactions $d_\mathrm{B} = R_B/L_\mathrm{abs} = 0.2 \ll 1$, b) antibunching for strong interactions, $d_\mathrm{B} = 2 > 1$.

In [Moos2017] we employed a Green's function approach to treat the two-excitation problem. In the following we want to review and discuss this approach.

A system of Rydberg polaritons under conditions of EIT is described by the truncated paraxial wave equation for the operators $\hat{\mathcal{E}}, \hat{\sigma}_\mathrm{ge}, \hat{\sigma}_\mathrm{gr}$, Eq. (1.5). As we showed in Section 2.1, for sufficiently strong interactions as well as sufficiently small excitation densities, the system can be described by a one-dimensional model.

Let us assume that the time evolution of the system is slow compared to the time scale set by the complex detuning, $\Gamma = \gamma + \mathrm{i}\Delta$, such that it is justified to adiabatically eliminate the optical polarization $\hat{\sigma}_\mathrm{ge}$. The resulting equations of motion for the operators $\hat{\mathcal{E}}, \hat{\sigma}_\mathrm{gr}$ are then given by

$$\mathrm{i}\frac{\partial}{\partial t}\begin{pmatrix}\hat{\mathcal{E}}\\ \hat{\sigma}_\mathrm{gr}\end{pmatrix} = -\frac{\mathrm{i}}{\Gamma}\begin{pmatrix} c\frac{\partial}{\partial z} + g^2 n & g\sqrt{n}\Omega \\ g\sqrt{n}\Omega & \Omega^2\end{pmatrix}\begin{pmatrix}\hat{\mathcal{E}}\\ \hat{\sigma}_\mathrm{gr}\end{pmatrix} + \int \mathrm{d}z\, V(z-z')\hat{\sigma}^\dagger_\mathrm{gr}(z')\hat{\sigma}_\mathrm{gr}(z')\hat{\mathrm{P}}_{\hat{\sigma}_\mathrm{gr}}\begin{pmatrix}\hat{\mathcal{E}}\\ \hat{\sigma}_\mathrm{gr}\end{pmatrix}, \tag{4.1}$$

where $\hat{\mathrm{P}}_{\hat{\sigma}_\mathrm{gr}}$ denotes the projector onto the atomic coherence, i.e., the second component of the vector $(\hat{\mathcal{E}}, \hat{\sigma}_\mathrm{gr})^t$. The matrix on the right hand side of the first line in Eq. (4.1) we denote as $\hat{H}_0$, corresponding to the free problem that has dark- and bright state solution. Including the interaction term in equation (4.1) results in a set of coupled integro-differential equations that cannot be solved directly. As it accounts for bound states we make a Green's function approach for two-excitation

wave function and use this to analyze the dynamics.The full wave function is given by

$$|\Psi(t)\rangle = |0\rangle + |\Psi_1(t)\rangle + |\Psi_2(t)\rangle + |\Psi_3(t)\rangle + \dots, \tag{4.2}$$

where $|0\rangle$ denotes the vacuum and $|\Psi_n\rangle$ denote the components with $n = 1, 2, 3, \dots$ excitations in the medium. For instance, the two-photon component is defined as

$$|\Psi_2(t)\rangle = \frac{1}{\mathcal{N}} \iint \mathrm{d}z_1\, \mathrm{d}z_2 \Big\{ \mathcal{EE}(z_1, z_2, t)\hat{\mathcal{E}}^\dagger(z_1)\hat{\mathcal{E}}^\dagger(z_2) + \mathcal{ES}(z_1, z_2, t)\hat{\mathcal{E}}^\dagger(z_1)\hat{\sigma}^\dagger_{\mathrm{gr}}(z_2) + \mathcal{SE}(z_1, z_2, t)\hat{\sigma}^\dagger_{\mathrm{gr}}(z_1)\hat{\mathcal{E}}^\dagger(z_2) + \mathcal{SS}(z_1, z_2, t)\hat{\sigma}^\dagger_{\mathrm{gr}}(z_1)\hat{\sigma}^\dagger_{\mathrm{gr}}(z_2) \Big\} |0\rangle\,, \tag{4.3}$$

where $\mathcal{N}$ is a normalization constant and $\mathcal{EE}(z_1, z_2, t) = \langle 0|\, \hat{\mathcal{E}}(z_1)\hat{\mathcal{E}}(z_2)\, |\Psi_2\rangle$ and analogously for the other components.

To analyze the creation and dynamics of photonic molecules, we specifically assume a two-photon state

$$|\Psi(t)\rangle = |\Psi_2(t)\rangle\,. \tag{4.4}$$

The complex detuning Γ in Eq. (4.1) in general couples the different components dissipatively in the presence of interactions, which act effectively as a space-dependent two-photon detuning, shifting photons out of the EIT transparency window. This dissipation manifests itself in quantum jumps at random times, e.g. projections of the two-photon wave function onto the single-photon wave function corresponding to the loss of a Rydberg polariton. In the far-detuned regime $|\Delta| \gg \gamma$ the probabilities of these quantum jumps are small, thus we neglect them. We note, however, that due to dissipation the norm of the wave function is not conserved during time evolution.

The two-photon wave function (4.3) is determined by the vector $\mathbf{\Psi}_2 = (\mathcal{EE}, \mathcal{ES}, \mathcal{SE}, \mathcal{SS})^T$. The time evolution of $\mathbf{\Psi_2}$ in real space is governed by the equation of motion,

$$\mathrm{i}\frac{\partial}{\partial t}\mathbf{\Psi}_2(z_1, z_2, t) = \hat{\mathcal{H}}(z_1, z_2)\mathbf{\Psi}_2(z_1, z_2, t), \tag{4.5}$$

i.e., a Schrödinger-like equation with the Hamiltonian $\hat{\mathcal{H}}$

$$\hat{\mathcal{H}}(z_1, z_2) = \hat{\mathcal{H}}_0(z_1, z_2) + V(z_1 - z_2)\hat{\mathrm{P}}_{\mathcal{SS}}. \tag{4.6}$$

Here $\hat{\mathcal{H}}_0 = \hat{H}_0(z_1)\otimes\mathbb{1}_2 + \mathbb{1}_2\otimes\hat{H}_0(z_2)$ denotes the free Hamiltonian and the operator $\hat{\mathrm{P}}_{\mathcal{SS}} = |\varphi_4\rangle\langle\varphi_4|$ with $|\varphi_4\rangle = (0, 0, 0, 1)^T$ is the projector onto the fourth component of the wave function, i.e. the component $\mathcal{SS}$ of two atomic Rydberg excitations . Analog to Chapter 2 this equation can be integrated numerically to find the time evolution of a two-photon wave packet.

Before we consider the numerical solutions in detail we summarize the Green's function approach

and the analytical results presented in [Moos2017]. A detailed derivation can be found in the appendix of this reference. Note that a similar approach exists using the T matrix [95]. We proceed as follows. First, we transform the coordinates z_1 and z_2 of the two-excitation wave function to relative and center-of-mass coordinates, $r = z_1 - z_2$ and $R = \frac{1}{2}(z_1 + z_2)$, respectively. Subsequently we perform a Fourier transform with respect to the center-of-mass coordinate R according to $f(R) = \int \mathrm{d}K \, \exp(\mathrm{i}KR)\tilde{f}(K)$. Then we have to solve the initial value problem in K-space

$$\begin{aligned} \mathrm{i}\frac{\partial}{\partial t}\mathbf{\Psi}_2(K,r,t) &= \hat{\mathcal{H}}\mathbf{\Psi}_2(K,r,t), \\ \mathbf{\Psi}_2(K,r,0) &= |\Psi_0\rangle\,, \end{aligned} \tag{4.7}$$

where we choose an initial state $|\Psi_0\rangle = f(K,r)\,|\varphi_1\rangle$, with only photonic excitation, $|\varphi_1\rangle := (1,0,0,0)^T$. It is straightforward to generalize the calculation to arbitrary initial states. Furthermore we restrict the calculation to negative detuning without loss of generality as the solution for positive detuning can directly be constructed from the solution for negative detuning (and vice versa). With our choice of initial state we can write a formal solution of the initial value problem, Eq. (4.7), that is given in spectral Fourier representation by

$$\mathcal{EE}(t) = \frac{1}{2\pi\mathrm{i}}\int_{-\infty}^{\infty} \mathrm{d}\omega\, \mathrm{e}^{-\mathrm{i}\omega t} f(K,r)\,\langle\varphi_1|\hat{G}(\omega)|\varphi_1\rangle\,, \quad t>0, \tag{4.8}$$

valid for $t > 0$. The full Green's operator $\hat{G}(\omega)$ is defined by

$$\hat{G}(\omega) := \frac{1}{\hat{\mathcal{H}} - \omega - \mathrm{i}0^+}. \tag{4.9}$$

For large times t and small distances r the expression (4.8) is dominated by the low-frequency contributions with $|\omega| \ll \Omega^2|\Gamma|$. To capture this limit we may approximate the Green's function in Eq. (4.8) by

$$\langle\varphi_1|\hat{G}(\omega)|\varphi_1\rangle \approx \cos^4(\theta) G(r,r',\omega), \tag{4.10}$$

where the Green's function $G(r,r',\omega)$ is determined by the integral equation

$$G(r,r',\omega) = G_0(r,r',\omega) - \sin^4(\theta)\int \mathrm{d}r''\, G_0(r,r'',\omega)W(r'',\omega)G(r'',r',\omega), \tag{4.11}$$

where G_0 denotes the Green's function of the electric-field component of a non-interacting polariton pair state with an effective mass m. The frequency-dependent effective potential and the complex effective mass are defined as

$$W(r,\omega) = \frac{V(r)}{1+\alpha_{00}(\omega)V(r)}, \qquad m = \mathrm{i}\frac{g^2 n}{4c\Gamma v_\mathrm{g}}, \tag{4.12}$$

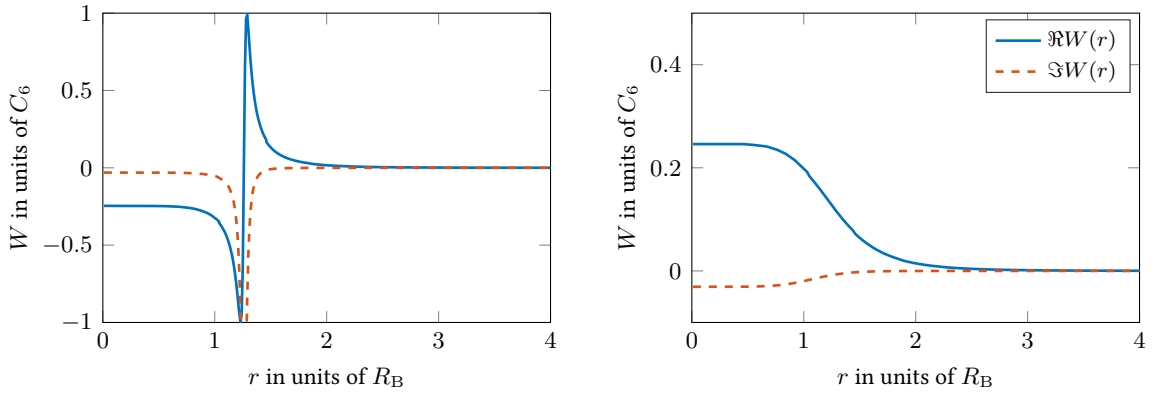

(a) Positive detuning, $\Delta = 8\gamma > 0$.

(b) Negative detuning, $\Delta = -8\gamma < 0$.

Figure 4.2: Real (solid blue lines) and imaginary part (dashed red lines) of effective potential $W(r)$, defined in Eq. (4.12) for (a) positive and (b) negative single-photon detuning $\Delta = \pm 8\gamma$ and $\Omega = \gamma$.

with $\alpha_{00}(\omega) = \mathrm{i}\Gamma/(2\Omega^2 - \mathrm{i}\omega\Gamma)$. In the limit of small ω the frequency dependence can be neglected and consequently we can set $\alpha_{00} \approx \frac{\mathrm{i}\Gamma}{2\Omega^2}$. In Figure 4.2 we plot the effective potential for positive and negative detuning Δ. For relative distances $r > R_\mathrm{B}$ the potential decays like the bare van der Waals potential for both signs of the detuning. For small distances the potential becomes a constant potential where the sign of the real part can be tuned by changing the sign of Δ, while the imaginary part is always negative (but small) indicating losses.

In the limit of slow light and large single photon detuning the Green's function G describes the evolution of a particle with the effective Hamiltonian

$$\hat{\mathcal{H}}_\mathrm{eff} = -\frac{1}{2m}\frac{\mathrm{d}^2}{\mathrm{d}r^2} + \sin^4(\theta)W(r,0). \tag{4.13}$$

In this limit the reduced mass is approximately given by the expression $m \approx \mathrm{sign}(\Delta)(4v_\mathrm{g}L_\mathrm{abs})^{-1}$. We observe that the reduced mass also changes its sign with Δ as the effective potential W does. The product of effective potential W and effective mass m always has a negative real part at small distances, indicating the existence of bound states for both positive and negative single-photon detuning.

4.2 Bound states – photonic molecule

In the following section we consider the spectral properties of the effective Hamiltonian. We analyze conditions for the existence of a single bound state and investigate the properties and internal structure of this bound state by means of the Green's function approach and numerical simulations.

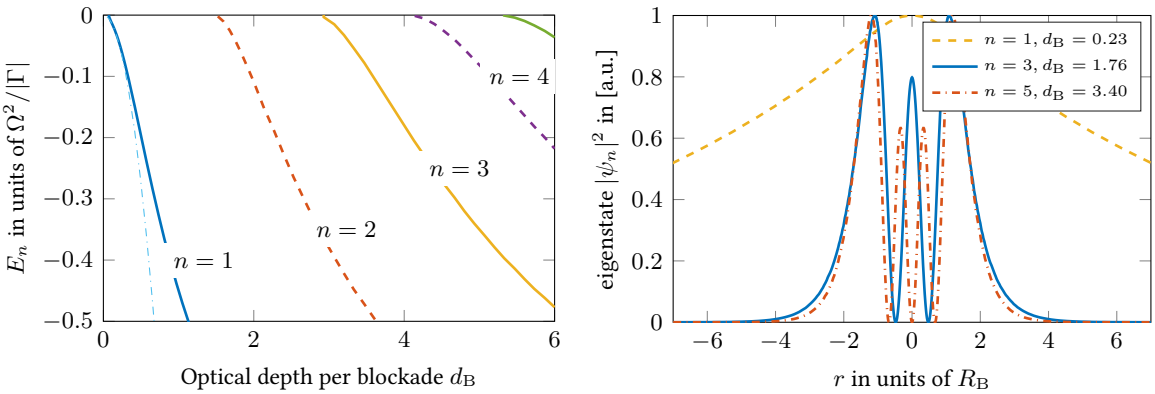

(a) Spectrum of effective Hamiltonian

(b) First symmetric eigenstates ψ_n.

Figure 4.3: Results of numerical diagonalization of the effective Hamiltonian $\hat{\mathcal{H}}_\mathrm{eff}$, Eq. (4.13) for a system of finite length with periodic boundary conditions and under the assumption $|\Delta| \gg \gamma$, where the non-Hermitian part of the Hamiltonian can be neglected. (a) Bound-state energies E_n in dependence of interaction strength, respectively optical depth per blockade volume d_B. The (light blue) dashed-dotted line is the approximate solution $E_0 \approx -\frac{\pi^2}{9} d_\mathrm{B}^2$ from Eq. (4.25). We restrict the plot to energies larger $-\Omega^2/2|\Gamma|$, as the effective Hamiltonian is only valid for small energies. (b) First three symmetric eigenstates ψ_n for different optical depth per blockade d_B corresponding to low energies $E_n = -0.05\Omega^2/|\Gamma|$ for $n = 1, 3, 5$. Note that the $r-$axis is scaled in units of R_B which is different for each shown state. We show only symmetric eigenstates, as antisymmetric states cannot be excited.

4.2.1 Bound states

In the far-detuned limit, $|\Delta| \gg \gamma$, the Green's function $G(r, r', \omega)$ can be written as a sum of bound eigenstates of the Hamiltonian, denoted by ψ_n, and scattering (continuum) states, denoted by ψ_E. In real space this sum is given by

$$G(r, r', \omega) = \sum_{n=1}^{N} \frac{\psi_n(r)\psi_n^*(r')}{\omega - E_n} + \int \mathrm{d}E \, \frac{\psi_E(r)\psi_E^*(r')}{\omega - E}, \tag{4.14}$$

with the bound state eigenenergies E_n that are in general complex and are increasing with increasing optical depth per blockade, $d_\mathrm{B} = R_\mathrm{B}/L_\mathrm{abs}$. A sufficient condition for the existence of bound states in the spectrum of a Hamiltonian is given by the product of (effective) mass and the area of the (effective) potential [96],

$$m \int_{-\infty}^{\infty} \mathrm{d}r \, W(r) < 0, \tag{4.15}$$

which is in our case fulfilled, as for negative single-photon detuning Δ the product of m and $W(r)$ is negative for all r. Furthermore the number N of bound states can be estimated [96] by

$$N \leq 1 + 2|m| \int_{-\infty}^{\infty} \mathrm{d}r \, |r| W(r). \tag{4.16}$$

This equation determines a condition when the number of bound states is smaller than 2, i.e., a condition for the existence of a unique bound state. For a constant effective mass the number of bound states depends on the area of the effective potential, i.e., depends on the strength of W. Using the definition of the effective potential and the effective mass, we can derive the condition for the regime where only unique bound state exists,

$$d_{\mathrm{B}} = \frac{R_{\mathrm{B}}}{L_{\mathrm{abs}}} \leq \sqrt{\frac{2\sqrt{3}}{\pi}} \approx 1.2861. \tag{4.17}$$

This regime is determined by the optical depth per blockade d_{B} being small, i.e., in the regime of weak interactions. To observe bound states one has to operate in this regime, where the relevant energies are close to zero, as can be explained as follows. Conditions of EIT require that the energies of the bound states have to be small compared to $\Omega^2/|\Gamma|$, i.e., deeply bound states are subject to losses respectively dispersion, depending on the single-photon detuning. Moreover, deeply bound states are strongly localized and thus difficult to excite by a flat initial photonic wave-packet. In Figure 4.3(a) we show the spectrum calculated for the Hamiltonian Eq. (4.13) in dependence on the optical depth per blockade, d_{B}. In Figure 4.3(b) the absolute value of the corresponding eigenstates for $n = 1, 3, 5$ are displayed, i.e., three lowest symmetric states. These states are calculated for different optical depths, such that they have the same energies E_n. We observe, that the $n = 1$-eigenstate exhibits a much larger spatial extent. For small d_{B} the effective Hamiltonian exhibits only a single bound state while for increasing d_{B} additional bound states exist. The energies of each of these bound states increases with d_{B}. In Figure 4.3(b) we show the first symmetric states, where we chose d_{B} such that their corresponding energies are equal. As can be seen, although they have equal energies, the spatial size of the higher bound states is on the order of the blockade radius R_{B} while the first bound state has a much larger extent compared to R_{B}. Note that $R_{\mathrm{B}} \sim d_{\mathrm{B}}^{-1}$ is different for the different curves. This and the increasing number of oscillations makes it hard to excite higher bound states. Consequently, only weakly bound states are feasible to create experimentally.

4.2.2 Internal structure of the bound state – photonic molecule

In the previous section we have shown that the $\mathcal{EE}$-component of a two-excitation dark-state polariton can be described using an effective Hamiltonian that possesses bound eigenstates. In particular for small d_{B} a single such state exists that has a large spatial extent.

Having identified this regime of a unique bound state we now turn to the calculation of the internal structure of this bound state in terms of the components of the two-excitation wave function $\mathbf{\Psi}_2$. To this end we simulate the time evolution of an two-photon wave-packet $\mathbf{\Psi}_2(K, r)$ numerically, using a discretization of space and a finite difference scheme for the relative coordinate r and setting the center-of-mass momentum $K = 0$. For small relative distances $|r| \lesssim R_\mathrm{B}$, i.e., inside the blockade radius, the $\mathcal{SS}$-component has to be strongly suppressed due to the Rydberg blockade, while for distances $|r| \gtrsim R_\mathrm{B}$ the effect of the interaction potential is negligible. Consequently, we expect the internal structure of the bound state wave function to be a dark-state polariton pair state, described by a product wave function $\Psi\Psi(K, r)$,

$$\mathcal{EE} = \cos^2\theta\,\Psi\Psi, \quad \mathcal{ES}_+ = -\sin\theta\cos\theta\,\Psi\Psi, \quad \mathcal{ES}_- = 0, \quad \mathcal{SS} = \sin^2\theta\,\Psi\Psi, \tag{4.18}$$

except inside the blockade radius. In Eq. (4.18) we defined $\mathcal{ES}_\pm = \frac{1}{2}(\mathcal{ES} \pm \mathcal{SE})$. Making this observation, we set the initial wave-packet as a product state of two polaritons, where we modify the $\mathcal{SS}$-component inside the blockade radius by multiplying it with $1/(1 - \frac{\Delta}{2\Omega^2}V(r))$. This suppresses initial $\mathcal{SS}$-excitation inside the blockade distance. Starting with this initial state we simulate a time evolution of the two-photon wave function according to Eq. (4.7) for positive as well as for negative detuning. After a time of $t = 20\frac{|\Delta|}{2\Omega^2}$ we get the results shown in Figure 4.4, where we display the $\mathcal{EE}$- and $\mathcal{SS}$-components as well as the symmetric and antisymmetric superpositions $\mathcal{ES}_\pm := \mathcal{ES} \pm \mathcal{ES}$. We observe that the $\mathcal{SS}$-component is strongly suppressed inside the blockade radius as expected, and thus the bound state has mainly photonic character in this regime. For larger distances, the internal structure is close to that of two dark-state polaritons, i.e., given by Eq. (4.18). A small but nonzero antisymmetric component $\mathcal{ES}_-$ and correspondingly a slightly increased spin excitation outside the blockaded region indicates small corrections. In the case of positive detuning sharp resonances in the $\mathcal{SS}$-component can be observed corresponding to the pole in the effective potential.

In the regime of small d_B where only a single bound state exists, we can write the photonic component of the wave function using Eq. (4.8) and Eq. (4.14) and obtain

$$\mathcal{EE}(r, t) = \cos^4\theta C_0 e^{-\mathrm{i}E_0 t}\psi_0(r) + \int \mathrm{d}E\, C(E) e^{-\mathrm{i}Et}\psi_E(r), \tag{4.19}$$

where C_0 and $C(E)$ denote the overlap integrals of initial state and bound and continuum states, respectively. To get the internal structure of the bound state we neglect the second term corresponding to the continuum part and insert the solution for the photonic part into the two-excitation Schrödinger equation (4.7). Assuming that $g^2 n/|\Delta| \gg \{cK, |E_0|\}$ one can calculate the remaining

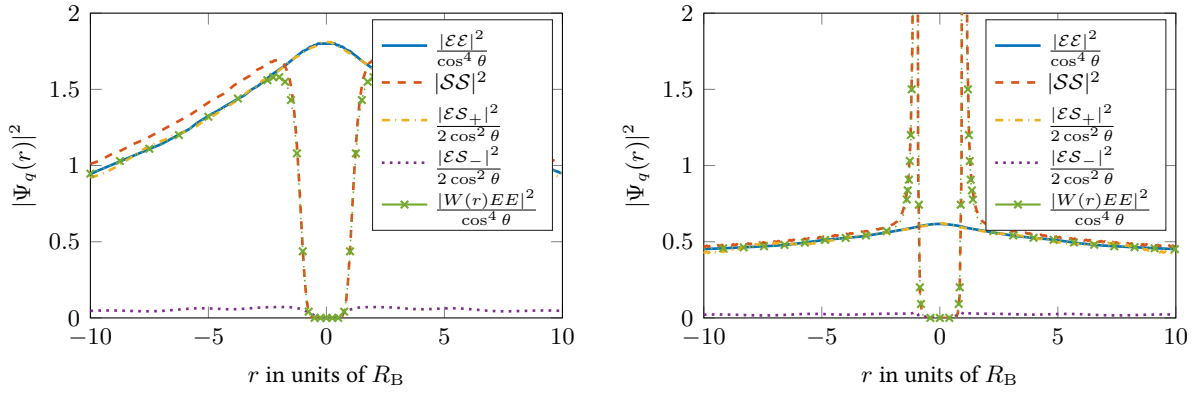

(a) negative detuning, $\Delta = -4\gamma$

(b) positive detuning, $\Delta = +4\gamma$

Figure 4.4: Photonic molecule state obtained from numerical time evolution of the paraxial Maxwell-Bloch equations for $K = 0$, $g = 20\Omega$, $d_\mathrm{B} = 0.2$, and $t = 20$ in units of $|\Delta|/2\Omega^2$. Shown are the amplitudes of the wave function components $\mathcal{EE}$, $\mathcal{ES}_\pm$, $\mathcal{SS}$, and $W(r)\mathcal{EE}$, and each scaled with powers of $\cos\theta$ according to Eq. (4.20) to make them comparable. (a) shows the result for negative detuning and (b) shows the result for positive detuning, where the SS-component exhibits resonances. Outside the blockade radius we find small deviations from the result we expect from Eq. (4.20).

components [Moos2017] and arrives at the two-photon wave function

$$\mathbf{\Psi}(r,t) = \cos^2\theta C_0 \begin{pmatrix} \cos^2\theta \\ -\sin\theta\cos\theta \\ -\sin\theta\cos\theta \\ \frac{\sin^2\theta}{1-\frac{\Delta}{2\Omega^2}V(r)} \end{pmatrix} \psi_0(r)\mathrm{e}^{-\mathrm{i}E_0 t},, \tag{4.20}$$

where the factor $\cos^2\theta$ in front is from projecting the intial state onto the state of two free polaritons and can be changed by choosing a different initial state. Eq. (4.20) describes a two-photon wave packet that exhibits bunching for small distances and propagates form-stable through the medium, i.e., a photon molecule state. This agrees well with the result shown in Figure 4.4 obtained by numerical wave function propagation. Note that for distances $|r| \gg R_\mathrm{B}$ it holds $V(r) \ll 2\Omega^2/\Delta$ and $\mathbf{\Psi}_2$ has the internal structure as a product of two Rydberg polaritons, cf. Eq. (4.18).

4.3 Time evolution of bound and scattering states

In the previous section we showed the existence of a photonic molecule pair state and calculated its internal structure. In doing so, we neglected the scattering continuum. However, in general the full state is a superposition of bound and scattering states, and as we assumed a flat initial photon

distribution, the scattering continuum has to play an important role in explaining the full numerical result. In this section we analyze the time evolution of the full state as well as the interplay of bound and continuum states.

In the limit of low excitation the spatial character of the interaction is not important, only the area of the interaction is relevant. Thus, the effective potential can be approximated by a point-like pseudopotential with the same area [Moos2017],

$$W_{\text{eff}}(r) = \frac{2\pi}{3}\frac{2\Omega^2}{|\Delta|}\frac{\sin^4\theta}{(1+\mathrm{i}\gamma/|\Delta|)^{5/6}}\delta(r/R_{\mathrm{B}}). \tag{4.21}$$

For convenience we introduce below dimensionless units such that time and space coordinates are measured in units of $(2\Omega^2/|\Delta|)^{-1}$ and R_{B}, respectively.

Within this approximation, one can show that the initial value problem with a uniformly distributed initial two-photon state admits analytical solutions, that are closed expressions [Moos2017] given by

$$\begin{aligned}\frac{\mathcal{EE}(r,t)}{\cos^4\theta} = {} & 2\exp\Big(-\mathrm{i}\frac{\beta\eta^2}{2}t - \beta\eta|r|\Big) + \operatorname{erf}\Big(\sqrt{\tfrac{i\beta}{2t}}|r|\Big) \\ & + \exp\Big(-\mathrm{i}\frac{\beta\eta^2}{2}t - \beta\eta|r|\Big)\left[1 + \operatorname{erf}\Big(-\operatorname{sign}[\Re(\beta\eta)]\sqrt{\tfrac{\beta\eta^2}{2\mathrm{i}}t} + \sqrt{\tfrac{\mathrm{i}\beta}{2t}}|r|\Big)\right].\end{aligned} \tag{4.22}$$

The constants β and η are defined by

$$\eta = \frac{2\pi}{3}\frac{1}{(1+\mathrm{i}\frac{\gamma}{|\Delta|})^{5/6}}, \qquad \beta = \frac{1}{2}\frac{d_{\mathrm{B}}^2}{(1+\mathrm{i}\frac{\gamma}{|\Delta|})}. \tag{4.23}$$

The first term $2\exp\big(-\mathrm{i}\frac{\beta\eta^2}{2}t - \beta\eta|r|\big)$ right hand side of Eq. (4.22) corresponds to a single bound state wavefunction of the effective potential $W_{\text{eff}}(r)$, if the condition $\Re(\beta\eta) > 0$ is fulfilled. This holds, if $|\Delta| > 0.8665\,\gamma$, i.e., under off-resonant driving conditions. This condition also shows that bound states require a sufficiently large single-photon detuning, i.e., an off-resonant EIT setup. From Eq. (4.22) we can read off the size of the bound state as being

$$r_{\mathrm{b}} \approx (\beta\eta)^{-1} \approx \frac{\pi}{3}d_{\mathrm{B}}^{-2}, \quad (\text{units of } R_{\mathrm{B}}), \tag{4.24}$$

which is much larger than the blockade distance R_{B}, for $d_{\mathrm{B}} \ll 1$. In Figure 4.5 we show the bound and scattering components according to Eq. (4.22) and a comparison of the sum of both with a numerically calculated state. We observe that in the vicinity of $r = 0$ the spatial structure of bound state and continuum state are the same.

The energy of the bound state can be read off Eq. (4.22). Expanding up to second order in γ/Δ we

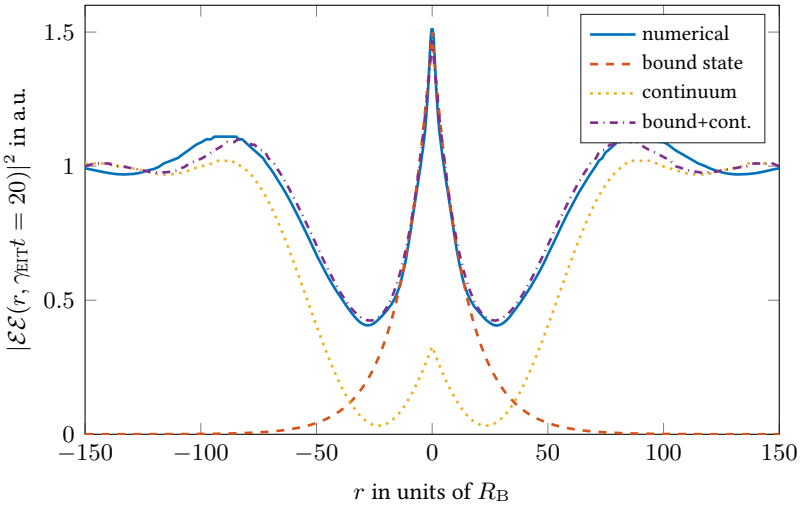

Figure 4.5: Second order correlation functions $|\mathcal{EE}(r,t)|^2$ of two photons as function of relative distance r and fixed time $t = 20$ (in units of $|\Delta|/2\Omega^2$). The solid blue line shows a numerical calculation for $K = 0$, $g/\Omega = 100$, $\Delta = -4\gamma$ in the weakly interacting regime with $d_{\mathrm{B}} = 0.2$. The dashed red and the dotted yellow line show the bound and continuum part of the wave function, respectively, according to Eq. (4.22), and the dash-dotted purple line shows the sum of both.

obtain

$$E_0 = -\frac{\pi^2}{9} d_{\mathrm{B}}^2 \left(1 - \mathrm{i}\frac{8}{3}\frac{\gamma}{\Delta} - \frac{44}{9}\frac{\gamma^2}{\Delta^2}\right), \tag{4.25}$$

which is complex-valued. The imaginary part gives rise to an exponential decay of the bound state with the rate

$$\gamma_{\mathrm{b}} \approx 2.924\, d_{\mathrm{B}}^2 \frac{\gamma}{\Delta}. \tag{4.26}$$

Note that both E_0 and γ_{b} are in units of $2\Omega^2/|\Delta|$. We observe a slow decay of the bound state, i.e., a long lifetime can be achieved in the regime of small optical depth per blockade, $d_{\mathrm{B}} \ll 1$, and also be improved by a large single-photon detuning.

Interplay of bound and continuum states. The analytical solution allows us to analyze the properties and the dynamical interplay of bound state and continuum states. At small distances $r = 0$ and for large times the analytical solution (4.22) can be simplified to the expression

$$\mathcal{EE}(0,t) = \cos^4\theta \left[2\exp\left(-\tfrac{\mathrm{i}\beta\eta^2}{2}t\right) - \frac{1}{\sqrt{\tfrac{\pi\beta\eta^2}{2\mathrm{i}}t}}\right], \tag{4.27}$$

where again the first term on the right hand side corresponds to the bound state and the second term to the scattering state contribution. This correlation function illustrates that both bound and continuum

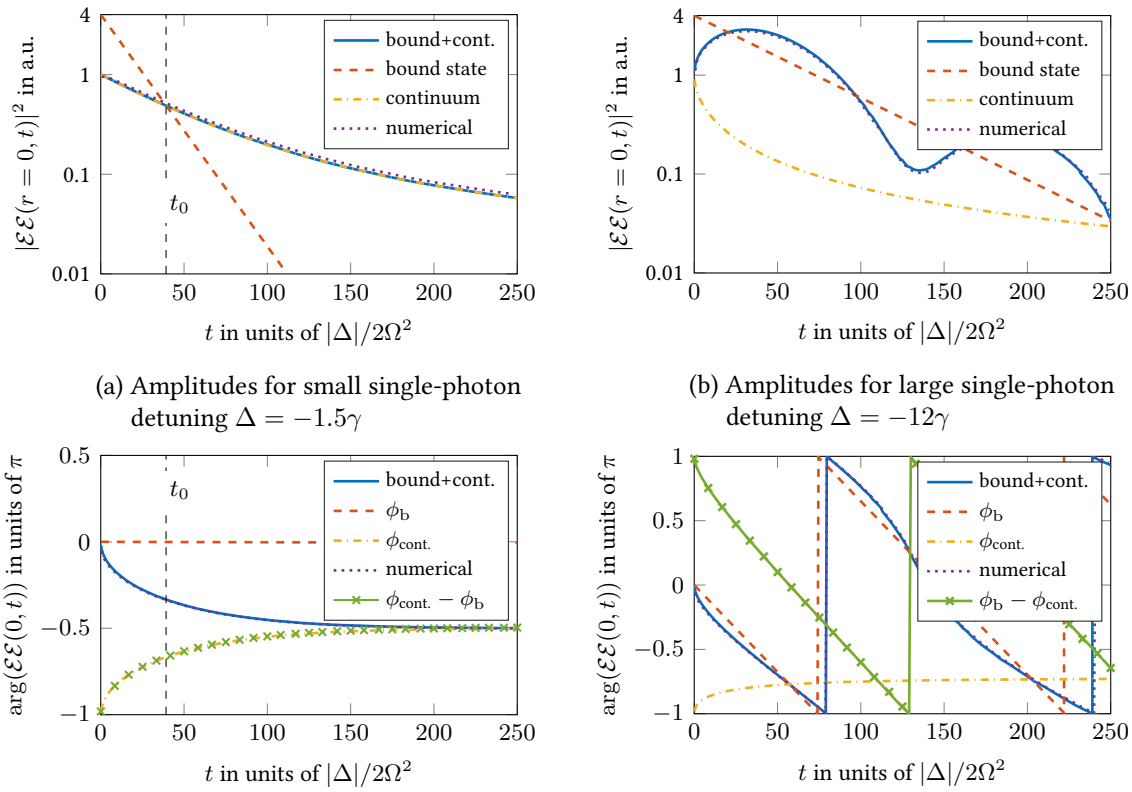

(a) Amplitudes for small single-photon detuning $\Delta = -1.5\gamma$

(b) Amplitudes for large single-photon detuning $\Delta = -12\gamma$

(c) Phases for small single-photon detuning $\Delta = -1.5\gamma$

(d) Phases for large single-photon detuning $\Delta = -12\gamma$

Figure 4.6: Time evolution of bound and scattering state components and full state of the two-photon wave function $\mathcal{EE}(r=0,t)$ at zero relative distance, calculated according to Eq. (4.22) and by using numerical simulations of the two-photon wave function. (a) and (c) are for a small single photon detuning of $\Delta = -1.5\,\gamma$, while (b) and (d) show results for $\Delta = -12\gamma$. (a) and (b) are log-log plots of the intensities and (c) and (d) show the time evolution of the phase arguments, in particular the difference in phase between bound and scattering components. The results are in the regime of slow light and weak interactions, where $d_\mathrm{B} = 0.2$ and $g\sqrt{n}/\Omega = 100$. The dashed vertical lines in (a) and (c) displays indicates the time scale t_0, where the character of the full state crosses over from bound state to scattering state. Note that for large detuning t_0 is larger than the maximal time displayed in (b) and (d).

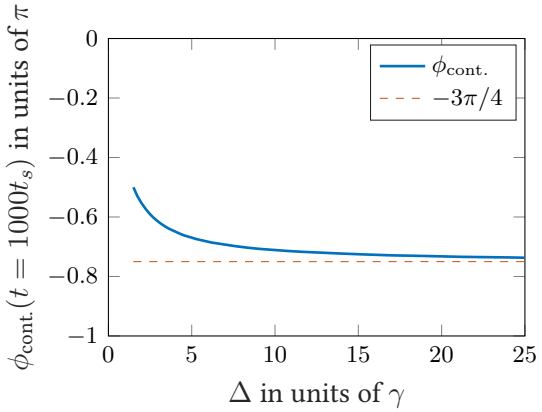

(a) Asymptotic phase of continuum contribution, calculated for $t_0 = 1000t_s$

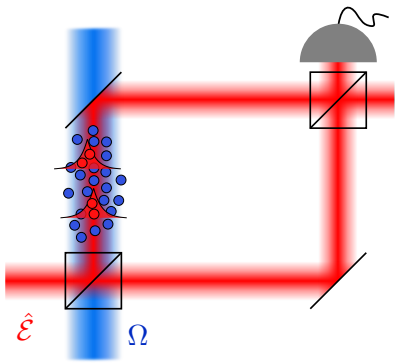

(b) Homodyne detection setup

Figure 4.7: (a) Asymtotic phase of continuum contribution for large t_0. (b) Sketch of interferometric setup that can be used to filter and detect bound-state and scattering-state contributions.

parts of the wave function contribute to the bunching. Initially, the contribution of the bound state is twice as large as the scattering states, but they interfere destructively, so the superposition of both sums up to the flat initial state. Then both evolve in time qualitatively different. While the bound state exhibits an exponential decay as discussed above, the continuum state decays algebraically in time, i.e., $\propto 1/\sqrt{t}$. The exponent of this is fixed, while the decay rate of the bound state can be changed by tuning the single-photon detuning. Moreover, considering the complex phases of the two components, Eq. (4.27) we find that the bound state acquires a dynamical phase, while the continuum contribution asymptotically approaches a constant phase. The interplay of this leads to an oscillatory behavior, as shown in Figure 4.6, which will be discussed below in more detail. Using Eq. (4.27) we can define a time scale t_0 such that for times $t < t_0$ the superposition is dominated by the bound state while for times $t > t_0$ the continuum state is dominant. It can be shown that t_0 is minimal for $\gamma/|\Delta| = \tan\frac{3\pi}{16} \approx 2/3$ where

$$t_0 \approx \frac{\pi}{2d_{\text{B}}^2}. \tag{4.28}$$

In the regime of weak interactions, $d_{\text{B}} < 1$, it holds $t_0 \gg 1$ in units of the inverse off-resonant EIT linewidth $|\Delta|/2\Omega^2$.

4.4 A scheme for detection of bound states

From equation (4.27) we obtain that the bound state acquires a dynamical phase of

$$\phi_{\text{b}}(t) = \frac{1}{2}\Re\{\beta\eta^2\}t, \tag{4.29}$$

that grows linearly in time. Thus, on the one hand, at the point $\gamma/|\Delta| = \tan\frac{3\pi}{16}$ the dynamical phase vanishes, as $\Re\{\beta\eta^2\} = 0$. On the other hand, the scattering continuum approaches asymptotically a constant value, depending on the single-photon detuning Δ. For $\gamma/|\Delta| = \tan\frac{3\pi}{16}$ this constant value is $-\pi/2$ and then decreases with increasing detuning to an asymptotic value of $-3\pi/4$. Although the continuum phase $\phi_{\text{cont.}}$ reaches this constant value only in the limit $t \to \infty$, already for intermediate times the phase is close to this asymptotic value and changes slowly in time, cf. Figures 4.6(c) and 4.6(d). Furthermore, as Figure 4.7(a) shows, the continuum phase is very robust, as it depends only on $|\Delta|/\gamma$, and thus can be tuned by changing the frequencies of the probe and control fields. This allows to build a detection setup for filtering bound and scattering state components.

When taking also the amplitude evolution into consideration, one can distinguish three regimes depending on the ratio $|\Delta|/\gamma$. For small single-photon detuning the scattering continuum dominates the dynamics at all times and attain a phase of $-\pi/2$. For intermediate detuning the photon bunching is dominated by the bound state at small times up to the crossover time t_0, where the continuum states start to dominate. Lastly, for large detuning the continuum states decay very quickly and the bunching is solely due to the bound state on all relevant time scales.

To observe the bound state, i.e., a photonic molecule state, one could try to perform experiments in the far-detuned regime, where the continuum decays much faster than the bound state. However, a far detuned EIT setup is experimentally challenging, it is much easier to work in the regime of small to intermediate detuning. The robustness of the phase ϕ_{b} of the scattering states makes it possible to filter the bound and scattering state components by employing interferometric techniques as e.g. the homodyne detection setup as sketched in Figure 4.7(b). In the regime of intermediate detuning the decay of the bound components is sufficiently slow and the phase of the continuum components is only changing slowly and close to their asymptotic value.

4.5 Conclusion

To summarize, we investigated the propagation of Rydberg polaritons under conditions of electromagnetically induced transparency and off-resonant driving, i.e., with a finite single-photon detuning. Particularly, we discussed the bunching that has been observed under these conditions [65], see also [66]. By using a Green's function approach we derived an effective model for two dark-state polaritons and analyzed its spectral properties, showing the existence of bound eigenstates. We showed that in the regime of weak interactions, manifesting in a small optical depth per blockade, the off-resonant model has a single eigenstate close to the scattering continuum, i.e., a photonic molecule. We argued that this low-energy bound state is experimentally accessible, while higher-order bound states are difficult to excite. Using two-photon wave function simulations of the full Maxwell-Bloch equations we confirmed the existence of bunching for sufficiently small values of the optical depth per blockade, as opposed to the anti-bunching that has been discussed in Chapter 2 in the case of

stronger interactions.

We showed that the bunching of photons arises from two contributions, i.e., additionally to the bound state, scattering states play a role. By using the Green's function approach we derived analytic expressions for the bound state and continuum wave functions in the limit of very weak interactions, where the effective interaction potential can be approximated by a δ potential. This expression allowed us to investigate the time dependence of the bound state and continuum components, where we found that the bound state decays exponentially, while the scattering state exhibit an algebraic time dependence. For small evolution times up to a certain cross-over time scale the bunching of polaritons is dominated by a superposition of bound and continuum wave function. For large times, however, the continuum contribution dominates the observed state. Since the continuum component asymptotically attains a constant phase, that depends only on the single-photon detuning we proposed to use an interferometric detection scheme to filter bound and continuum components. This allows for an isolation and observation of photonic molecules by using standard interferometric methods.

Chapter 5

General conclusion and outlook

The aim of this thesis was to investigate few- and many-body properties of interacting Rydberg polaritons. To this end, we derived conditions, when a three-dimensional setup can effectively described by a one-dimensional model. Using this as a starting point we showed in Chapter 2 that the physics of Rydberg polariton can be described by a field theory of a single field. We derived the master equation governing the time evolution of this field and discussed the properties of its various dissipative and unitary terms. We could confirm this result on the few-excitation level by comparing with numerical simulation of the full Maxwell-Bloch equations of photons propagating in a gas of Rydberg atoms. Moreover, we found a regime, where the master equation reduces to a Hamiltonian description, i.e., the time evolution becomes unitary.

Building on the few-body results, we analyzed many-body properties of the Rydberg polariton field theory in the regime of unitary description and small excitation densities. In Chapter 3 we showed on the basis of correlation functions obtained by density-matrix renormalization group simulations, that the many-body physics is very well described by a Luttinger liquid theory. Thus, in the case of strong interactions, the correlations on large length scales are dominated by a density wave, giving rise to a Wigner crystal of photons. As the blockade distance increases with the interaction strength, this regime is inaccessible for propagating polaritons while keeping sufficiently large excitation densities. We proposed a solution to this problem, by using a dynamical protocol turning propagating polaritons into a stationary density-wave of Rydberg excitations and at the same time increasing the interaction strength, while keeping excitation densities finite. Releasing this density wave from the medium by turning it back into a propagating polariton pulse generates a regular train of photons. As an outlook, one could extend the results by imposing a lattice potential on the polaritons giving rise to sine-Gordon physics [32] that allows for true crystalline order[97]. In this case a stationary light setup [49, 98] should be used.

Finally, in Chapter 4, we investigated a different regime of weak interactions, where under off-resonant driving conditions bunching of photons has been observed [65]. By utilizing a Green's function approach and deriving an effective Hamiltonian for the two-excitation problem, we found that this bunching can be explained by an interplay of continuum states and bound states, photonic

molecule states. We showed that the bound states have a Rydberg polariton-like structure except for small distances inside the blockade radius. An analysis of the time evolution of the continuum and bound contributions during propagation revealed a robust asymptotic phase for the continuum states, allowing for an isolation and subsequent observation of the photonic molecule. Building on this result, many further questions can be addressed. A natural next step would be to extend the results to more particles, as bunching has very recently been observed for three particles [66]. Even beyond that, one could investigate interactions between pair-states possibly yielding a many-body theory of photonic molecules.

In conclusion, let me observe that Rydberg quantum optics is a vibrant and exciting research field. The combination of slowly propagating polaritons with strong nonlocal van der Waals-type interactions produces interesting properties ranging from the few-excitation level to many-body physics giving rise to many possible applications.

Appendices

Appendix A

Derivation of the Rydberg polariton model

In this appendix we present details on the derivation of the Rydberg polariton model used in the main text. Specifically, we derive the Heisenberg-Langevin equations for a quantized probe field propagating under conditions of electromagnetically induced transparency (EIT) [1] starting from the Hamiltonian of quantum optics. Furthermore, we find the polariton as a dark-state eigensolution of this Hamiltonian and derive corrections using perturbation theory.

We remark that for all calculations we set $\hbar = 1$.

A.1 Hamiltonian of quantum optics

A transversal electrical field consisting of a probe field and a classical control field

$$\hat{\mathbf{E}}(\mathbf{r},t) = \hat{\mathbf{E}}_{\mathrm{p}}(\mathbf{r},t) + \mathbf{E}_{\mathrm{c}}(\mathbf{r},t), \tag{A.1}$$

where we assume that the fields are linear polarized parallel to the polarization vectors $\boldsymbol{\epsilon}_{\mathrm{p}}$ and $\boldsymbol{\epsilon}_{\mathrm{c}}$, respectively. Furthermore we assume that the probe field is varying around a central k-mode and frequency, $\mathbf{k}_{\mathrm{p}} = k_{\mathrm{p}}\mathbf{e}_z$ and $\omega_{\mathrm{p}} = ck_{\mathrm{p}}$, respectively. Thus we can write the probe field as

$$\hat{\mathbf{E}}(\mathbf{r},t) = \sum_{\mathbf{q}} \sqrt{\frac{\omega_{\mathbf{q}}}{2\epsilon_0 V}} \left(\hat{a}_{\mathbf{q}}(t)\boldsymbol{\epsilon}_p e^{\mathrm{i}\mathbf{q}\cdot\mathbf{r}} + \mathrm{H.a.}\right) = \sqrt{\frac{\omega_{\mathrm{p}}}{2\epsilon_0}} \left(\boldsymbol{\epsilon}_{\mathrm{p}}\hat{\mathcal{E}}(\mathbf{r},t)e^{\mathrm{i}(k_{\mathrm{p}}z-\omega_{\mathrm{p}}t)} + \mathrm{H.a.}\right) \tag{A.2}$$

where V denotes the quantization volume and in the first equation we used the general definition of a linear polarized, quantized field, that reduces to (A.2) under our assumptions, with the slowly varying operator

$$\hat{\mathcal{E}}(\mathbf{r},t) \equiv \frac{1}{\sqrt{V}} \sum_{\mathbf{q}} \sqrt{\tfrac{\omega_{\mathbf{q}}}{\omega_{\mathrm{p}}}} \hat{\tilde{a}}_{\mathbf{q}} e^{-\mathrm{i}(\Delta\omega_{\mathbf{q}}t - \Delta\mathbf{q}\cdot\mathbf{r})}. \tag{A.3}$$

Here we defined $\hat{\tilde{a}}_{\mathbf{q}} = \hat{a}_{\mathbf{q}} e^{+\mathrm{i}\omega_{\mathbf{q}}t}$ and $\Delta\omega_{\mathbf{q}} = \omega_{\mathbf{q}} - \omega_{\mathrm{p}}$, $\Delta\mathbf{q} = \mathbf{q} - \mathbf{k}_{\mathrm{p}}$. Note that $\hat{\mathcal{E}}(\mathbf{r},t) \propto V^{-1/2}$ is a normalized operator, and thus $\hat{\mathcal{E}}^\dagger\hat{\mathcal{E}}$ gives the photon number density. Using the bosonic commutation relations of the creation and annihilation operators, $[\hat{a}_{\mathbf{k}}, \hat{a}^\dagger_{\mathbf{k}'}] = \delta_{\mathbf{k},\mathbf{k}'}$, we can derive commutation relations for the slowly varying field operators

$$[\hat{\mathcal{E}}(\mathbf{r},t), \hat{\mathcal{E}}^\dagger(\mathbf{r}',t)] \approx \delta(\mathbf{r}-\mathbf{r}'). \tag{A.4}$$

The classical probe field is given by

$$\mathbf{E}(\mathbf{r},t) = \boldsymbol{\epsilon}_{\mathrm{c}} E_{\mathrm{c}}(\mathbf{r},t) e^{\mathrm{i}(k_{\mathrm{c}} z - \omega_{\mathrm{c}} t)} + \mathrm{c.c.} \tag{A.5}$$

yielding for the full field operator

$$\hat{\mathbf{E}}(\mathbf{r},t) = \sqrt{\frac{\omega_{\mathrm{p}}}{2\epsilon_0}} \left(\boldsymbol{\epsilon}_{\mathrm{p}} \hat{\mathcal{E}}(\mathbf{r},t) e^{\mathrm{i}(k_{\mathrm{p}} z - \omega_{\mathrm{p}} t)} + \mathrm{H.a.} \right) + \left(\boldsymbol{\epsilon}_{\mathrm{c}} E_{\mathrm{c}}(\mathbf{r},t) e^{\mathrm{i}(k_{\mathrm{c}} z - \omega_{\mathrm{c}} t)} + \mathrm{c.c.} \right). \tag{A.6}$$

The atomic medium consists of 3 (or 2) states $|\mu\rangle$ with corresponding energies ω_μ and the free Hamiltonian of an atom at position $\mathbf{r}_i$ is given by

$$\hat{\mathcal{H}}_{\mathrm{a}} = \sum_{\mu} \omega_\mu \hat{\sigma}^i_{\mu\mu}, \tag{A.7}$$

where we introduced the spin flip operators $\hat{\sigma}^i_{\mu\nu} = |\mu\rangle_i \langle\nu|_i$. For these we can deduce the commutation relations by using the orthogonality of the atomic states $\langle \mu_i | \nu_j \rangle = \delta_{i,j}\delta_{\mu,\nu}$ yielding

$$[\sigma^i_{\mu\nu}, \sigma^j_{\alpha\beta}] = \delta_{i,j} \left\{ \delta_{\nu,\alpha} \sigma^i_{\mu\beta} - \delta_{\beta,\mu} \sigma^i_{\alpha\nu} \right\}. \tag{A.8}$$

The coupling of an atom and the electromagnetic field is in dipole approximation described by the Hamiltonian

$$\hat{\mathcal{H}}_{\mathrm{af}} = -\hat{\mathbf{d}} \cdot \hat{\mathbf{E}}(\mathbf{r}_i). \tag{A.9}$$

Using the identity $\mathbb{1} = \sum_\mu \hat{\sigma}^i_{\mu\mu}$, we can write the dipole operator in the form

$$\hat{\mathbf{d}} = \sum_{\mu} |\mu\rangle_i \langle\mu|_i \, \hat{\mathbf{d}} \sum_{\nu} |\nu\rangle_i \langle\nu|_i = \sum_{\mu,\nu} \wp_{\mu\nu} \hat{\sigma}^i_{\mu\nu}, \tag{A.10}$$

where we denote the dipole matrix element $\wp_{\mu\nu} = \langle\mu| \hat{\mathbf{d}} |\nu\rangle$ which we assume to be the same for all atoms (, which trivially holds if they are identical).

A.1.1 Three-level atoms

Now we restrict ourselves to atoms with three levels denoted by $|\mathrm{g}\rangle$, $|\mathrm{e}\rangle$ and $|\mathrm{r}\rangle$, where the free Hamiltonian of an atom is given by

$$\hat{\mathcal{H}}_{\mathrm{a}} = \omega_{\mathrm{g}} \hat{\sigma}_{\mathrm{gg}} + \omega_{\mathrm{e}} \hat{\sigma}_{\mathrm{ee}} + \omega_{\mathrm{r}} \hat{\sigma}_{\mathrm{rr}}. \tag{A.11}$$

Without loss of generality we set in the following $\omega_g \to 0$, which is equivalent to performing the unitary transformation

$$\hat{\mathcal{H}}_a \to U\hat{\mathcal{H}}U^\dagger + i(\partial_t U)U^\dagger \tag{A.12}$$

(see below) with $U = \exp\{\mathrm{i}\omega_\mathrm{g}(\hat{\sigma}_\mathrm{gg} + \hat{\sigma}_\mathrm{ee} + \hat{\sigma}_\mathrm{rr})\}$, such that the atomic Hamiltonian becomes

$$\hat{\mathcal{H}}_\mathrm{a} = \omega_\mathrm{eg}\hat{\sigma}_\mathrm{ee} + \omega_\mathrm{rg}\hat{\sigma}_\mathrm{rr} \tag{A.13}$$

where $\omega_{\mu\nu} = \omega_\mu - \omega_\nu$. Moreover, we assume that the transition $|g\rangle \leftrightarrow |r\rangle$ is dipole-forbidden and that the non-zero matrix elements $\wp_{\mu\nu}$ are real. Thus the dipole operator is given by $\hat{\mathbf{d}} = \wp_{ge}(\hat{\sigma}_\mathrm{ge} + \hat{\sigma}_\mathrm{eg}) + \wp_{er}(\hat{\sigma}_\mathrm{er} + \hat{\sigma}_\mathrm{re})$. We use this and the electromagnetic field in the dipole interaction Hamiltonian, Eq. (A.9) and furthermore assume for simplicity that $\wp_\mathrm{ge} \perp \boldsymbol{\epsilon}_\mathrm{c}$ and $\wp_\mathrm{er} \perp \boldsymbol{\epsilon}_\mathrm{p}$. Then the dipole interaction Hamiltonian becomes

$$\begin{aligned}\hat{\mathcal{H}}_\mathrm{af} = -\sqrt{\frac{\omega_\mathrm{p}}{2\epsilon_0}}\wp_\mathrm{ge}\cdot\boldsymbol{\epsilon}_\mathrm{p}\left(\hat{\mathcal{E}}(\mathbf{r},t)e^{\mathrm{i}(k_\mathrm{p}z-\omega_\mathrm{p}t)} + \mathrm{H.a.}\right)\left(\hat{\sigma}_\mathrm{ge} + \hat{\sigma}_\mathrm{ge}^\dagger\right) \\ - \wp_\mathrm{er}\cdot\boldsymbol{\epsilon}_\mathrm{c}\left(E_\mathrm{c}e^{\mathrm{i}(k_\mathrm{c}z-\omega_\mathrm{c}t)} + \mathrm{c.c.}\right)\left(\hat{\sigma}_\mathrm{er} + \hat{\sigma}_\mathrm{re}\right).\end{aligned} \tag{A.14}$$

We perform a unitary transformation to a frame rotating with optical frequencies $\omega_\mathrm{p}, \omega_\mathrm{c}$ generated by

$$U = e^{it\{\omega_\mathrm{p}\hat{\sigma}_\mathrm{ee} + (\omega_\mathrm{p}+\omega_\mathrm{c})\hat{\sigma}_\mathrm{rr}\}}. \tag{A.15}$$

This transforms the free atomic Hamiltonian to

$$\hat{\mathcal{H}}_\mathrm{a} = (\omega_\mathrm{eg} - \omega_\mathrm{p})\hat{\sigma}_\mathrm{ee} + (\omega_\mathrm{rg} - \omega_\mathrm{p} - \omega_\mathrm{c})\hat{\sigma}_\mathrm{rr} = \Delta\hat{\sigma}_\mathrm{ee} + \delta\hat{\sigma}_\mathrm{rr}, \tag{A.16}$$

where $\omega_{\mu\nu} = \omega_\mu - \omega_\nu$ and where we introduced the one- and two-photon detuning $\Delta = \omega_\mathrm{eg} - \omega_\mathrm{p}$ and $\delta = \omega_\mathrm{re} - \omega_\mathrm{c} + \Delta$, respectively. The atom-field coupling Hamiltonian gets transformed to

$$\begin{aligned}\hat{\mathcal{H}}_\mathrm{af} = -\sqrt{\frac{\omega_\mathrm{p}}{2\epsilon_0}}\wp_\mathrm{ge}\cdot\boldsymbol{\epsilon}_\mathrm{p}\left(\hat{\mathcal{E}}(\mathbf{r},t)e^{\mathrm{i}(k_\mathrm{p}z-\omega_\mathrm{p}t)} + \mathrm{H.a.}\right)\left(\hat{\sigma}_\mathrm{ge}e^{-\mathrm{i}\omega_\mathrm{p}t} + \hat{\sigma}_\mathrm{ge}^\dagger e^{\mathrm{i}\omega_\mathrm{p}t}\right) \\ - \wp_\mathrm{er}\cdot\boldsymbol{\epsilon}_\mathrm{c}\left(E_\mathrm{c}e^{\mathrm{i}(k_\mathrm{c}z-\omega_\mathrm{c}t)} + \mathrm{c.c.}\right)\left(\hat{\sigma}_\mathrm{er}e^{-\mathrm{i}\omega_\mathrm{c}t} + \hat{\sigma}_\mathrm{re}e^{\mathrm{i}\omega_\mathrm{c}t}\right).\end{aligned} \tag{A.17}$$

To simplify the Hamiltonian we perform a rotating wave approximation (RWA) thereby neglecting fast oscillating terms proportional to $e^{\pm 2\mathrm{i}\omega_j t}, j = \mathrm{p}, \mathrm{c}$. Defining the control field Rabi frequency $\Omega = \wp_\mathrm{er}\cdot\boldsymbol{\epsilon}_\mathrm{c}E_\mathrm{c}^*$ and $g = \sqrt{\frac{\omega_\mathrm{p}}{2\epsilon_0}}\wp_\mathrm{ge}\cdot\boldsymbol{\epsilon}_\mathrm{p}$ we get the full Hamiltonian in rotating wave approximation

$$\hat{\mathcal{H}} = \hat{\mathcal{H}}_\mathrm{a} + \hat{\mathcal{H}}_\mathrm{af} = \Delta\hat{\sigma}_\mathrm{ee} + \delta\hat{\sigma}_\mathrm{rr} - \left\{g\hat{\mathcal{E}}^\dagger(\mathbf{r},t)\hat{\sigma}_\mathrm{ge}e^{-\mathrm{i}k_\mathrm{p}z} + \Omega^*\hat{\sigma}_\mathrm{re}e^{-\mathrm{i}k_\mathrm{c}z} + \mathrm{H.a.}\right\}. \tag{A.18}$$

A.1.2 Coarse graining and continuum limit

For an ensemble of N atoms we write the full Hamiltonian as a sum over all atoms j at positions $\mathbf{r}_j$

$$\hat{\mathcal{H}} = \sum_j \left\{ \Delta\hat{\sigma}^j_{\mathrm{ee}} + \delta\hat{\sigma}^j_{\mathrm{rr}} - \left[g\hat{\mathcal{E}}^\dagger(\mathbf{r}_j,t)\hat{\sigma}^j_{\mathrm{ge}} e^{-\mathrm{i}k_{\mathrm{p}}z_j} + \Omega^*\hat{\sigma}^j_{\mathrm{re}} e^{-\mathrm{i}k_{\mathrm{c}}z_j} + \mathrm{H.a.} \right] \right\}. \tag{A.19}$$

If $N \gg 1$ we can split the atoms into bins, small volumes $V(\mathbf{r}_j)$ centered at $\mathbf{r}_j$ containing $N(\mathbf{r}_j) \gg 1$ atoms, where $\sum_j N(\mathbf{r}_j) = N$. We furthermore assume that the bins are sufficiently small such that $\hat{\mathcal{E}}(\mathbf{r})$ and $\exp\{-\mathrm{i}k_{\mathrm{p/c}}z\}$ are approximately constant for each bin. Then we can introduce continuous atomic spin-flip operators by

$$\hat{\sigma}_{\mu\nu}(\mathbf{r}) = \frac{1}{N(\mathbf{r})} \sum_{k\in V(\mathbf{r})} \hat{\sigma}^k_{\mu\nu}, \tag{A.20}$$

which allows us to write the Hamiltonian in the form

$$\hat{\mathcal{H}} = \sum_j N(\mathbf{r}_j) \left\{ \Delta\hat{\sigma}_{\mathrm{ee}}(\mathbf{r}_j) + \delta\hat{\sigma}_{\mathrm{rr}}(\mathbf{r}_j) - \left[g\hat{\mathcal{E}}^\dagger(\mathbf{r}_j)\hat{\sigma}_{\mathrm{ge}}(\mathbf{r}_j) e^{-\mathrm{i}k_{\mathrm{p}}z_j} + \Omega^*\hat{\sigma}_{\mathrm{re}}(\mathbf{r}_j) e^{-\mathrm{i}k_{\mathrm{c}}z_j} + \mathrm{H.a.} \right] \right\} \tag{A.21}$$

Finally, performing a continuum limit $\sum_j V(\mathbf{r}_j)\frac{N(\mathbf{r}_j)}{V(\mathbf{r}_j)} \to \int \mathrm{d}^3\mathbf{r}\, n(\mathbf{r})$, by letting $V(\mathbf{r}) \to 0$ while $\frac{N(\mathbf{r})}{V(\mathbf{r})} \to n(\mathbf{r})$ which is the atomic density at position $\mathbf{r}$. This yields the continuum Hamiltonian

$$\hat{\mathcal{H}} = \int \mathrm{d}^3\mathbf{r}\, n(\mathbf{r}) \left\{ \Delta\hat{\sigma}_{\mathrm{ee}}(\mathbf{r}) + \delta\hat{\sigma}_{\mathrm{rr}}(\mathbf{r}) - \left[g\hat{\mathcal{E}}^\dagger(\mathbf{r})\hat{\sigma}_{\mathrm{ge}}(\mathbf{r}) e^{-\mathrm{i}k_{\mathrm{p}}z} + \Omega^*\hat{\sigma}_{\mathrm{re}}(\mathbf{r}) e^{-\mathrm{i}k_{\mathrm{c}}z} + \mathrm{H.a.} \right] \right\} \tag{A.22}$$

The commutation relations of the continuous spin-flip operators can be derived as follows [69]

$$\begin{aligned}
\left[\hat{\sigma}_{\alpha\beta}(\mathbf{r}), \hat{\sigma}_{\mu\nu}(\mathbf{r}')\right] &= \frac{1}{N^2} \sum_{k\in V(\mathbf{r})} \sum_{l\in V(\mathbf{r}')} \left[\hat{\sigma}^k_{\alpha\beta}, \hat{\sigma}^l_{\mu\nu}\right] \\
&= \delta_{\mathbf{r},\mathbf{r}'} \frac{1}{N^2} \sum_{k,l\in V(\mathbf{r})} \delta_{k,l} \left(\delta_{\beta,\mu}\hat{\sigma}^k_{\alpha\nu} - \delta_{\alpha,\nu}\hat{\sigma}^k_{\mu\beta} \right) \\
&= \frac{1}{N} \delta_{\mathbf{r},\mathbf{r}'} \left(\delta_{\beta,\mu}\hat{\sigma}_{\alpha\nu}(\mathbf{r}) - \delta_{\alpha,\nu}\hat{\sigma}_{\mu\beta}(\mathbf{r}) \right)
\end{aligned}$$

In the continuum limit we get finally

$$\left[\hat{\sigma}_{\alpha\beta}(\mathbf{r}), \hat{\sigma}_{\mu\nu}(\mathbf{r}')\right] = \frac{1}{n}\delta^3(\mathbf{r}-\mathbf{r}') \left(\delta_{\beta,\mu}\hat{\sigma}_{\alpha\nu}(\mathbf{r}) - \delta_{\alpha,\nu}\hat{\sigma}_{\mu\beta}(\mathbf{r}) \right), \tag{A.23}$$

where the Kronecker delta changes to the Dirac delta function.

A.2 Dark-state polaritons

In the following section we derive equations of motion for the dark-state polariton. To this end we start from Heisenberg-Langevin equations for the atomic operators and the truncated paraxial wave equation for the electromagnetic field from which we derive Maxwell-Bloch equations for a reduced set of operators. We diagonalize these equations of motion in k-space to find the dark-state polariton eigenmode and use a perturbation theory to find its equations of motion.

A.2.1 Heisenberg-Langevin equations

The Heisenberg-Langevin equations for the atomic occupations and coherences are given by

$$\partial_t \hat{\sigma}_{\mathrm{gg}} = \Gamma_{\mathrm{eg}}\hat{\sigma}_{\mathrm{ee}} + \mathrm{i}g\left(\hat{\mathcal{E}}^\dagger \hat{\sigma}_{\mathrm{ge}} e^{-\mathrm{i}k_{\mathrm{p}}z} - \hat{\mathcal{E}}\hat{\sigma}_{\mathrm{eg}} e^{\mathrm{i}k_{\mathrm{p}}z}\right) + \hat{F}_{\mathrm{gg}}, \tag{A.24a}$$

$$\begin{aligned}\partial_t \hat{\sigma}_{\mathrm{ee}} = &-\Gamma_{\mathrm{eg}}\hat{\sigma}_{\mathrm{ee}} + \Gamma_{\mathrm{re}}\hat{\sigma}_{\mathrm{rr}} - \mathrm{i}g\left(\hat{\mathcal{E}}^\dagger \hat{\sigma}_{\mathrm{ge}} e^{-\mathrm{i}k_{\mathrm{p}}z} - \hat{\mathcal{E}}\hat{\sigma}_{\mathrm{eg}} e^{\mathrm{i}k_{\mathrm{p}}z}\right) \\ &- \mathrm{i}\left(\Omega^* \hat{\sigma}_{\mathrm{re}} e^{-\mathrm{i}k_{\mathrm{c}}z} - \Omega\hat{\sigma}_{\mathrm{er}} e^{\mathrm{i}k_{\mathrm{c}}z}\right) + \hat{F}_{\mathrm{ee}},\end{aligned} \tag{A.24b}$$

$$\partial_t \hat{\sigma}_{\mathrm{rr}} = -\Gamma_{\mathrm{re}}\hat{\sigma}_{\mathrm{rr}} + \mathrm{i}\left(\Omega^* \hat{\sigma}_{\mathrm{re}} e^{-\mathrm{i}k_{\mathrm{c}}z} - \Omega\hat{\sigma}_{\mathrm{er}} e^{\mathrm{i}k_{\mathrm{c}}z}\right) + \hat{F}_{\mathrm{rr}}, \tag{A.24c}$$

$$\partial_t \hat{\sigma}_{\mathrm{ge}} = -(\gamma_{\mathrm{ge}} + \mathrm{i}\Delta)\hat{\sigma}_{\mathrm{ge}} - \mathrm{i}g\hat{\mathcal{E}} e^{\mathrm{i}k_{\mathrm{p}}z}(\hat{\sigma}_{\mathrm{ee}} - \hat{\sigma}_{\mathrm{gg}}) + \mathrm{i}\Omega e^{\mathrm{i}k_{\mathrm{c}}z}\hat{\sigma}_{\mathrm{gr}} + \hat{F}_{\mathrm{ge}}, \tag{A.24d}$$

$$\partial_t \hat{\sigma}_{\mathrm{re}} = -(\gamma_{\mathrm{re}} + \mathrm{i}(\Delta - \delta))\hat{\sigma}_{\mathrm{re}} + \mathrm{i}g\hat{\mathcal{E}} e^{\mathrm{i}k_{\mathrm{p}}z}\hat{\sigma}_{\mathrm{rg}} - \mathrm{i}\Omega e^{\mathrm{i}k_{\mathrm{c}}z}(\hat{\sigma}_{\mathrm{ee}} - \hat{\sigma}_{\mathrm{rr}}) + \hat{F}_{\mathrm{re}}, \tag{A.24e}$$

$$\partial_t \hat{\sigma}_{\mathrm{gr}} = -(\gamma_{\mathrm{gr}} + \mathrm{i}\delta)\hat{\sigma}_{\mathrm{gr}} - \mathrm{i}g\hat{\mathcal{E}} e^{\mathrm{i}k_{\mathrm{p}}z}\hat{\sigma}_{\mathrm{er}} + \mathrm{i}\Omega^* \hat{\sigma}_{\mathrm{ge}} e^{-\mathrm{i}k_{\mathrm{c}}z} + \hat{F}_{\mathrm{gr}}. \tag{A.24f}$$

Γ_{eg} and Γ_{re} are spontaneous emission rates from states $|\mathrm{e}\rangle$ to $|\mathrm{g}\rangle$ and from $|\mathrm{r}\rangle$ to $|\mathrm{e}\rangle$, respectively, since we have a ladder configuration and the transition from Rydberg to ground state is dipole forbidden. The rates $\gamma_{\mu\nu}$ are so-called transverse decay rates combining spontaneous decay rates and dephasing rates. The operators $\hat{F}_\mu$ are Langevin noise operators, that are δ-correlated in space and time with zero mean value,

$$\langle \hat{F}_\mu \rangle = 0 \tag{A.25a}$$

$$\langle \hat{F}_\mu^\dagger(\mathbf{r}, t)\hat{F}_\nu(\mathbf{r}', t')\rangle = D_{\mu\nu}\delta^3(\mathbf{r} - \mathbf{r}')\delta(t - t'). \tag{A.25b}$$

The coefficients $D_{\mu\nu}$ are denoted diffusion coefficients and can be determined by the generalized dissipation-fluctuation theorem [99]. The Langevin noise operators are introduced to preserve commutation relations of the operators when introducing decay. However, in the regime of EIT there is typically only a small excitation of excited and spin (Rydberg) state present and therefore the error arising from omitting the Langevin noise operators is small. Hence we will omit them in the following for convenience. Together with the truncated paraxial wave equation, Eq. (A.30), that will be derived below, the Heisenberg-Langevin equations form a closed set of equations of motion, called

the Maxwell-Bloch equations.

The time evolution of the electromagnetic field $\hat{\mathbf{E}}(\mathbf{r},t)$ is coupled to the polarization of the atomic medium, according to Maxwell's equation,

$$[\partial_t^2 - c^2\nabla^2]\hat{\mathbf{E}}(\mathbf{r},t) = -\frac{1}{\epsilon_0}\partial_t^2\hat{\mathbf{P}}(\mathbf{r},t). \tag{A.26}$$

The polarization of the medium is defined by the average over all single atom dipole operators. In the continuum limit it is given by

$$\hat{\mathbf{P}}(\mathbf{r},t) = n(\mathbf{r})\left(\wp_{\mathrm{ge}}\hat{\sigma}_{\mathrm{ge}}(\mathbf{r},t)e^{-\mathrm{i}\omega_{\mathrm{p}}t} + \wp_{\mathrm{er}}\hat{\sigma}_{\mathrm{er}}(\mathbf{r},t)e^{-\mathrm{i}\omega_{\mathrm{c}}t} + \mathrm{H.a.}\right), \tag{A.27}$$

where we used slowly varying operators $\hat{\sigma}_{\mu\nu}$ as they are defined in the rotating frame we are using, see Eq. (3.12). We put this definition together with the definition of the electromagnetic field, (A.6), into Maxwell's equation. Furthermore, we assume as before for simplicity that $\wp_{\mathrm{ge}} \perp \boldsymbol{\epsilon}_{\mathrm{c}}$ and $\wp_{\mathrm{er}} \perp \boldsymbol{\epsilon}_{\mathrm{p}}$ and the polarizations of the probe and control fields are orthogonal to each other, i.e., $\boldsymbol{\epsilon}_{\mathrm{p}} \perp \boldsymbol{\epsilon}_{\mathrm{c}}$. As we are interested in the dynamics of the probe field, we project the Maxwell equation onto $\boldsymbol{\epsilon}_{\mathrm{p}}$, yielding

$$\begin{aligned}\left[\partial_t^2 - c^2\partial_z^2 - c^2\nabla_\perp^2\right]\sqrt{\frac{\omega_{\mathrm{p}}}{2\epsilon_0}}\left(\hat{\mathcal{E}}(\mathbf{r},t)e^{\mathrm{i}(k_{\mathrm{p}}z-\omega_{\mathrm{p}}t)} + \mathrm{H.a.}\right)& \\ = -\frac{1}{\epsilon_0}n(\mathbf{r})\boldsymbol{\epsilon}_{\mathbf{p}}\cdot\wp_{\mathbf{ge}}\,\partial_t^2\left(\hat{\sigma}_{\mathrm{ge}}(\mathbf{r},t)e^{-i\omega_{\mathrm{p}}t} + \mathrm{H.a.}\right),&\end{aligned} \tag{A.28}$$

where we split the spatial derivative into z- and transversal derivative. We use the definition $g = \sqrt{\frac{\omega_{\mathrm{p}}}{2\epsilon_0}}\wp_{\mathrm{ge}}\cdot\boldsymbol{\epsilon}_{\mathrm{p}}$ of the atom-field coupling strength, the dispersion relation of the free probe field, $\omega_{\mathrm{p}} = ck_{\mathrm{p}}$ and arrive at:

$$\begin{aligned}\left[\partial_t^2\hat{\mathcal{E}} - c^2\partial_z^2\hat{\mathcal{E}} - 2\mathrm{i}\omega_{\mathrm{p}}(\partial_t\hat{\mathcal{E}} + c\partial_z\hat{\mathcal{E}}) - c^2\nabla_\perp^2\hat{\mathcal{E}}\right]e^{\mathrm{i}(k_{\mathrm{p}}z-\omega_{\mathrm{p}}t)} + \mathrm{H.a.}& \\ = -\frac{2}{\omega_{\mathrm{p}}}n(\mathbf{r})g\left[\partial_t^2\hat{\sigma}_{\mathrm{ge}} - 2\mathrm{i}\omega_{\mathrm{p}}\hat{\sigma}_{\mathrm{ge}} - \omega_{\mathrm{p}}^2\hat{\sigma}_{\mathrm{ge}}\right]e^{-\mathrm{i}\omega_{\mathrm{p}}t} + \mathrm{H.a.}&\end{aligned} \tag{A.29}$$

We observe that the operators $\hat{\sigma}_{\mathrm{ge}}$ and $\hat{\mathcal{E}}$ are slowly varying in time and space and time, respectively. Thus we can make the estimations $|\partial_t^2\hat{\mathcal{E}}| \ll \omega_{\mathrm{p}}|\partial_t\hat{\mathcal{E}}|$, $|\partial_z^2\hat{\mathcal{E}}| \ll k_{\mathrm{p}}|\partial_z\hat{\mathcal{E}}|$ for the probe field and $|\partial_t^2\hat{\sigma}_{\mathrm{ge}}| \ll \omega_{\mathrm{p}}|\partial_t\hat{\sigma}_{\mathrm{ge}}| \ll \omega_{\mathrm{p}}^2|\hat{\sigma}_{\mathrm{ge}}|$ for the atomic coherence and simplify Eq. (A.29) by neglecting the higher order derivatives, accordingly. Comparing the coefficients of the exponential functions we arrive finally at the equation

$$\left[\partial_t + c\partial_z - \mathrm{i}\frac{c}{2k_{\mathrm{p}}}\nabla_\perp^2\right]\hat{\mathcal{E}}(\mathbf{r},t) = \mathrm{i}gn(\mathbf{r})\hat{\sigma}_{\mathrm{ge}}(\mathbf{r},t)e^{-\mathrm{i}k_{\mathrm{p}}z}, \tag{A.30}$$

the truncated paraxial wave equation that will be one of the fundamental equations for our calculations.

A.2.2 Maxwell-Bloch equations

In the following we want to make further assumptions and approximations to derive a reduced set of equations for the relevant operators. In the regime of a weak quantized probe field we can assume that the probe field is much weaker than the control field, i.e., $g\langle\hat{\mathcal{E}}\rangle \ll \Omega$. Under this assumption we can treat the probe field perturbatively. If we furthermore make the reasonable assumption that the atoms are initially all in their ground state, we obtain in zeroth order of $g\hat{\mathcal{E}}$ that $\hat{\sigma}_{\mathrm{gg}}^{(0)} = 1$. Including the paraxial wave equation (reduced to one spatial dimension for the moment) the equations in first order in $g\hat{\mathcal{E}}$ read

$$\begin{aligned}
\partial_t\hat{\mathcal{E}} &= -c\partial_z\hat{\mathcal{E}} + \mathrm{i}gn\hat{\sigma}_{\mathrm{ge}}^{(1)}e^{-\mathrm{i}k_{\mathrm{p}}z} \\
\partial_t\hat{\sigma}_{\mathrm{ge}}^{(1)} &= -(\gamma_{\mathrm{ge}} + \mathrm{i}\Delta)\hat{\sigma}_{\mathrm{ge}}^{(1)} + \mathrm{i}g\hat{\mathcal{E}}e^{\mathrm{i}k_{\mathrm{p}}z} + \mathrm{i}\Omega\hat{\sigma}_{\mathrm{gr}}^{(1)}e^{\mathrm{i}k_{\mathrm{c}}z} \\
\partial_t\hat{\sigma}_{\mathrm{gr}}^{(1)} &= -(\gamma_{\mathrm{gr}} + \mathrm{i}\delta)\hat{\sigma}_{\mathrm{gr}}^{(1)} + \mathrm{i}\Omega^*\hat{\sigma}_{\mathrm{ge}}^{(1)}e^{-\mathrm{i}k_{\mathrm{c}}z}
\end{aligned} \tag{A.31}$$

We omit the perturbation orders in the following and absorb a factor of $1/\sqrt{n}$ as well as the spatial oscillations with the wavevector k_{p} and the wave vector mismatch $k_{\mathrm{p}} - k_{\mathrm{c}}$ into the operators $\hat{\sigma}_{\mathrm{ge}}$ and $\hat{\sigma}_{\mathrm{gr}}$, respectively, by transforming

$$\hat{\sigma}_{\mathrm{ge}} \to \frac{1}{\sqrt{n}}\hat{\sigma}_{\mathrm{ge}}e^{+\mathrm{i}k_{\mathrm{p}}z}, \qquad \hat{\sigma}_{\mathrm{gr}} \to \frac{1}{\sqrt{n}}\hat{\sigma}_{\mathrm{gr}}e^{\mathrm{i}(k_{\mathrm{p}}-k_{\mathrm{c}})z}, \tag{A.32}$$

i.e., transforming also to spatially slowly varying operators. Multiplying the second and last equation by $\sqrt{n}$ results in the final Maxwell-Bloch equations

$$\begin{aligned}
\partial_t\hat{\mathcal{E}}(\mathbf{r},t) &= -c\partial_z\hat{\mathcal{E}}(\mathbf{r},t) + ig\sqrt{n}\hat{\sigma}_{\mathrm{ge}}(\mathbf{r},t) \\
\partial_t\hat{\sigma}_{\mathrm{ge}}(\mathbf{r},t) &= -(\gamma_{\mathrm{ge}} + \mathrm{i}\Delta)\hat{\sigma}_{\mathrm{ge}}(\mathbf{r},t) + \mathrm{i}g\sqrt{n}\hat{\mathcal{E}}(\mathbf{r},t) + \mathrm{i}\Omega\hat{\sigma}_{\mathrm{gr}}(\mathbf{r},t) \\
\partial_t\hat{\sigma}_{\mathrm{gr}}(\mathbf{r},t) &= -(\gamma_{\mathrm{gr}} + \mathrm{i}\delta)\hat{\sigma}_{\mathrm{gr}}(\mathbf{r},t) + \mathrm{i}\Omega^*\hat{\sigma}_{\mathrm{ge}}(\mathbf{r},t),
\end{aligned} \tag{A.33}$$

that are the fundamental equations of motion for our calculations and numerical simulations of interacting Rydberg dark-state polaritons considered in this thesis.

A.2.3 Perturbation theory in k-space

In this section we want to derive an effective equation of motion for the dark-state polaritons by using perturbation theory. We transform the spatial coordinate z to the momentum space according to $f(z,t) = \int \mathrm{d}k\, e^{-\mathrm{i}kz}f(k,t)$. As we want to solve a system of equations of motion for the three operators $\hat{\mathcal{E}}, \hat{\sigma}_{\mathrm{gr}}$ and $\hat{\sigma}_{\mathrm{ge}}$ we define $\hat{\mathbf{y}} = (\hat{\mathcal{E}}, \hat{\sigma}_{\mathrm{gr}}, \hat{\sigma}_{\mathrm{ge}})^t$, such that the equations can be rewritten in the

form

$$\mathrm{i}\partial_t \hat{\mathbf{y}} = (H_0 + H_1)\hat{\mathbf{y}}, \tag{A.34}$$

$$H_0 = \begin{pmatrix} 0 & 0 & -g\sqrt{n} \\ 0 & 0 & -\Omega \\ -g\sqrt{n} & -\Omega & -2\mathrm{i}\Gamma \end{pmatrix}, \quad H_1 = \begin{pmatrix} -ck & 0 & 0 \\ 0 & \delta & 0 \\ 0 & 0 & 0 \end{pmatrix}, \tag{A.35}$$

where we set $\Gamma = \frac{1}{2}(\gamma_{\mathrm{ge}} + \mathrm{i}\Delta)$ and $\gamma_{\mathrm{gr}} = 0$ and H_1 denotes the perturbation Hamiltonian. For simplicity we perform a rotation transformation

$$R(\theta) = \begin{pmatrix} \cos\theta & -\sin\theta & 0 \\ \sin\theta & \cos\theta & 0 \\ 0 & 0 & 1 \end{pmatrix}, \quad R(\theta) \begin{pmatrix} \hat{\mathcal{E}} \\ \hat{\sigma}_{\mathrm{gr}} \\ \hat{\sigma}_{\mathrm{ge}} \end{pmatrix} = \begin{pmatrix} \hat{\Psi} \\ \hat{\Phi} \\ \hat{\sigma}_{\mathrm{ge}} \end{pmatrix} \equiv \hat{\mathbf{x}}, \tag{A.36}$$

where the second equation defines the dark-state polariton $\hat{\Psi}$ and the bright-state polariton $\hat{\Phi}$. Applying this transformation to Eq. (A.34) yields after rearranging terms

$$\mathrm{i}\partial_t \hat{\mathbf{x}} = [R(\theta)(H_0 + H_1)R^{-1}(\theta) - \mathrm{i}\dot{\theta}R(\theta)\partial_\theta R^{-1}(\theta)]\hat{\mathbf{x}}. \tag{A.37}$$

Choosing the mixing angle $\theta = \mathrm{atan}(g\sqrt{n}/\Omega)$ we get

$$RH_0R^{-1} = \begin{pmatrix} 0 & 0 & 0 \\ 0 & 0 & -\Omega_{\mathrm{eff}} \\ 0 & -\Omega_{\mathrm{eff}} & -2\mathrm{i}\Gamma \end{pmatrix}, \tag{A.38}$$

$$RH_1R^{-1} = \frac{1}{\Omega_{\mathrm{eff}}^2} \begin{pmatrix} g^2n\delta - \Omega^2 ck & -g\Omega(ck+\delta) & 0 \\ -g\Omega(ck+\delta) & \Omega^2\delta - g^2nck & 0 \\ 0 & 0 & 0 \end{pmatrix} \tag{A.39}$$

and

$$R(\theta)\partial_\theta R^{-1}(\theta) = \begin{pmatrix} 0 & 1 & 0 \\ -1 & 0 & 0 \\ 0 & 0 & 0 \end{pmatrix}, \tag{A.40}$$

where we defined $\Omega_{\mathrm{eff}} = \sqrt{g^2n + \Omega^2}$.

The unperturbed matrix RH_0R^{-1} can be diagonalized giving the eigenvalues and (not yet normal-

ized) eigenstates

$$|n^0\rangle = (1,0,0)^t, \quad E_0 = 0 \tag{A.41}$$

and

$$|m^0_\pm\rangle = \frac{(0, E_\mp/\Omega_{\text{eff}}, 1)^t}{\sqrt{|E_\mp|^2/\Omega^2_{\text{eff}} + 1}}, \quad E_\pm = -(\mathrm{i}\Gamma \pm \sqrt{\Omega^2_{\text{eff}} - \Gamma^2}). \tag{A.42}$$

The state $|n^0\rangle$ corresponds to the operator $\hat{\Psi}$ and has in zeroth order perturbation theory the eigenenergy $E_0 = 0$, i.e. is a dark-state. We want now to calculate energy corrections arising by the coupling matrix $\tilde{H}_1 \equiv RH_1R^{-1}$. Perturbation theory yields up to second order

$$\mathrm{i}\partial t\hat{\Psi} = \left[\langle n^0|\tilde{H}_1|n^0\rangle - \sum_{\alpha=\pm} \frac{|\langle m^0_\alpha|\tilde{H}_1|n^0\rangle|^2}{E_\alpha}\right]\hat{\Psi} \tag{A.43}$$

$$= \left[-ck\cos^2\theta + \delta\sin^2\theta\right]\hat{\Psi} - \mathrm{i}(\dot{\theta} + \sin\theta\cos\theta(ck+\delta))^2\left[\frac{2\Gamma}{\Omega^2_{\text{eff}}} - \frac{\gamma}{|\Gamma|^2 + \Omega^2_{\text{eff}} + |\Gamma^2 - \Omega^2_{\text{eff}}|}\right]\hat{\Psi} \tag{A.44}$$

Note that in the limits $\Delta \gg \gamma$ and $\Delta \ll \gamma$, respectively, the term in the last (square) bracket becomes

$$\frac{\mathrm{i}\Delta}{\Omega^2_{\text{eff}}} = \frac{\mathrm{i}\Delta\sin^2\theta}{g^2n} \quad \text{and} \quad \frac{\gamma}{2\Omega^2_{\text{eff}}} = \frac{\gamma\sin^2\theta}{2g^2n}, \tag{A.45}$$

respectively, where we assumed $\Omega^2_{\text{eff}} > \gamma^2$ for the last expression. Furthermore, we used the identity $\sin^2\theta = g^2n/\Omega^2_{\text{eff}}$, as this takes care of the θ- (and thus also time-) dependence of Ω_{eff}.

We can now derive a simple solution of this equation as given in [21] by integrating the time variable, yielding

$$\hat{\Psi}(k,t) = \hat{\Psi}(k,0)\exp\left\{\mathrm{i}\int_0^t \mathrm{d}\tau\ \left[ck\cos^2\theta(\tau) - \delta\sin^2\theta(\tau)\right]\right\} \times \exp\left\{-\frac{\gamma + \mathrm{i}2\Delta}{g^2n}\int_0^t \mathrm{d}\tau\ \sin^2\theta(\tau)[\dot{\theta}(\tau) + \sin\theta(\tau)\cos\theta(\tau)(ck+\delta)]^2\right\} \times \exp\left\{-\tfrac{\gamma}{g^2n}\int_0^t \mathrm{d}\tau\, A_\Gamma(\tau)\right\}. \tag{A.46}$$

The first exponential factor consist of two terms, describing propagation of the polariton with time-dependent group velocity $v_{\text{g}}(t) = c\cos^2\theta(t)$ and an additional phase factor due to the two-photon detuning δ. The second exponential factor describes losses and dispersion of the polariton, where one

of the two processes may dominate, depending on the ratio Δ/γ. Furthermore it describes corrections arising from non-adiabatic switching of θ and a finite two-photon δ [21]. The last exponential factor with $A_\Gamma(\tau)$ only contributes if γ is comparable to Δ, a regime that we are not interested in. Let us now discuss the first and second exponential factor.

A.2.4 Adiabatic elimination

Equations of motion for the dark-state polaritons coupled to bright-state polaritons can also be derived by adiabatic elimination of $\hat{\sigma}_{\mathrm{ge}}$. Starting from (A.33) and setting $\frac{d}{dt}\hat{\sigma}_{\mathrm{ge}} = 0$ leads to

$$\hat{\sigma}_{\mathrm{ge}}^{(0)} = +\mathrm{i}\frac{g\sqrt{n}}{\Gamma}\hat{\mathcal{E}} + \mathrm{i}\frac{\Omega}{\Gamma}\hat{\sigma}_{\mathrm{gr}} \tag{A.47}$$

Inserting this into the equations of motion we get

$$\frac{d}{dt}\hat{\mathcal{E}} = -c\partial_z\hat{\mathcal{E}} - \frac{g^2 n}{\Gamma}\hat{\mathcal{E}} - \frac{g\sqrt{n}\Omega}{\Gamma}\hat{\sigma}_{\mathrm{gr}} \tag{A.48}$$

$$\frac{d}{dt}\hat{\sigma}_{\mathrm{gr}} = -(\gamma_{gr} + \mathrm{i}\delta)\hat{\sigma}_{\mathrm{gr}} - \frac{|\Omega|^2}{\Gamma}\hat{\sigma}_{\mathrm{gr}} - \frac{g\sqrt{n}\Omega^*}{\Gamma}\hat{\mathcal{E}} \tag{A.49}$$

Finally, transforming to the polariton degrees of freedom according to Eq. (A.36) yields a set of coupled equations,

$$\frac{d}{dt}\hat{\Psi} = -c\cos^2\theta\frac{\partial}{\partial z}\hat{\Psi} - c\sin\theta\cos\theta\frac{\partial}{\partial z}\hat{\Phi} - \dot{\theta}\hat{\Phi} \tag{A.50}$$

$$\frac{d}{dt}\hat{\Phi} = -\frac{\Omega_{\mathrm{eff}}^2}{\Gamma}\hat{\Phi} - \sin^2\theta\frac{\partial}{\partial z}\hat{\Phi} - c\sin\theta\cos\theta\frac{\partial}{\partial z}\hat{\Psi} + \dot{\theta}\hat{\Psi} \tag{A.51}$$

describing the time evolution of Rydberg polaritons.

Appendix B

Laguerre-Gauss transition elements

In this appendix we present the details on the calculations in section 2.1. In particular we present the integration of the angular integrals by means of residue calculus and furthermore the derivation of the approximate integration of the radial integrals.

B.1 Laguerre-Gaussian modes

Let us first reconsider the Definition of the Laguerre-Gauss modes. These are defined by

$$u_{pl}(r,\varphi,z) = \frac{C_{pl}}{w(z)}\left(\frac{r\sqrt{2}}{w(z)}\right)^{|l|} e^{-r^2/w^2(z)+\mathrm{i}l\varphi} e^{-\mathrm{i}k_\mathrm{p}r^2/2R(z)} e^{\mathrm{i}(2p+|l|+1)\zeta(z)} L_p^{|l|}\left(\frac{2r^2}{w^2(z)}\right), \tag{B.1}$$

where the normalization constant is given by

$$C_{pl}^{-2}(z) = 2\pi\int \mathrm{d}r\, r\left|\frac{1}{w(z)}\left(\frac{r\sqrt{2}}{w(z)}\right)^{|l|} e^{-r^2/w^2(z)} L_p^{|l|}\Big(\frac{2r^2}{w^2(z)}\Big)\right|^2 = \frac{\pi}{2}\frac{(|l|+p)!}{p!}. \tag{B.2}$$

B.2 Effective interaction potentials

The effective potentials for a mode scattering as considered in the main text are defined by integration of angular and radial coordinates,

$$\widetilde{V}_{\mathbf{pl}}(z,z') := C_6 \iint_0^{2\pi} \mathrm{d}\varphi\,\mathrm{d}\varphi' \iint_0^{\infty} r\mathrm{d}r\, r'\mathrm{d}r' \frac{u^*_{p_1l_1}(\mathbf{r})u^*_{p_2l_2}(\mathbf{r}')u_{p_3l_3}(\mathbf{r}')u_{p_4l_4}(\mathbf{r})}{[r^2+r'^2+2rr'\cos(\varphi-\varphi')+(z-z')^2]^3}, \tag{B.3}$$

where in polar coordinates $\mathbf{r} = (r,\varphi,z)$.

B.2.1 Angular integration

The angular integration can be done analytically by means of the residue theorem [60]. We consider the integral

$$\iint \mathrm{d}\varphi\,\mathrm{d}\varphi' \frac{e^{-\mathrm{i}q'\varphi'}e^{-\mathrm{i}q\varphi}}{[\alpha+\beta\cos(\varphi-\varphi')]^3}, \tag{B.4}$$

where we introduced the notation $q = l_1 - l_4$, $q' = l_2 - l_3$, $\alpha = r^2 + r'^2 + (z - z')^2$ and $\beta = 2rr'$ for simplicity. We restrict ourselves to the case $\alpha > 0$ which can be justified by assuming that no double Rydberg excitation can exist for $z = z'$. We want to perform the integration over φ. We do this using the residue theorem applied to a rational function of trigonometric functions [60], which allows us to calculate the double integral as

$$\int \mathrm{d}\varphi' \, e^{-\mathrm{i}q'\varphi'} 2\pi\mathrm{i} \sum_{|z_0|<1} \mathrm{Res}_{z_0}(f), \tag{B.5}$$

i.e. a sum of residues of the function

$$f(z) = \frac{8\mathrm{i}z^{2-q}}{(2\alpha z + \beta e^{\mathrm{i}\varphi'} + z^2 e^{-\mathrm{i}\varphi'})^3}. \tag{B.6}$$

This function has the poles $z = 0$ for $q > 2$ and

$$z_\pm = -\frac{\alpha}{\beta} e^{\mathrm{i}\varphi'} \left(1 \pm \sqrt{1 - \frac{\beta^2}{\alpha^2}}\right). \tag{B.7}$$

As can easily be seen, it holds $\alpha > \beta$. Thus $|z_+| > 1$ and $|z_-| < 1$ and therefore only z_- and $z = 0$ may contribute to the integral. A calculation of the residue yields

$$\mathrm{Res}_{z_-}(f) = \mathrm{i} z_-^{-q} \frac{(q^2-1)\beta^2 - (q^2+2)\alpha^2 + 3q\alpha\sqrt{\alpha^2 - \beta^2}}{2(\alpha^2 - \beta^2)^{5/2}}. \tag{B.8}$$

In particular the remaining φ'-dependence of the integral is given by $z_-^{-p} \propto e^{-\mathrm{i}p\varphi'}$. We can easily integrate over the variable φ', resulting in

$$\int_0^{2\pi} \mathrm{d}\varphi' \, e^{-\mathrm{i}(p'+p)\varphi'} = 2\pi\delta_{p,-p'}. \tag{B.9}$$

Thus, the full integral (B.4) is vanishing except for the case, when $q = -q'$. For $q > 2$ also the residue $\mathrm{Res}_{z=0}(f)$ yields a finite contribution to the integral. However, as the full integral (B.4) is invariant under changing $q \leftrightarrow q'$ and proportional to $\delta_{q,-q'}$ it has to be independent of the sign of p. Thus we can take the result for $q < 0$ and replace $q \to -|q|$ to get the result that is valid for arbitrary q,

$$2\pi^2 \delta_{q,-q'} \left(\frac{-\alpha + \sqrt{\alpha^2 - \beta^2}}{\beta}\right)^{|q|} \frac{(q^2+2)\alpha^2 - (q^2-1)\beta^2 + 3|q|\alpha\sqrt{\alpha^2 - \beta^2}}{(\alpha^2 - \beta^2)^{5/2}}. \tag{B.10}$$

Inserting the definition of q, q' we get the relation $\delta_{l_1 - l_4, l_3 - l_2} = \delta_{l_1 + l_2, l_3 + l_4}$, i.e. a conservation rule for angular momentum.

B.2.2 Approximate radial integration

For the radial integrals no closed expression can be given. However, in certain limits regarding $z - z'$, an approximate result can be derived for the integrals that reproduces the exact integrals quite well, as demonstrated in the main text. Here we want to get a brief derivation of these results. To this end we consider the limit $\alpha \gg \beta$, as holds eg. for sufficiently large $z - z'$. Expanding around $\beta/\alpha = 0$ yields for the integral in first order

$$I_\varphi = \delta_{q,-q'} 2\pi^2 (1 + |q|)(2 + |q|)(-1)^{|q|} \frac{(rr')^{|q|}}{(r^2 + r'^2 + (z - z')^2)^{|q|+3}}. \tag{B.11}$$

Now we restrict ourselves to the case of initial Gaussian modes, i.e., $p_3 = p_4 = l_3 = l_4 = 0$, and denote $l \equiv |q| = |l_1|$. Here we have to integrate

$$\widetilde{V}_{\mathbf{pl}}(z, z') := C_6 \iint_0^\infty r \mathrm{d}r \, r' \mathrm{d}r' \, I_\varphi^l(r, r', z, z'). \tag{B.12}$$

We are in particular interested in the intermediate regime for distances larger than a few beam waists w_0 and smaller than a few Rayleigh lengths z_R where the diagonal scattering potential is the dominant contribution to the potential. In this regime all potentials decay as a power law with different exponents. By making some assumptions we can derive an approximate closed analytical expression for the integrals over r, r' and hence the potentials in this regime as follows. In the limit of $|z - z'| \gg rr'$ the full integral (2.15) can be written for Gaussian in-going modes ($p_3 = p_4 = l_3 = l_4 = 0$) and taking only lowest order of rr' as

$$\begin{aligned}\tilde{V}_{\mathbf{pl}}(z, z') = \delta_{l_1,-l_2} \frac{(-1)^{l+1}}{2^{2l+1}} (l + 1)(l + 2) \sqrt{\frac{p_1! p_2!}{(p_1 + l)!(p_2 + l)!}} e^{-\mathrm{i}(p_1+l)\zeta(z)} e^{-\mathrm{i}(p_2+l)\zeta(z')} \\ \times (w(z)w(z'))^l \int_0^\infty \mathrm{d}s \, s^l e^{-s} L_{p_1}^l(s) \int_0^\infty \mathrm{d}s' \, s'^l e^{-s'} L_{p_2}^l(s') \frac{1}{[r(s)^2 + r'(s')^2 + (z - z'^2)]^{l+3}},\end{aligned} \tag{B.13}$$

where we made the substitutions $s = s(r, z) = 2r^2/w^2(z)$ and analog for s' and $r(s)$ indicates the inverse of this substitution. Moreover, we set $l := |l_1| = |l_2|$. For $z, z' \gg s, s'$ we can make a series expansion of the fraction in the integral with respect to s, s', in the point $s = s' = 0$, yielding a power series, that we will not consider here in detail, but analyze the contribution of its terms to the integral as follows. Let us consider the m^{th} power $\sim s^m$ of this series. Using Rodrigues representation [57] of the associated Laguerre polynomials, $s^l e^{-s} L_p^l(s) = \frac{\mathrm{d}^p}{\mathrm{d}s^p}\left(e^{-s} s^{p+l}\right)$, we can derive the expression

$$\int_0^\infty \mathrm{d}s \, s^{l+m} e^{-s} L_p^l(s) = \frac{(l + m)!}{p!} \prod_{j=0}^{p-1} (j - m). \tag{B.14}$$

From this result we can directly read off, that the power s^m of the power series of the fraction in (B.13) only contributes to the integral, if $m \geq p$, all lower orders of the power series cancel. For the leading order of the power series the integral becomes $(-1)^p(l+p)!$. Taking only the leading order and repeating the argument for the second integral as well, we can finally determine the asymptotic behavior in the intermediate regime in leading order as

$$\tilde{V}_{\mathbf{pl}}(z, z') \propto (z - z')^{-\alpha}, \quad \alpha = 6 + 2(p_1 + p_2) + 2l, \tag{B.15}$$

where we used that the terms of the power series of order $(ss')^m$ are proportional to $(z-z')^{-6-2l-2m}$.

Appendix C

Equations of motion for single- and two particle density matrix

Here we want to derive the equation of motion under the master equation (2.35) in the main text for single- and two-particle correlations assuming, that initially only up to two excitations exist in the system. In this case it is justified to keep only expectation values up to second order in $\hat{\Psi}(z)$ and $\hat{\Psi}^\dagger(z)$.

Equation of motion for single particle density matrix

$$\begin{aligned}
\frac{d}{dt}\langle\hat{\Psi}^\dagger(x)\hat{\Psi}(x)\rangle &= iv_{\mathrm{g}}L_{\mathrm{abs}}\frac{\Delta}{\gamma}\sin^4\theta\left\langle[\partial_{xx}\hat{\Psi}^\dagger(x)]\hat{\Psi}(x)-\hat{\Psi}^\dagger(x)\partial_{xx}\hat{\Psi}(x)\right\rangle \\
&+ 2iv_{\mathrm{g}}\frac{\Delta}{\Omega_{\mathrm{eff}}^2}\sin^4\theta\partial_x\int dz\,V(x-z)\,\langle\hat{\Psi}^\dagger(x)\hat{\Psi}^\dagger(z)\hat{\Psi}(z)\hat{\Psi}(x)\rangle \\
&+ v_{\mathrm{g}}L_{\mathrm{abs}}\sin^4\theta\left\langle[\partial_{xx}\hat{\Psi}^\dagger(x)]\hat{\Psi}(x)+\hat{\Psi}^\dagger(x)\partial_{xx}\hat{\Psi}(x)\right\rangle \\
&+ 2iv_{\mathrm{g}}\frac{\gamma}{\Omega_{\mathrm{eff}}^2}\sin^4\theta\int dz\,V(x-z)\left\langle[\partial_x\hat{\Psi}^\dagger(x)]\hat{\Psi}^\dagger(z)\hat{\Psi}(z)\hat{\Psi}(x)-\hat{\Psi}^\dagger(x)\hat{\Psi}^\dagger(z)\hat{\Psi}(z)[\partial_x\hat{\Psi}(x)]\right\rangle \\
&- 2\frac{\gamma}{\Omega_{\mathrm{eff}}^2}\sin^4\theta\cos^2\theta(2-\sin^2\theta)\int dz V^2(x-z)\,\langle\hat{\Psi}^\dagger(x)\hat{\Psi}^\dagger(y)\hat{\Psi}(x)\hat{\Psi}(y)\rangle
\end{aligned} \tag{C.1}$$

Equation of motion of two particle density matrix

$$\begin{aligned}
&\frac{d}{dt}\langle\hat{\Psi}^\dagger(x)\hat{\Psi}^\dagger(y)\hat{\Psi}(y)\hat{\Psi}(x)\rangle = \\
&iv_{\mathrm{g}}L_{\mathrm{abs}}\frac{\Delta}{\gamma}\sin^4\theta\left\{[(\partial_{xx}+\partial_{yy})\hat{\Psi}^\dagger(x)\hat{\Psi}^\dagger(y)]\hat{\Psi}(y)\hat{\Psi}(x)-\hat{\Psi}^\dagger(x)\hat{\Psi}^\dagger(y)(\partial_{xx}+\partial_{yy})\hat{\Psi}(y)\hat{\Psi}(x)\right\} \\
&+ 2v_{\mathrm{g}}\frac{\Delta}{\Omega_{\mathrm{eff}}^2}\sin^4\theta(\partial_x+\partial_y)\left[V(x-y)\,\langle\hat{\Psi}^\dagger(x)\hat{\Psi}^\dagger(y)\hat{\Psi}(y)\hat{\Psi}(x)\rangle\right] \\
&- 4\frac{\gamma}{\Omega_{\mathrm{eff}}^2}\sin^4\theta\cos^2\theta V^2(x-y)\,\langle\hat{\Psi}^\dagger(x)\hat{\Psi}^\dagger(y)\hat{\Psi}(x)\hat{\Psi}(y)\rangle \\
&- v_{\mathrm{g}}L_{\mathrm{abs}}\sin^4\theta\left\{[(\partial_{xx}+\partial_{yy})\hat{\Psi}^\dagger(x)\hat{\Psi}^\dagger(y)]\hat{\Psi}(y)\hat{\Psi}(x)+\hat{\Psi}^\dagger(x)\hat{\Psi}^\dagger(y)(\partial_{xx}+\partial_{yy})\hat{\Psi}(y)\hat{\Psi}(x)\right\} \\
&+ 2iv_{\mathrm{g}}\frac{\gamma}{\Omega_{\mathrm{eff}}^2}\sin^4\theta V(x-y)\left\langle\left[(\partial_x+\partial_y)\hat{\Psi}^\dagger(x)\hat{\Psi}^\dagger(y)\right]\hat{\Psi}(x)\hat{\Psi}(y)-\hat{\Psi}^\dagger(x)\hat{\Psi}^\dagger(y)\left[(\partial_x+\partial_y)\hat{\Psi}(x)\hat{\Psi}(y)\right]\right\rangle
\end{aligned} \tag{C.2}$$

Appendix D

Finite differences on a non-uniform grid

We want to derive a finite difference scheme for the first derivative of a function f given at a discretized nonuniform grid as sketched in Figure D.1 To this end we consider three sampling points x_i, x_{i-1}, x_{i-2}. Approximating the function f by the Taylor expansion at the point x_i yields

$$f(x) = f(x_i) + (x - x_i)f'(x_i) + \frac{1}{2}(x - x_i)^2 f''(x_i) + \dots \tag{D.1}$$

We evaluate this at the sampling points x_{i-1} and x_{i-2}, where we use the definitions $\Delta = x_i - x_{i-1}$ and $\delta = x_{i-1} - x_{i-2}$,

$$f(x_{i-1}) = f(x_i) - \Delta f'(x_i) + \frac{1}{2}\Delta^2 f''(x_i) + \dots, \tag{D.2}$$

$$f(x_{i-2}) = f(x_i) - (\Delta + \delta)f'(x_i) + \frac{1}{2}(\Delta + \delta)^2 f''(x_i) + \dots \tag{D.3}$$

Multiplying these two equations with α and β, resp., then calculating the sum and requiring $\alpha + \beta = 1$ we find an expression for the first derivative, where the contribution of the second derivative vanishes:

$$f'(x_i) = \frac{\delta + 2\Delta}{\Delta(\Delta + \delta)} f(x_i) - \frac{\Delta + \delta}{\delta\Delta} f(x_{i-1}) + \frac{\Delta}{\delta(\delta + \Delta)} f(x_{i-2}) \tag{D.4}$$

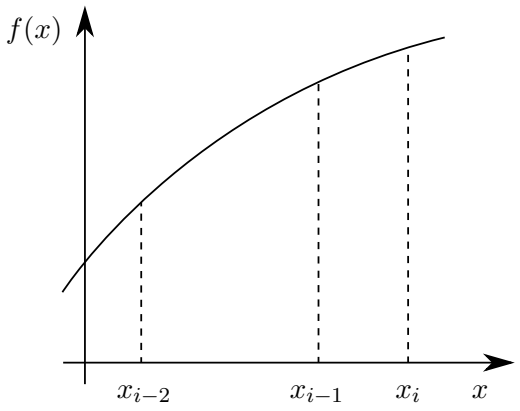

Figure D.1: Sketch of nonuniform grid.

In the case of a uniform grid we regain the well known coefficients $\{3/2, -2, 1/2\}$ for a second order backward finite difference scheme. This expression is of second order accuracy.

References

[1] M. Fleischhauer, A. Imamoglu, and J. P. Marangos. Electromagnetically induced transparency: Optics in coherent media. *Rev. Mod. Phys.*, **77**, (2005), 633–673. doi: 10.1103/RevModPhys.77.633.

[2] M. Fleischhauer and M. D. Lukin. Dark-State Polaritons in Electromagnetically Induced Transparency. *Phys. Rev. Lett.*, **84**, (2000), 5094–5097. doi: 10.1103/PhysRevLett.84.5094.

[3] M. Fleischhauer and M. D. Lukin. Quantum memory for photons: Dark-state polaritons. *Phys. Rev. A*, **65**, (2002), 022314. doi: 10.1103/PhysRevA.65.022314.

[4] S. E. Harris, J. E. Field, and A. Kasapi. Dispersive properties of electromagnetically induced transparency. *Phys. Rev. A*, **46**, (1992), R29–R32. doi: 10.1103/PhysRevA.46.R29.

[5] T. F. Gallagher. *Rydberg Atoms*. Cambridge Monographs on Atomic, Molecular and Chemical Physics. Cambridge, UK: Cambridge University Press, 2005. isbn: 978-0-521-02166-1.

[6] M. Saffman, T. G. Walker, and K. Mølmer. Quantum information with Rydberg atoms. *Reviews of Modern Physics*, **82**, (2010), 2313–2363. doi: 10.1103/RevModPhys.82.2313.

[7] O. Firstenberg, C. S. Adams, and S. Hofferberth. Nonlinear quantum optics mediated by Rydberg interactions. *Journal of Physics B: Atomic, Molecular and Optical Physics*, **49**, (2016), 152003. doi: 10.1088/0953-4075/49/15/152003.

[8] T. Peyronel, O. Firstenberg, Q.-Y. Liang, S. Hofferberth, A. V. Gorshkov, T. Pohl, M. D. Lukin, and V. Vuletić. Quantum nonlinear optics with single photons enabled by strongly interacting atoms. *Nature*, **488**, (2012), 57–60. doi: 10.1038/nature11361.

[9] H. J. Carmichael. *Statistical Methods in Quantum Optics 1: Master Equations and Fokker-Planck Equations*. Theoretical and Mathematical Physics. Springer Berlin Heidelberg, 1999.

[10] T. Giamarchi. *Quantum Physics in One Dimension*. International Series of Monogr. Clarendon Press, 2004. isbn: 978-0-19-852500-4.

[11] M. O. Scully and M. S. Zubairy. *Quantum Optics*. 1st ed. Cambridge, UK: Cambridge University Press, 1997. isbn: 978-0-521-43595-6.

[12] C. Gerry and P. Knight. *Introductory Quantum Optics*. 1st ed. Cambridge, UK: Cambridge University Press, 2005. isbn: 978-0-521-52735-4.

[13] W. Louisell. *Quantum statistical properties of radiation*. Wiley Series in Pure and Applied Optics Series. John Wiley & Sons Canada, Limited, 1990. isbn: 978-0-471-52365-9.

[14] C. L. G. Alzar, M. A. G. Martinez, and P. Nussenzveig. Classical analog of electromagnetically induced transparency. *American Journal of Physics*, **70**, (2002), 37–41. doi: 10.1119/1.1412644.

[15] K. Boller, A. Imamoğlu, and S. E. Harris. Observation of electromagnetically induced transparency. *Phys. Rev. Lett.*, **66**, (1991), 2593–2596. doi: 10.1103/PhysRevLett.66.2593.

[16] J. D. Jackson. *Classical electrodynamics*. 3rd ed. New York: Wiley, 1999. isbn: 978-0-471-30932-1.

[17] A. Kasapi, M. Jain, G. Y. Yin, and S. E. Harris. Electromagnetically Induced Transparency: Propagation Dynamics. *Phys. Rev. Lett.*, **74**, (1995), 2447–2450. doi: 10.1103/PhysRevLett.74.2447.

[18] M. Xiao, Y.-q. Li, S.-z. Jin, and J. Gea-Banacloche. Measurement of Dispersive Properties of Electromagnetically Induced Transparency in Rubidium Atoms. *Phys. Rev. Lett.*, **74**, (1995), 666–669. doi: 10.1103/PhysRevLett.74.666.

[19] L. V. Hau, S. E. Harris, Z. Dutton, and C. H. Behroozi. Light speed reduction to 17 metres per second in an ultracold atomic gas. *Nature*, **397**, (1999), 594–598. doi: 10.1038/17561.

[20] C. Mewes and M. Fleischhauer. Two-photon linewidth of light "stopping" via electromagnetically induced transparency. *Phys. Rev. A*, **66**, (2002), 033820. doi: 10.1103/PhysRevA.66.033820.

[21] C. Mewes. *Decoherence and decoherence suppression in quantum memories with collective atomic excitations*. Dissertation. Technische Universität Kaiserslautern, 2004.

[22] P. J. Mohr, D. B. Newell, and B. N. Taylor. CODATA recommended values of the fundamental physical constants: 2014. *Rev. Mod. Phys.*, **88**, (2016), 035009. doi: 10.1103/RevModPhys.88.035009.

[23] J. Deiglmayr, M. Reetz-Lamour, T. Amthor, S. Westermann, A. de Oliveira, and M. Weidemüller. Coherent excitation of Rydberg atoms in an ultracold gas. *Optics Communications*, **264**, (2006). Quantum Control of Light and Matter, 293–298. doi: 10.1016/j.optcom.2006.02.058.

[24] A. Reinhard, T. C. Liebisch, B. Knuffman, and G. Raithel. Level shifts of rubidium Rydberg states due to binary interactions. *Phys. Rev. A*, **75**, (2007), 032712. doi: 10.1103/PhysRevA.75.032712.

[25] T. G. Walker and M. Saffman. Consequences of Zeeman degeneracy for the van der Waals blockade between Rydberg atoms. *Phys. Rev. A*, **77**, (2008), 032723. doi: 10.1103/PhysRevA.77.032723.

[26] L. Ballentine. *Quantum Mechanics: A Modern Development*. World Scientific, 2014. isbn: 978-981-4578-57-8.

[27] K. Mølmer, Y. Castin, and J. Dalibard. Monte Carlo wave-function method in quantum optics. *J. Opt. Soc. Am. B*, **10**, (1993), 524–538. doi: 10.1364/JOSAB.10.000524.

[28] M. B. Plenio and P. L. Knight. The quantum-jump approach to dissipative dynamics in quantum optics. *Rev. Mod. Phys.*, **70**, (1998), 101–144. doi: 10.1103/RevModPhys.70.101.

[29] A. J. Daley. Quantum trajectories and open many-body quantum systems. *Advances in Physics*, **63**, (2014), 77–149. doi: 10.1080/00018732.2014.933502.

[30] W. Itano, J. Bergquist, and D. Wineland. Early observations of macroscopic quantum jumps in single atoms. *International Journal of Mass Spectrometry*, **377**, (2015). Special Issue: MS 1960 to Now, 403–409. doi: 10.1016/j.ijms.2014.07.005.

[31] R. Dum, A. S. Parkins, P. Zoller, and C. W. Gardiner. Monte Carlo simulation of master equations in quantum optics for vacuum, thermal, and squeezed reservoirs. *Phys. Rev. A*, **46**, (1992), 4382–4396. doi: 10.1103/PhysRevA.46.4382.

[32] A. Gogolin, A. Nersesyan, and A. Tsvelik. *Bosonization and Strongly Correlated Systems*. 1. paperback ed., re-issue. Cambridge, UK: Cambridge University Press, 2004. isbn: 978-0-521-61719-2.

[33] D. Sénéchal. An introduction to bosonization (1999). arXiv: cond-mat/9908262.

[34] M. A. Cazalilla. Bosonizing one-dimensional cold atomic gases. *Journal of Physics B Atomic Molecular Physics*, **37**, (2004), S1–S47. doi: 10.1088/0953-4075/37/7/051.

[35] F. D. M. Haldane. Effective Harmonic-Fluid Approach to Low-Energy Properties of One-Dimensional Quantum Fluids. *Phys. Rev. Lett.*, **47**, (1981), 1840–1843. doi: 10.1103/PhysRevLett.47.1840.

[36] J. Clarke and F. K. Wilhelm. Superconducting quantum bits. *Nature*, **453**, (2008), 1031–1042. doi: doi:10.1038/nature07128.

[37] C. O'Brien, N. Lauk, S. Blum, G. Morigi, and M. Fleischhauer. Interfacing Superconducting Qubits and Telecom Photons via a Rare-Earth-Doped Crystal. *Phys. Rev. Lett.*, **113**, (2014), 063603. doi: 10.1103/PhysRevLett.113.063603.

[38] A. Grankin, E. Brion, E. Bimbard, R. Boddeda, I. Usmani, A. Ourjoumtsev, and P. Grangier. Quantum-optical nonlinearities induced by Rydberg-Rydberg interactions: A perturbative approach. *Phys. Rev. A*, **92**, (2015), 043841. doi: 10.1103/PhysRevA.92.043841.

[39] J. D. Pritchard, D. Maxwell, A. Gauguet, K. J. Weatherill, M. P. A. Jones, and C. S. Adams. Cooperative atom-light interaction in a blockaded Rydberg ensemble. *Phys. Rev. Lett.*, **105**, (2010), 3–6. doi: 10.1103/PhysRevLett.105.193603.

[40] C. Ates, S. Sevin çli, and T. Pohl. Electromagnetically induced transparency in strongly interacting Rydberg gases. *Phys. Rev. A*, **83**, (2011), 041802. doi: 10.1103/PhysRevA.83.041802.

[41] D. Petrosyan, J. Otterbach, and M. Fleischhauer. Electromagnetically Induced Transparency with Rydberg Atoms. *Phys. Rev. Lett.*, **107**, (2011), 213601. doi: 10.1103/PhysRevLett.107.213601.

[42] A. V. Gorshkov, J. Otterbach, M. Fleischhauer, T. Pohl, and M. D. Lukin. Photon-Photon Interactions via Rydberg Blockade. *Phys. Rev. Lett.*, **107**, (2011), 133602. doi: 10.1103/PhysRevLett.107.133602.

[43] S. Baur, D. Tiarks, G. Rempe, and S. Dürr. Single-Photon Switch Based on Rydberg Blockade. *Phys. Rev. Lett.*, **112**, (2014), 073901. doi: 10.1103/PhysRevLett.112.073901.

[44] H. Gorniaczyk, C. Tresp, J. Schmidt, H. Fedder, and S. Hofferberth. Single-Photon Transistor Mediated by Interstate Rydberg Interactions. *Phys. Rev. Lett.*, **113**, (2014), 053601. doi: 10.1103/PhysRevLett.113.053601.

[45] D. Tiarks, S. Baur, K. Schneider, S. Dürr, and G. Rempe. Single-Photon Transistor Using a Förster Resonance. *Phys. Rev. Lett.*, **113**, (2014), 053602. doi: 10.1103/PhysRevLett.113.053602.

[46] M. Nielsen and I. Chuang. *Quantum Computation and Quantum Information: 10th Anniversary Edition*. 10th ed. Cambridge, UK: Cambridge University Press, 2010. isbn: 978-1-139-49548-6.

[47] D. Paredes-Barato and C. S. Adams. All-Optical Quantum Information Processing Using Rydberg Gates. *Phys. Rev. Lett.*, **112**, (2014), 040501. doi: 10.1103/PhysRevLett.112.040501.

[48] A. Siegman. *Lasers*. 1st ed. Sausalito, Calif.: Univ. Science Books, 1986. isbn: 978-0-935702-11-8.

[49] F. E. Zimmer, J. Otterbach, R. G. Unanyan, B. W. Shore, and M. Fleischhauer. Dark-state polaritons for multicomponent and stationary light fields. *Phys. Rev. A*, **77**, (2008), 063823. doi: 10.1103/PhysRevA.77.063823.

[50] M. Fleischhauer, J. Otterbach, and R. G. Unanyan. Bose-Einstein Condensation of Stationary-Light Polaritons. *Phys. Rev. Lett.*, **101**, (2008), 163601. doi: 10.1103/PhysRevLett.101.163601.

[51] M. Bajcsy, S. Hofferberth, V. Balic, T. Peyronel, M. Hafezi, A. S. Zibrov, V. Vuletic, and M. D. Lukin. Efficient All-Optical Switching Using Slow Light within a Hollow Fiber. *Phys. Rev. Lett.*, **102**, (2009), 203902. doi: 10.1103/PhysRevLett.102.203902.

[52] G. Epple, K. Kleinbach, T. Euser, N. Joly, T. Pfau, P. S. J. Russell, and R. Löw. Rydberg atoms in hollow-core photonic crystal fibres. *Nat. Commun.*, **5**, (2014). doi: doi:10.1038/ncomms5132.

[53] M. Langbecker, M. Noaman, N. Kjærgaard, F. Benabid, and P. Windpassinger. Rydberg excitation of cold atoms inside a hollow-core fiber. *Phys. Rev. A*, **96**, (2017), 041402. doi: 10.1103/PhysRevA.96.041402.

[54] O. Svelto and D. Hanna. *Principles of Lasers*. 4th ed. Springer US, 1998. isbn: 978-0-306-45748-7.

[55] M. Abramowitz and I. Stegun. *Handbook of Mathematical Functions: With Formulas, Graphs, and Mathematical Tables*. Dover Books on Mathematics. New York: Dover Publications Inc., 1964. isbn: 978-0-486-61272-0.

[56] G. Arfken and H.-J. Weber. *Mathematical Methods for Physicists*. 6. ed., internat. ed. Amsterdam: Elsevier Academic Press, 2005. isbn: 978-0-12-088584-8.

[57] E. W. Weisstein. *"Associated Laguerre Polynomial." From MathWorld–A Wolfram Web Resource*. Visited on 21/10/17. url: http://mathworld.wolfram.com/AssociatedLaguerrePolynomial.html.

[58] M. D. Lukin, M. Fleischhauer, R. Cote, L. M. Duan, D. Jaksch, J. I. Cirac, and P. Zoller. Dipole Blockade and Quantum Information Processing in Mesoscopic Atomic Ensembles. *Phys. Rev. Lett.*, **87**, (2001), 037901. doi: 10.1103/PhysRevLett.87.037901.

[59] T. Holstein and H. Primakoff. Field Dependence of the Intrinsic Domain Magnetization of a Ferromagnet. *Phys. Rev.*, **58**, (1940), 1098–1113. doi: 10.1103/PhysRev.58.1098.

[60] E. W. Weisstein. *"Trigonometric Substitution." From MathWorld–A Wolfram Web Resource*. Visited on 21/10/17. url: http://mathworld.wolfram.com/TrigonometricSubstitution.html.

[61] W. Fischer and I. Lieb. *Funktionentheorie: Komplexe Analysis in einer Veränderlichen*. 9th ed. vieweg studium; Aufbaukurs Mathematik. Vieweg+Teubner Verlag, 2005. isbn: 978-3-8348-0013-8.

[62] D. Tiarks, S. Schmidt, G. Rempe, and S. Dürr. Optical Pi phase shift created with a single-photon pulse. *Science Advances*, **2**, (2016), e1600036–e1600036. doi: 10.1126/sciadv.1600036.

[63] *MATLAB, Release 2017a*. The MathWorks, Inc. Natick, Massachusetts, USA., 2017.

[64] T. A. Driscoll, N. Hale, and L. N. Trefethen. *Chebfun Guide*. 2014. url: http://www.chebfun.org/docs/guide/.

[65] O. Firstenberg, T. Peyronel, Q.-Y. Liang, A. V. Gorshkov, M. D. Lukin, and V. Vuletić. Attractive photons in a quantum nonlinear medium. *Nature*, **502**, (2013), 71–5. doi: 10.1038/nature12512.

[66] Q.-Y. Liang, A. V. Venkatramani, S. H. Cantu, T. L. Nicholson, M. J. Gullans, A. V. Gorshkov, J. D. Thompson, C. Chin, M. D. Lukin, and V. Vuletic. Observation of three-photon bound states in a quantum nonlinear medium (2017). arXiv: 1709.01478v2.

[67] M. J. Gullans, J. D. Thompson, Y. Wang, Q.-Y. Liang, V. Vuletić, M. D. Lukin, and A. V. Gorshkov. Effective Field Theory for Rydberg Polaritons. *Phys. Rev. Lett.*, **117**, (2016), 113601. doi: 10.1103/PhysRevLett.117.113601.

[68] J. Otterbach, M. Moos, D. Muth, and M. Fleischhauer. 2013. url: https://link.aps.org/supplemental/10.1103/PhysRevLett.111.113001.

[69] J. Otterbach. *Single- and Many-Body Phenomena of Dark-State Polaritons*. Dissertation. Technische Universität Kaiserslautern, 2011.

[70] H. Breuer and F. Petruccione. *The Theory of Open Quantum Systems*. 1st ed. Oxford: Oxford University Press, 2010. isbn: 978-0-19-921390-0.

[71] C. Gardiner and P. Zoller. *Quantum Noise: A Handbook of Markovian and Non-Markovian Quantum Stochastic Methods with Applications to Quantum Optics*. 3rd ed. Springer Series in Synergetics. Springer, 2004. isbn: 978-3-540-22301-6.

[72] R. Puri. *Mathematical Methods of Quantum Optics*. Physics and astronomy online library. Springer, 2001. isbn: 978-3-540-67802-1.

[73] E. Wigner. On the Interaction of Electrons in Metals. *Phys. Rev.*, **46**, (1934), 1002–1011. doi: 10.1103/PhysRev.46.1002.

[74] D. Muth. *Dynamics in strongly correlated quantum gases*. Dissertation. Technische Universität Kaiserslautern, 2012.

[75] D. F. Phillips, A. Fleischhauer, A. Mair, R. L. Walsworth, and M. D. Lukin. Storage of Light in Atomic Vapor. *Phys. Rev. Lett.*, **86**, (2001), 783–786. doi: 10.1103/PhysRevLett.86.783.

[76] A. V. Gorshkov, A. André, M. D. Lukin, and A. S. Sørensen. Photon storage in Λ-type optically dense atomic media. II. Free-space model. *Phys. Rev. A*, **76**, (2007), 033805. doi: 10.1103/PhysRevA.76.033805.

[77] B. Dóra, M. Haque, and G. Zaránd. Crossover from Adiabatic to Sudden Interaction Quench in a Luttinger Liquid. *Phys. Rev. Lett.*, **106**, (2011), 156406. doi: 10.1103/PhysRevLett.106.156406.

[78] E. Perfetto and G. Stefanucci. On the thermalization of a Luttinger liquid after a sequence of sudden interaction quenches. *EPL (Europhysics Letters)*, **95**, (2011), 10006. doi: 10.1209/0295-5075/95/10006.

[79] S. R. White. Density matrix formulation for quantum renormalization groups. *Phys. Rev. Lett.*, **69**, (1992), 2863–2866. doi: 10.1103/PhysRevLett.69.2863.

[80] E. H. Lieb and W. Liniger. Exact Analysis of an Interacting Bose Gas. I. The General Solution and the Ground State. *Phys. Rev.*, **130**, (1963), 1605–1616. doi: 10.1103/PhysRev.130.1605.

[81] D. E. Chang, V. Gritsev, G. Morigi, V. Vuletic, M. D. Lukin, and E. A. Demler. Crystallization of strongly interacting photons in a nonlinear optical fibre. *Nat. Phys.*, **4**, (2008), 884–889. doi: doi:10.1038/nphys1074.

[82] R. Citro, E. Orignac, S. De Palo, and M. L. Chiofalo. Evidence of Luttinger-liquid behavior in one-dimensional dipolar quantum gases. *Phys. Rev. A*, **75**, (2007), 051602. doi: 10.1103/PhysRevA.75.051602.

[83] M. Dalmonte, G. Pupillo, and P. Zoller. One-Dimensional Quantum Liquids with Power-Law Interactions: The Luttinger Staircase. *Phys. Rev. Lett.*, **105**, (2010), 140401. doi: 10.1103/PhysRevLett.105.140401.

[84] S. A. Söffing, M. Bortz, I. Schneider, A. Struck, M. Fleischhauer, and S. Eggert. Wigner crystal versus Friedel oscillations in the one-dimensional Hubbard model. *Phys. Rev. B*, **79**, (2009), 195114. doi: 10.1103/PhysRevB.79.195114.

[85] L. Karpa, G. Nikoghosyan, F. Vewinger, M. Fleischhauer, and M. Weitz. Frequency Matching in Light-Storage Spectroscopy of Atomic Raman Transitions. *Phys. Rev. Lett.*, **103**, (2009), 093601. doi: 10.1103/PhysRevLett.103.093601.

[86] M. A. Cazalilla and M.-C. Chung. Quantum Quenches in the Luttinger model and its close relatives. *Journal of Statistical Mechanics: Theory and Experiment*, **2016**, (2016), 064004. doi: 10.1088/1742-5468/2016/06/064004.

[87] A. Iucci and M. A. Cazalilla. Quantum quench dynamics of the Luttinger model. *Phys. Rev. A*, **80**, (2009), 063619. doi: 10.1103/PhysRevA.80.063619.

[88] A. Polkovnikov, K. Sengupta, A. Silva, and M. Vengalattore. Colloquium: Nonequilibrium dynamics of closed interacting quantum systems. *Rev. Mod. Phys.*, **83**, (2011), 863–883. doi: 10.1103/RevModPhys.83.863.

[89] F. Pollmann, M. Haque, and B. Dóra. Linear quantum quench in the Heisenberg XXZ chain: Time-dependent Luttinger-model description of a lattice system. *Phys. Rev. B*, **87**, (2013), 041109. doi: 10.1103/PhysRevB.87.041109.

[90] R. Sachdeva, T. Nag, A. Agarwal, and A. Dutta. Finite-time interaction quench in a Luttinger liquid. *Phys. Rev. B*, **90**, (2014), 045421. doi: 10.1103/PhysRevB.90.045421.

[91] P. Chudzinski and D. Schuricht. Time evolution during and after finite-time quantum quenches in Luttinger liquids. *Phys. Rev. B*, **94**, (2016), 075129. doi: 10.1103/PhysRevB.94.075129.

[92] G. D. Mahan. *Many-Particle Physics*. 3rd ed. Physics of Solids and Liquids. New York: Springer Science+Business Media, 2000. isbn: 978-1-4419-3339-3.

[93] R. Lim and M. V. Berry. Superadiabatic tracking of quantum evolution. *Journal of Physics A: Mathematical and General*, **24**, (1991), 3255. doi: 10.1088/0305-4470/24/14/014.

[94] K. Jachymski, P. Bienias, and H. P. Büchler. Three-Body Interaction of Rydberg Slow-Light Polaritons. *Phys. Rev. Lett.*, **117**, (2016), 053601. doi: 10.1103/PhysRevLett.117.053601.

[95] P. Bienias, S. Choi, O. Firstenberg, M. F. Maghrebi, M. Gullans, M. D. Lukin, A. V. Gorshkov, and H. P. Büchler. Scattering resonances and bound states for strongly interacting Rydberg polaritons. *Phys. Rev. A*, **90**, (2014), 053804. doi: 10.1103/PhysRevA.90.053804.

[96] B. Simon. *Trace Ideals and Their Applications*. 2nd ed. Vol. 120. Mathematical Surveys and Monographs. Providence, Rhode Island: American Mathematical Society, 2005. isbn: 978-0-8218-4988-0. doi: 10.1090/surv/120.

[97] H. P. Büchler. Crystalline phase for one-dimensional ultra-cold atomic bosons. *New Journal of Physics*, **13**, (2011), 093040. doi: 10.1088/1367-2630/13/9/093040.

[98] M. Bajcsy, A. S. Zibrov, and M. D. Lukin. Stationary pulses of light in an atomic medium. *Nature*, **426**, (2003), 638–641. doi: 10.1038/nature02176.

[99] H. B. Callen and T. A. Welton. Irreversibility and Generalized Noise. *Phys. Rev.*, **83**, (1951), 34–40. doi: 10.1103/PhysRev.83.34.

List of publications

The following list provides an overview on the publications underlying this thesis. The material presented in this thesis is largely contained in these publications, partially with textual overlap. All publications are results from collaborations of several authors who all contributed substantially to the theoretical and numerical work and the writing of the manuscripts unless otherwise noted. Specific contributions of individual authors are provided below.

Publications in peer-reviewed journals:

[Höning2012] M. Höning, M. Moos, and M. Fleischhauer. Critical exponents of steady-state phase transitions in fermionic lattice models. *Phys. Rev. A.,* **86,** 013606 (2012). DOI: 10.1103/PhysRevA.86.013606.

This publication is a collaboration of M. Höning and M. Fleischhauer and myself. In particular most of the analytic and numerical work was done by M. Höning. I contributed to the quantum optical example presented in the publication.

[Otterb2013] J. Otterbach, M. Moos, D. Muth, and M. Fleischhauer. Wigner Crystallization of Single Photons in Cold Rydberg Ensembles. *Phys. Rev. Lett.,* **111**, 113001 (2013). DOI: 10.1103/PhysRevLett.111.113001.

This work was done in collaboration with J. Otterbach, D. Muth and M. Fleischhauer. Specifically, J. Otterbach contributed mainly the analytic calculation of the dark-state polariton model, D. Muth provided the numerical DMRG simulations of the correlation functions and extraction of the Luttinger K parameter while I mainly did the analytic and numerical calculations of the time-dependent Luttinger liquid theory.

[Moos2015] M. Moos, M. Höning, R. Unanyan, and M. Fleischhauer. Many-body physics of Rydberg dark-state polaritons in the strongly interacting regime. *Phys. Rev. A,* **92,** 053846 (2015). DOI:10.1103/PhysRevA.92.053846.

This publication is a collaboration of Razmik Unanyan, Michael Fleischhauer and myself, with minor contributions from Michael Höning. In particular all analytical calculations and the numerical wave-function simulations were done by me.

[Moos2017] M. Moos, R. Unanyan, and M. Fleischhauer. Creation and detection of photonic molecules in Rydberg gases. *Phys. Rev. A,* **96,** 023853 (2017). DOI:10.1103/PhysRevA.96.023853.

This publication is a collaboration of Razmik Unanyan, Michael Fleischhauer and myself. Razmik Unanyan mainly did the analytical calculations using the Green's function approach while I provided all numerical results and contributed to the analytical calculations.

Lebenslauf

Persönliche Daten

Name	Matthias Moos
Geburstdatum, -ort	07.10.1986, Ludwigshafen am Rhein
Familienstand	ledig
Staatsangehörigkeit	Deutsch

Ausbildung

09/2011 – 12/2017	Promotionsstudium in Physik, Technische Universität Kaiserslautern, Arbeitsgruppe Theoretische Quantenoptik, Prof. Dr. Fleischhauer. Angestrebter Abschluss: Dr. rer. nat.
05/2011	Diplomarbeit in Physik: „Badinduzierte Korrelationen in bosonischen Gittermodellen“.
10/2006 – 08/2011	Studium der Physik. Technische Universität Kaiserslautern, Abschluss als Diplom-Physiker mit Note 1,2 (sehr gut).
09/1997 – 03/2006	Gymnasium, Paul-von-Denis-Schulzentrum, Schifferstadt. Abschluss: Abitur mit Note 1,4 (sehr gut).

Berufliche Laufbahn

seit 08/2016	Wissenschaftlicher Mitarbeiter im Fachbereich Physik, Technische Universität Kaiserslautern
07/2015 – 07/2016	Wissenschaftliche Hilfskraft im Fachbereich Physik, Technische Universität Kaiserslautern
09/2011 – 06/2015	Wissenschaftlicher Mitarbeiter im Fachbereich Physik, Technische Universität Kaiserslautern
06/2011 – 08/2011	Wissenschaftliche Hilfskraft im Fachbereich Physik, Technische Universität Kaiserslautern
10/2010 – 03/2011	Wissenschaftliche Hilfskraft im Fachbereich Physik, Technische Universität Kaiserslautern

Stipendien

07/2015 – 07/2016	Stipendium des Fachbereichs Physik, Technische Universität Kaiserslautern

Sprachkenntnisse

Deutsch	Muttersprache
Englisch	fließend
Französisch	Grundkenntnisse

Sonstige Qualifikationen

Lehre	Betreuung von Übungsgruppen zu den Vorlesungen Mathematische Grundlagen der Physik, Elektrodynamik und Statistische Mechanik

Kaiserslautern, den 10. Januar 2018

Danksagung

An dieser Stelle möchte ich mich bei allen Menschen bedanken, die mich in meiner Zeit an der Uni und unterstützt und begleitet haben und zur Entstehung dieser Arbeit beigetragen haben.

Mein erster Dank geht an meinen Doktorvater Michael, der mir das Schreiben dieser Arbeit ermöglichte und mich mit unzähligen Anregungen und Ideen und konstruktiver Kritik begleitet und immer neue Wege aufgezeigt hat. Vielen Dank für Deine Unterstützung und Dein Vertrauen.

Weiter gilt mein Dank meinen ehemaligen und aktuellen Kollegen Nikolai, Michael, Fabian, Razmik und Johannes. Ohne die Zusammenarbeit mit Euch und viele Diskussionen über Physik, Mathematik, numerische und sonstige Probleme wäre diese Arbeit sicher nicht möglich gewesen. An dieser Stelle möchte ich auch allen anderen ehemaligen und aktuellen Mitgliedern der AG Theoretische Quantenoptik, insbesondere David, Christopher, Thomas, Lukas, Max, Fabian und Dominik meinen Dank aussprechen, sei es für Diskussionen, lustige Momente, gemeinsame Kaffeepausen oder für tolle gemeinsame Tage in den Alpen und auf Konferenzen.

Ein großer Dank gilt auch meinen Eltern die mir stets mit Rat und Tat zur Seite stehen und meinen Geschwistern und Freunden für wundervolle gemeinsam verbrachte Zeit und Unterstützung in allen Lebenslagen.

Zu guter Letzt geht mein Dank an meine liebe Sarah. Danke für die geteilte Zeit und deine Unterstützung insbesondere in der Schlussphase meiner Arbeit.